

92-112

3346/III

F-100

CORRELATION

PROGRESS REPORT

on

CORRELATION OF LABORATORY TESTS WITH
FULL SCALE SHIP PLATE FRACTURE TESTS

by

M. GENSAMER, E. P. KLLER, T. A. PRATER,
F. C. WAGNER, J. O. MACK AND J. L. FISHER
PENNSYLVANIA STATE COLLEGE
Under Navy Contract NObs-31217

COMMITTEE ON SHIP CONSTRUCTION
DIVISION OF ENGINEERING & INDUSTRIAL RESEARCH
NATIONAL RESEARCH COUNCIL

Advisory to

BUREAU OF SHIPS, NAVY DEPARTMENT
Under Contract NObs-34231

Serial No. SSC-9

Copy No. 10

March 19, 1947

NATIONAL RESEARCH COUNCIL
2101 Constitution Avenue
Washington, D. C.

March 19, 1947

Chief, Bureau of Ships
Navy Department
Washington, D. C.

Dear Sir:

Attached is Report Serial No, SSC-9, entitled "Correlation of Laboratory Tests with Full Scale Ship Plate Fracture Tests". This report has been submitted by the contractor as a progress report of the work done on Research Project SR-96 under Contract NOBs-31217 between the Bureau of Ships, Navy Department and the Pennsylvania State College.

The report has been reviewed and acceptance recommended by representatives of the Committee on Ship Construction, Division of Engineering and Industrial Research, NRC, in accordance with the terms of the contract between the Bureau of Ships, Navy Department and the National Academy of Sciences.

Very truly yours,



Frederick M. Feiker, Chairman
Division of Engineering and
Industrial Research

Enclosure

PREFACE

The Navy Department through the Bureau of Ships is distributing this report to those agencies and individuals that were actively associated with this research program. This report represents a part of the research work contracted for under the section of the Navy's directive "to investigate the design and construction of welded steel merchant vessels."

The distribution of this report is as follows:

Copy No. 1 - Chief, Bureau of Ships, Navy Department
Copy No. 2 - Dr. D. W. Bronk, Chairman, National Research Council

Committee on Ship Construction

Copy No. 3 - V. H. Schnee, Chairman
Copy No. 4 - J. L. Bates
Copy No. 5 - H. C. Boardman
Copy No. 6 - Paul Field
Copy No. 7 - M. A. Grossman
Copy No. 8 - C. H. Herty, Jr.
Copy No. 9 - A. B. Kinzel
Copy No. 10 - J. M. Lessells
Copy No. 11 - L. P. McAllister
Copy No. 12 - G. S. Mikhalapov
Copy No. 13 - J. Ormondroyd
Copy No. 14 - H. W. Pierce
Copy No. 15 - E. C. Smith
Copy No. 16 - Finn Jonassen, Research Coordinator

Members of Project Advisory Committees SR-89, SR-92 and SR-96:

Copy No. 16 - Finn Jonassen, Chairman
Copy No. 7 - M. A. Grossman
Copy No. 8 - C. H. Herty, Jr.
Copy No. 10 - J. M. Lessells
Copy No. 11 - L. P. McAllister
Copy No. 13 - J. Ormondroyd
Copy No. 14 - H. W. Pierce
Copy No. 15 - E. C. Smith
Copy No. 17 - W. M. Wilson
Copy No. 18 - E. M. MacCutcheon, Jr., U. S. Coast Guard, Liaison
Copy No. 19 - E. Rassman, Bureau of Ships, Liaison
Copy No. 20 - Comdr. R. D. Schmidtman, U. S. Coast Guard, Liaison
Copy No. 21 - T. L. Soc-Hoo, Bureau of Ships, Liaison
Copy No. 22 - John Vasta, U. S. Maritime Commission, Liaison
Copy No. 23 - R. E. Wiley, Bureau of Ships, Liaison
Copy No. 24 - J. L. Wilson, American Bureau of Shipping, Liaison

Ship Structure Committee

- Copy No. 25 - Rear Admiral Ellis Reed-Hill, USCG, Chairman
- Copy No. 26 - Rear Admiral Charles D. Wheelock, USN, Bureau of Ships
- Copy No. 27 - Captain T. L. Schumacher, USN, Maritime Commission
- Copy No. 28 - David Arnott, American Bureau of Shipping
- Copy No. 3 - V. H. Schnee, Committee on Ship Construction, Liaison

Ship Structure Sub-Committee

- Copy No. 29 - Captain L. V. Honsinger, USN, Bureau of Ships, Chairman
- Copy No. 30 - Captain R. A. Hinners, USN, David Taylor Model Basin
- Copy No. 20 - Comdr. R. D. Schmidtman, USCG
- Copy No. 31 - D. P. Brown, American Bureau of Shipping
- Copy No. 18 - E. M. MacCutcheon, Jr., USCG
- Copy No. 32 - R. M. Robertson, Office of Naval Research, USN
- Copy No. 22 - John Vasta, U. S. Maritime Commission
- Copy No. 33 - I. J. Wanless, U. S. Maritime Commission
- Copy No. 24 - J. L. Wilson, American Bureau of Shipping
- Copy No. 16 - Finn Jonassen, Liaison Representative, NRC
- Copy No. 34 - Wm. Spraragen, Liaison Representative, NRC

Navy Department

- Copy No. 35 - Comdr. R. H. Lambert, USN, Bureau of Ships
- Copy No. 36 - Comdr. R. S. Mandelkorn, USN, Bureau of Ships
- Copy No. 37 - A. G. Bissell, Bureau of Ships
- Copy No. 38 - J. W. Jenkins, Bureau of Ships
- Copy No. 39 - Noah Kahn, New York Naval Shipyard
- Copy No. 40 - I. R. Kramer, Office of Naval Research
- Copy No. 41 - W. R. Osgood, David Taylor Model Basin
- Copy No. 42 - N. E. Promisel, Bureau of Aeronautics
- Copy No. 23 - R. E. Wiley, Bureau of Ships
- Copy No. 43 - K. D. Williams, Bureau of Ships
- Copy No. 44 - Naval Academy, Post Graduate School
- Copy No. 45 - Naval Research Laboratory
- Copy No. 46 - Philadelphia Naval Shipyard
- Copy No. 47 - U. S. Naval Engineering Experiment Station
- Copies 48 and 49 - Publications Board, Navy Department via Bureau of Ships, Code 330c
- Copies 50 and 51 - Technical Library, Bureau of Ships, Code 337-L

U. S. Coast Guard

- Copy No. 52 - Captain R. B. Lank, Jr., USCG
- Copy No. 53 - Captain G. A. Tyler, USCG
- Copy No. 54 - Testing and Development Division

U. S. Maritime Commission

- Copy No. 55 - E. E. Martinsky

Representatives of American Iron and Steel
Institute Committee on Manufacturing Problems

- Copy No. 56 - C. M. Parker, Secretary, General Technical Committee
American Iron and Steel Institute
Copy No. 57 - L. C. Bibber, Carnegie-Illinois Steel Corporation
Copy No. 8 - C. H. Herty, Jr., Bethlehem Steel Company
Copy No. 15 - E. C. Smith, Republic Steel Corporation

Welding Research Council

- Copy No. 58 - C. A. Adams
Copy No. 59 - Everett Chapman
Copy No. 60 - LaMotte Grover
Copy No. 34 - Wm. Spraragen

-
- Copy No. 61 - Dean F. M. Feiker, Chairman, Division of Engineering and
Industrial Research, NRC
Copy No. 62 - Dr. Clyde Williams, Chairman, Committee on Engineering Materials
Copy No. 3 - V. H. Schnee, Chairman, Committee on Ship Construction
Copy No. 16 - Finn Jonassen, Research Coordinator, Committee on Ship Construction
Copy No. 63 - M. Gensamer, Investigator, Research Project SR-96
Copy No. 64 - E. P. Klier, Investigator, Research Project SR-96
Copy No. 65 - T. A. Prater, Investigator, Research Project SR-96
Copy No. 66 - F. C. Wagner, Investigator, Research Project SR-96
Copy No. 67 - J. O. Mack, Investigator, Research Project SR-96
Copy No. 68 - J. L. Fisher, Investigator, Research Project SR-96
Copy No. 69 - A. Boodberg, Investigator, Research Project SR-92
Copy No. 70 - W. H. Bruckner, Investigator, Research Project SR-93
Copy No. 71 - E. Paul DeGarmo, Investigator, Research Project SR-92
Copy No. 72 - R. A. Hechtman, Investigator, Research Project SR-93
Copy No. 73 - S. C. Hollister, Investigator, Research Project SR-89
Copy No. 74 - C. H. Lorig, Investigator, Research Project SR-97
Copy No. 75 - Albert Muller, Investigator, Research Project SR-92
Copy No. 76 - M. P. O'Brien, Technical Representative, Research Project SR-92
Copy No. 77 - E. R. Parker, Investigator, Research Project SR-92
Copy No. 78 - C. E. Sims, Investigator, Research Project SR-87
Copy No. 17 - W. M. Wilson, Investigator, Research Project SR-93
Copy No. 79 - E. T. Barron, Carnegie-Illinois Steel Corporation
Copy No. 80 - N. M. Newmark, College of Engineering, University of Illinois
Copy No. 81 - W. P. Roop, Division of Engineering, Swarthmore College
Copy No. 82 - T. T. Watson, Lukens Steel Company
Copy No. 83 - File Copy, Committee on Ship Construction
Copies 84 thru 88 - Library of Congress via Bureau of Ships, Code 330c
Copy No. 89 - NACA, Committee on Materials Research Coordination, USN
Copy No. 90 - Copy No. 96 -
Copy No. 91 - Copy No. 97 -
Copy No. 92 - Copy No. 98 -
Copy No. 93 - Copy No. 99 -
Copy No. 94 - Copy No. 100 -
Copy No. 95 -

(Copies 90 thru 100 - Bureau of Ships)
Total Number of Copies - 100

PROGRESS REPORT

Navy Bureau of Ships Contract NObs-31217
Project SR-96

CORRELATION OF LABORATORY TESTS WITH
FULL SCALE SHIP PLATE FRACTURE TESTS

Date: September 15, 1946

By: M. Gensamer
E. P. Klier
T. A. Prater
F. C. Wagner
J. O. Mack
J. L. Fisher

Mineral Industries Experiment Station
School of Mineral Industries
The Pennsylvania State College
State College, Pennsylvania

TABLE OF CONTENTS

	<u>Page</u>
Abstract	II
List of Tables	III
List of Figures	IV
Introduction	1
Steels	4
Part I - Impact Testing	5
Resume of Testing Program	5
Testing Procedure	7
The Graphical Representation of Data	7
The Tabulation of Impact Test Data	10
Results of Impact Testing	10
V-Notch Specimens	10
Keyhole-Notch Specimens	12
Full Plate Thickness Specimens	14
Discussion of Impact Test Data § A,B,C.	14
Impact Specimens from Large Plate Tests	16
Strain on Impact Test Data	17
Grain Size on Impact Test Data	19
Impact Test Data - Steel C	20
Plate Gage on Impact Test Data - Steel C	20
Discussion and Conclusions	21
Part II - Metallographic Study	27
Experimental Results	28
Discussion and Conclusions	32
Bibliography	33
Tables	34-45
Appendix A - Mill Data	46-51
Figures	52

ABSTRACT

The present report summarizes the results which have been obtained to date on notched beam impact testing, and metallographic examination of the ship plate steels which have been used on Navy Research Projects NObs-31217, 31222 and 31224.

In Part I of this report it is shown that the standard Charpy impact test using either the V- or keyhole-notch or a special 3/4" wide specimen is not capable of evaluating the ship plate according to the data which have been obtained for large plate specimens. However, by using Charpy keyhole-notch specimens which have been strained 10% in tension and which have been allowed to stand at room temperature for one month, test data have been obtained which allow the prediction with fair accuracy of the transition temperature in the large plates.

In Part II the microstructures of the project steels have been considered. It has been shown that no simple alteration in microstructures can be found to account for the profound variation in energy absorption characteristics in the series of steels which have been studied. It has been shown that variations in grain size in a given steel cause large changes in the energy absorption characteristics of that steel. However, this factor alone is not responsible for the wide range of energy absorption characteristics which have been found in these steels.

LIST OF TABLES

	<u>Page</u>
Table 1-	Steels Investigated on Projects SR-92, -93 and -96. 34
Table 2-	Chemical Analyses of the Steels 35
Table 3-	Gas Analyses by Battelle Memorial Institute 36
Table B-	The Temperature of Transition in Degrees Fahrenheit at 25% and at 50% of Maximum Energy Absorption for the Standard LH Charpy V-Notch Specimen. 37
Table C-	The Temperature of Transition in Degrees Fahrenheit at 25% and at 50% of Maximum Energy Absorption for the Standard LH Charpy Keyhole Notch Specimen. 38
Table D-	The Temperature of Transition in Degrees Fahrenheit at 25% and at 50% of Maximum Energy Absorption for the LH Rectangular Notch, Full Plate Thickness Specimens. 39
Table E-	The Temperature of Transition in Degrees Fahrenheit at 25% and at 50% of Maximum Energy Absorption for the Standard LH Charpy Keyhole Notch Specimen. Specimens taken from 72-inch Wide Test Plates. 40
Table F-	The Temperature of Transition in Degrees Fahrenheit at 25% and at 50% Maximum Energy Absorption for the Standard LH Charpy Keyhole-Notch Specimen. 41-42
Table K-	The Temperature of Transition in Degrees Fahrenheit at 25% and at 50% of Maximum Energy Absorption for Plates of Steel C of Various Gages. 43
Table L-	The Lowest Temperature for Maximum Energy Absorption for the Impact Test Specimens for the Project Steels. 44
Table M-	Results of Measurements on Microstructures. 45

LIST OF FIGURES

	Page
Fig. A	Schematic Energy Absorption Curves for Steels for the Standard Charpy Keyhole Notch Specimen. 52
Fig. A-1	Temperature-Energy Absorption Curve for 60 Keyhole Notch Specimens, Steel E. 53
Fig. A-2	Temperature-Energy Absorption Curve for 60 Keyhole Notch Specimens, Steel Dr. 53
Fig. B-1	Temperature-Energy Absorption Curve for V-Notch Specimens of 12 Steels 54
Fig. B-2	Temperature-Energy Absorption Curve for V-Notch Specimens, Steel A 55
Fig. B-3	Temperature-Energy Absorption Curve for V-Notch Specimens, Steel Br. 55
Fig. B-4	Temperature-Energy Absorption Curve for V-Notch Specimens, Steel Bn. 55
Fig. B-5	Temperature-Energy Absorption Curve for V-Notch Specimens, Steel C 55
Fig. B-6	Temperature-Energy Absorption Curve for V-Notch Specimens, Steel Dr. 56
Fig. B-7	Temperature-Energy Absorption Curve for V-Notch Specimens, Steel Dn. 56
Fig. B-8	Temperature-Energy Absorption Curve for V-Notch Specimens, Steel E. 56
Fig. B-9	Temperature-Energy Absorption Curve for V-Notch Specimens, Steel F. 56
Fig. B-10	Temperature-Energy Absorption Curve for V-Notch Specimens, Steel H. 57
Fig. B-11	Temperature-Energy Absorption Curve for V-Notch Specimens, Steel N. 57
Fig. B-12	Temperature-Energy Absorption Curve for V-Notch Specimens, Steel Q. 57
Fig. B-13	Temperature-Energy Absorption Curve for V-Notch Specimens, Steel G. 57

Fig. C-1	Temperature-Energy Absorption Curves for Keyhole Notch Specimens for 12 Steels.	58
Fig. C-2	Temperature-Energy Absorption Curve for Keyhole Notch Specimens, Steel A.	59
Fig. C-3	Temperature-Energy Absorption Curve for Keyhole Notch Specimens, Steel Br.	59
Fig. C-4	Temperature-Energy Absorption Curve for Keyhole Notch Specimens, Steel Bn.	59
Fig. C-5	Temperature-Energy Absorption Curve for Keyhole Notch Specimens, Steel C.	59
Fig. C-6	Temperature-Energy Absorption Curve for Keyhole Notch Specimens, Steel Dr.	60
Fig. C-7	Temperature-Energy Absorption Curve for Keyhole Notch Specimens, Steel Dn.	60
Fig. C-8	Temperature-Energy Absorption Curve for Keyhole Notch Specimens, Steel E.	60
Fig. C-9	Temperature-Energy Absorption Curve for Keyhole Notch Specimens, Steel F.	60
Fig. C-10	Temperature-Energy Absorption Curve for Keyhole Notch Specimens, Steel H.	61
Fig. C-11	Temperature-Energy Absorption Curve for Keyhole Notch Specimens, Steel N.	61
Fig. C-12	Temperature-Energy Absorption Curve for Keyhole Notch Specimens, Steel Q.	61
Fig. C-13	Temperature-Energy Absorption Curve for Keyhole Notch Specimens, Steel G.	61
Fig. D-1	Temperature-Energy Absorption Curves for Rectangular Notch, Full Plate Thickness Specimens for 12 Steels.	62
Fig. D-2	Comparison of Temperature-Energy Absorption Curves of Rectangular Notch, Full Plate Thickness Specimens and Standard Charpy Specimens of Steel A.	63
Fig. D-3	Comparison of Temperature-Energy Absorption Curves of Rectangular Notch, Full Plate Thickness Specimens and Standard Charpy Specimens of Steel Br.	63
Fig. D-4	Comparison of Temperature-Energy Absorption Curves of Rectangular Notch, Full Plate Thickness Specimens and Standard Charpy Specimens of Steel Bn.	63

Fig. D-5	Comparison of Temperature-Energy Absorption Curves of Rectangular Notch, Full Plate Thickness Specimens and Standard Charpy Specimens of Steel C.	63
Fig. D-6	Comparison of Temperature-Energy Absorption Curves of Rectangular Notch, Full Plate Thickness Specimens and Standard Charpy Specimens of Steel D.	64
Fig. D-7	Comparison of Temperature-Energy Absorption Curves of Rectangular Notch, Full Plate Thickness Specimens and Standard Charpy Specimens of Steel Dn.	64
Fig. D-8	Comparison of Temperature-Energy Absorption Curves of Rectangular Notch, Full Plate Thickness Specimens and Standard Charpy Specimens of Steel E.	64
Fig. D-9	Comparison of Temperature-Energy Absorption Curves of Rectangular Notch, Full Plate Thickness Specimens and Standard Charpy Specimens of Steel F.	64
Fig. D-10	Comparison of Temperature-Energy Absorption Curves of Rectangular Notch, Full Plate Thickness Specimens and Standard Charpy Specimens of Steel H.	65
Fig. D-11	Comparison of Temperature-Energy Absorption Curves of Rectangular Notch, Full Plate Thickness Specimens and Standard Charpy Specimens of Steel N.	65
Fig. D-12	Comparison of Temperature-Energy Absorption Curves of Rectangular Notch, Full Plate Thickness Specimens and Standard Charpy Specimens of Steel Q.	65
Fig. D-13	Comparison of Temperature-Energy Absorption Curves of Rectangular Notch, Full Plate Thickness Specimens and Standard Charpy Specimens of Steel G.	66
Fig. D-a	Comparison of Energy Absorption vs. Temperature for the Standard Charpy Keyhole and V-Notch Specimens and the Large Plate Specimens, (Schematic).	66
Fig. D-b	Comparison of Energy Absorption Data for Steels, Obtained in Large Plate and Standard Charpy Tests.	66
Fig. E-A	Location of Impact Specimens in Large Plate Specimens	67
Fig. E-1	Summary of Temperature-Energy Absorption Curves for Keyhole Notch Specimens for Sections of Steel A.	68
Fig. E-2	Summary of Temperature-Energy Absorption Curves for Keyhole Notch Specimens for Sections of Steel B.	68

Fig. E-3	Summary of Temperature-Energy Absorption Curves for Keyhole Notch Specimens for Sections of Steel Bn.	68
Fig. E-4	Summary of Temperature-Energy Absorption Curves for Keyhole Notch Specimens for Sections of Steel C.	68
Fig. E-5	Summary of Temperature-Energy Absorption Curves for Keyhole Notch Specimens for Sections of Steel Dr.	69
Fig. E-6	Summary of Temperature-Energy Absorption Curves for Keyhole Notch Specimens for Sections of Steel Dn.	69
Fig. E-7	Summary of Temperature-Energy Absorption Curves for Keyhole Notch Specimens for Sections of Steel E.	69
Fig. E-8	Temperature-Energy Absorption Curve for Keyhole Notch Specimens, Steel A, Plate A1A.	69
Fig. E-9	Temperature-Energy Absorption Curve for Keyhole Notch Specimens, Steel A, Plate A2A.	70
Fig. E-10	Temperature-Energy Absorption Curve for Keyhole Notch Specimens, Steel Br, Plate B1A.	70
Fig. E-11	Temperature-Energy Absorption Curve for Keyhole Notch Specimens, Steel Br, Plate B3A.	70
Fig. E-12	Temperature-Energy Absorption Curve for Keyhole Notch Specimens, Steel Bn, Plate B2A.	70
Fig. E-13	Temperature-Energy Absorption Curve for Keyhole Notch Specimens, Steel Bn, Plate B4A.	71
Fig. E-14	Temperature-Energy Absorption Curve for Keyhole Notch Specimens, Steel C, Plate C1A.	71
Fig. E-15	Temperature-Energy Absorption Curve for Keyhole Notch Specimens, Steel C, Plate C2A.	71
Fig. E-16	Temperature-Energy Absorption Curve for Keyhole Notch Specimens, Steel C, Plate C4A.	71
Fig. E-17	Temperature-Energy Absorption Curve for Keyhole Notch Specimens, Steel Dr, Plate 17-7.	72
Fig. E-18	Temperature-Energy Absorption Curve for Keyhole Notch Specimens, Steel Dr, Plate 17-A7.	72
Fig. E-19	Temperature-Energy Absorption Curve for Keyhole Notch Specimens, Steel Dr, Plate 5-1.	72
Fig. E-20	Temperature-Energy Absorption Curve for Keyhole Notch Specimens, Steel Dn, Plate 14-7.	72

VIII

Fig. E-21	Temperature-Energy Absorption Curve for Keyhole Notch Specimens, Steel Dn, Plate 5-7.	73
Fig. E-22	Temperature-Energy Absorption Curve for Keyhole Notch Specimens, Steel Dn, Plate 11-1.	73
Fig. E-23	Temperature-Energy Absorption Curve for Keyhole Notch Specimens, Steel Dn, Plate 15-7.	73
Fig. E-24	Temperature-Energy Absorption Curve for Keyhole Notch Specimens, Steel E, Plate 23-7.	73
Fig. E-25	Temperature-Energy Absorption Curve for Keyhole Notch Specimens, Steel E, Plate CG-1.	74
Fig. E-26	Temperature-Energy Absorption Curve for Keyhole Notch Specimens, Steel E, Plate 13-A7.	74
Fig. E-27	Temperature-Energy Absorption Curve for Keyhole Notch Specimens, Steel N, Plate N1A.	75
Fig. E-28	Temperature-Energy Absorption Curve for Keyhole Notch Specimens, Steel C, Plate C3A.	75
Fig. E-29	Temperature-Energy Absorption Curve for Keyhole Notch Specimens, Steel Br, Plate B5A.	75
Fig. E-30	Temperature-Energy Absorption Curve for Keyhole Notch Specimens, Steel A, Plate A3A.	76
Fig. E-31	Temperature-Energy Absorption Curve for Keyhole Notch Specimens, Steel Dn, Plate 2-1K.	76
Fig. E-32	Temperature-Energy Absorption Curve for Keyhole Notch Specimens, Steel Dn, Plate 12A1KN.	77
Fig. E-33	Temperature-Energy Absorption Curve for Keyhole Notch Specimens, Steel Dr, Plate 18A1K.	77
Fig. E-34	Temperature-Energy Absorption Curve for Keyhole Notch Specimens, Steel E, Plate 18A1R.	77
Fig. F-1	Summary, Temperature-Energy Absorption Curves for Keyhole Notch Specimens Prestrained 2%, 5% and 10%, Steel A.	78
Fig. F-2	Summary, Temperature-Energy Absorption Curves for Keyhole Notch Specimens Prestrained 2%, 5% and 10%, Steel Br.	78
Fig. F-3	Summary, Temperature-Energy Absorption Curves for Keyhole Notch Specimens Prestrained 2%, 5% and 10%, Steel Bn.	78

Fig. F-4	Summary, Temperature-Energy Absorption Curves for Keyhole Notch Specimens Prestrained 2%, 5% and 10%, Steel C.	79
Fig. F-5	Summary, Temperature-Energy Absorption Curves for Keyhole Notch Specimens Prestrained 2%, 5% and 10%, Steel Dr.	79
Fig. F-6	Summary, Temperature-Energy Absorption Curves for Keyhole Notch Specimens Prestrained 2%, 5% and 10%, Steel Dn.	79
Fig. F-7	Summary, Temperature-Energy Absorption Curves for Keyhole Notch Specimens Prestrained 2%, 5% and 10%, Steel E.	80
Fig. F-8	Summary, Temperature-Energy Absorption Curves for Keyhole Notch Specimens Prestrained 2%, 5% and 10%, Steel H.	80
Fig. F-8a	Summary, Temperature-Energy Absorption Curves for Keyhole Notch Specimens Prestrained 10%.	80
Fig. F-9	Temperature-Energy Absorption Curves for Keyhole Notch Specimens Prestrain 2%, Steel A.	81
Fig. F-10	Temperature-Energy Absorption Curves for Keyhole Notch Specimens Prestrain 5%, Steel A.	81
Fig. F-11	Temperature-Energy Absorption Curves for Keyhole Notch Specimens Prestrain 10%, Steel A.	81
Fig. F-12	Temperature-Energy Absorption Curves for Keyhole Notch Specimens Prestrain 2%, Steel Br.	82
Fig. F-13	Temperature-Energy Absorption Curves for Keyhole Notch Specimens Prestrain 5%, Steel Br.	82
Fig. F-14	Temperature-Energy Absorption Curves for Keyhole Notch Specimens Prestrain 10%, Steel Br.	82
Fig. F-15	Temperature-Energy Absorption Curves for Keyhole Notch Specimens Prestrain 2%, Steel Bn.	83
Fig. F-16	Temperature-Energy Absorption Curves for Keyhole Notch Specimens Prestrain 5%, Steel Bn.	83
Fig. F-17	Temperature-Energy Absorption Curves for Keyhole Notch Specimens Prestrain 10%, Steel Bn.	83
Fig. F-18	Temperature-Energy Absorption Curves for Keyhole Notch Specimens Prestrain 2%, Steel C.	84
Fig. F-19	Temperature-Energy Absorption Curves for Keyhole Notch Specimens Prestrain 5%, Steel C.	84
Fig. F-20	Temperature-Energy Absorption Curves for Keyhole Notch Specimens Prestrain 10%, Steel C.	84

Fig. F-21	Temperature-Energy Absorption Curves for Keyhole Notch Specimens Prestrain 2%, Steel Dr.	85
Fig. F-22	Temperature-Energy Absorption Curves for Keyhole Notch Specimens Prestrain 5%, Steel Dr.	85
Fig. F-23	Temperature-Energy Absorption Curves for Keyhole Notch Specimens Prestrain 10%, Steel Dr.	85
Fig. F-24	Temperature-Energy Absorption Curves for Keyhole Notch Specimens Prestrain 2%, Steel Dn.	86
Fig. F-25	Temperature-Energy Absorption Curves for Keyhole Notch Specimens Prestrain 5%, Steel Dn.	86
Fig. F-26	Temperature-Energy Absorption Curves for Keyhole Notch Specimens Prestrain 10%, Steel Dn.	86
Fig. F-27	Temperature-Energy Absorption Curves for Keyhole Notch Specimens Prestrain 2%, Steel E.	87
Fig. F-28	Temperature-Energy Absorption Curves for Keyhole Notch Specimens Prestrain 5%, Steel E.	87
Fig. F-29	Temperature-Energy Absorption Curves for Keyhole Notch Specimens Prestrain 10%, Steel E.	87
Fig. F-30	Temperature-Energy Absorption Curves for Keyhole Notch Specimens Prestrain 2%, Steel H.	88
Fig. F-31	Temperature-Energy Absorption Curves for Keyhole Notch Specimens Prestrain 5%, Steel H.	88
Fig. F-32	Temperature-Energy Absorption Curves for Keyhole Notch Specimens Prestrain 10%, Steel H.	88
Fig. G-1	Summary, Temperature-Energy Absorption Curves for Keyhole Notch Specimens Steel N Treated for Different Ferrite Grain Size.	89
Fig. G-2	Temperature-Energy Absorption Curve, Keyhole Notch Specimens Steel N Normalized from 1650°F.	89
Fig. G-3	Temperature-Energy Absorption Curve, Keyhole Notch Specimens Steel N Normalized from 1750°F.	89
Fig. G-4	Temperature-Energy Absorption Curve, Keyhole Notch Specimens Steel N Furnace Cooled from 1850°F.	89
Fig. G-5	Photomicrographs of Steel N after Different Heat Treatments	90
Fig. H-1	Summary, Temperature-Energy Absorption Curves, Keyhole Notch Specimens for Four Plates of Steel C.	91

Fig. H-2	Summary, Temperature-Energy Absorption Curves, V-Notch Specimens for Four Plates of Steel C	91
Fig. H-3	Summary, Temperature-Energy Absorption Curves, Full Plate Thickness Specimens for Four Plates of Steel C.	91
Fig. H-4	Temperature-Energy Absorption Curve Keyhole Notch Specimens Steel C, Plate C3.	92
Fig. H-5	Temperature-Energy Absorption Curve Keyhole Notch Specimens Steel C, Plate C5.	92
Fig. H-6	Temperature-Energy Absorption Curve Keyhole Notch Specimens Steel C, Plate C6.	92
Fig. H-7	Temperature-Energy Absorption Curve V-Notch Specimens Steel C, Plate C3.	93
Fig. H-8	Temperature-Energy Absorption Curve V-Notch Specimens Steel C, Plate C5.	93
Fig. H-9	Temperature-Energy Absorption Curve V-Notch Specimens Steel C, Plate C6.	93
Fig. H-10	Temperature-Energy Absorption Curve, Full Plate Thickness Specimens Steel C, Plate C3.	94
Fig. H-11	Temperature-Energy Absorption Curve, Full Plate Thickness Specimens Steel C, Plate C5.	94
Fig. H-12	Temperature-Energy Absorption Curve, Full Plate Thickness Specimens Steel C, Plate C6.	94
Fig. K-1	Summary, Temperature-Energy Absorption Curve, Keyhole Notch Specimens, Steel C. Plates of Varying Thickness.	95
Fig. K-2	Summary, Temperature-Energy Absorption Curve, V-Notch Specimens, Steel C, Plates of Varying Thickness.	95
Fig. K-3	Temperature-Energy Absorption Curve Keyhole Notch Specimens, Steel C, 1/2" Plate Core.	95
Fig. K-4	Temperature-Energy Absorption Curve Keyhole Notch Specimens, Steel C, 5/8" Plate Core.	96
Fig. K-5	Temperature-Energy Absorption Curve Keyhole Notch Specimens, Steel C, 1" Plate Rim.	96
Fig. K-6	Temperature-Energy Absorption Curve Keyhole Notch Specimens, Steel C, 1" Plate Core.	96
Fig. K-7	Temperature-Energy Absorption Curve Keyhole Notch Specimens, Steel C, 1-1/8" Plate Rim.	97
Fig. K-8	Temperature-Energy Absorption Curve Keyhole Notch Specimens, Steel C, 1-1/8" Plate Core.	97

Fig. K-9	Temperature-Energy Absorption Curves, V-Notch Specimens, Steel C, 1/2" Plate Core.	97
Fig. K-10	Temperature-Energy Absorption Curves, V-Notch Specimens, Steel C, 5/8" Plate Core.	98
Fig. K-11	Temperature-Energy Absorption Curves, V-Notch Specimens, Steel C, 1" Plate Rim.	98
Fig. K-12	Temperature-Energy Absorption Curves, V-Notch Specimens, Steel C, 1" Plate Core	98
Fig. K-13	Temperature-Energy Absorption Curves, V-Notch Specimens, Steel C, 1-1/8" Plate Rim	99
Fig. K-14	Temperature-Energy Absorption Curves, V-Notch Specimens, Steel C, 1-1/8" Plate Core.	99
Fig. L-A	Breaking Energy-Temperature Relationship between Static Bend Test and Impact Bend Test on Fine Grained 0.24% C Steel.	100
Fig. M-1	Photomicrographs, Longitudinal and Transverse Sections, Etched Steel E. (Rim)	101
Fig. M-1a	Photomicrographs, Longitudinal and Transverse Sections, Etched Steel E. (Core)	102
Fig. M-2	Photomicrographs, Longitudinal and Transverse Sections, Etched Steel C.	103
Fig. M-3	Photomicrographs, Longitudinal and Transverse Sections, Etched Steel A.	104
Fig. M-4	Photomicrographs, Longitudinal and Transverse Sections, Etched Steel Br.	105
Fig. M-5	Photomicrographs, Longitudinal and Transverse Sections, Etched Steel Bn.	106
Fig. M-6	Photomicrographs, Longitudinal and Transverse Sections, Etched Steel Dr.	107
Fig. M-7	Photomicrographs, Longitudinal and Transverse Sections, Etched Steel Dn.	108
Fig. M-8	Photomicrographs, Longitudinal and Transverse Sections, Etched Steel Q.	109
Fig. M-9	Photomicrographs, Longitudinal and Transverse Sections, Etched Steel F.	110
Fig. M-10	Photomicrographs, Longitudinal and Transverse Sections, Etched Steel G.	111

Fig. M-11	Photomicrographs, Longitudinal and Transverse Sections, Etched Steel H.	112
Fig. M-12	Photomicrographs, Longitudinal and Transvers Sections, Etched Steel N.	113
Fig. L-13	The Plot of Transition Temperature in Degrees Fahrenheit against Grain Size.	114

CORRELATION OF LABORATORY TESTS WITH
FULL SCALE SHIP PLATE FRACTURE TESTS

INTRODUCTION

Research Projects SR-92,¹ SR-93,² and SR-96³ were established to study the fracture characteristics of steel plate used in merchant vessel construction. The sections tested under Research Projects SR-92 and SR-93 were large scale and so designed as to simulate, insofar as possible in a testing laboratory, service conditions which might be encountered in merchant vessels. It is evident that such large scale tests cannot become widely used, so the need for some small scale test to correlate with the results of the large scale tests is obvious. The objective of Research Project SR-96 is to supply this small scale laboratory test.

The general features of ship plate failure by cracking are such as to suggest the use of the standard impact test as a possible means of evaluating merchant vessel plate. The most serious type of ship plate failure has the appearance of a brittle failure, a type of failure readily obtainable in the notched-beam impact test. An impact test which appears to be uniquely suited to the requirements of this problem is the standard Charpy Impact Test, as by this testing procedure, testing can be conducted rapidly and at various temperatures.

The impact test, while being moderately simple to carry out, is an exceedingly difficult test to analyze on a fundamental basis. Thus, despite the possible successful use of this test to evaluate the steels to be used in a given structure, it probably could not offer a means of understanding the factors which give rise to the differing physical properties

1, 2, 3 - See Bibliography

* These projects were started under OSRD contracts and were then designated as NRC-92, 93 and 96 respectively. These projects are now sponsored by the Bureau of Ships under contract NObs-31222 at the University of California, NObs-31224 at the University of Illinois, and NObs-31217 at the Pennsylvania State College.

in a given group of steels. To further the understanding of these fundamental factors, a second approach to the problem of ship plate fracture has been undertaken.

At normal temperatures tensile test coupons of ship plate possess high ductility. If the temperature of test is lowered sufficiently, this ductility will ultimately disappear. In the process of losing ductility with decreasing temperature, the steel undergoes a change such that the character of the fracture is affected. The fractures go from ductile to brittle, and are frequently referred to as shear and cleavage fractures, respectively. (It is well to point out, however, that there is reason to believe that a cleavage type fracture need not always be a brittle fracture.)

The fracturing process is not well understood. One of the reasons why this is so, is the great disparity in tensile strengths as calculated theoretically and as measured experimentally. In addition to this there is no fully developed theory of plasticity for metals. These conditions exist largely because of the paucity of data on the plastic deformation and fracture of metals. The fracturing of metals has been explained as follows:

- a. Two quantities, known as the fracture strength (σ_f) and the flow strength (σ_s) exist and have the following

properties. The fracture strength designates that unit of stress in tension on a unit section which will cause rupture without plastic deformation but seemingly not by change in temperature. The flow strength is that unit of stress in tension on a unit section which will cause plastic deformation.

- b. In general, for metals, the yield strength lies below the fracture strength, so that with increasing unit stress the

metal is first plastically deformed.

- c. Plastic deformation results in work hardening whereby the flow strength is raised to higher stress levels. This elevation in the flow strength continues until it becomes equal to the fracture strength at which point the metal breaks.

Assuming that a complete knowledge of the effects of temperature and stress conditions on the flow- and fracture-strengths were available, and that the concepts attendant thereto are valid, it should be possible to predict the behavior of a given steel under any specified service conditions. The evaluation of the fracture- and flow-strengths of the project steels have in part been obtained, but due to certain experimental difficulties have not been completed as yet.

Additional quantities which may prove to be of much importance in the analysis of fracture in ship plate are velocity effects, commonly specified as the rate of straining, and strain gradients. Several data are in the literature showing that for a given test condition an increase in the rate of straining frequently enhances the development of a brittle failure. In the second place, it has been shown conclusively that ductile failures are always accompanied by extensive regions plastically deformed, while brittle failures are unaccompanied by such regions of plastically deformed material.

All steels were subjected to a metallographic examination. Certain differences in micro-structures have been detected, but as might be expected, these differences are subtle and are difficult to interpret.

The report contained herein presents the results of the extensive

investigation of the impact properties of the steels which have been available on the related projects SR-92, -93 and -96. The results of a preliminary metallographic examination of the steels are included.

Data on the fracture- and flow-strengths of the steels; the results of the measurements on strain gradients; and the effects of velocity of testing on these factors will be contained in a progress report to be released in the future.

The following persons have constituted the staff and have contributed to the various phases of the investigation:

M. Gensamer	Technical Representative
E. P. Klier	Supervisor
T. A. Prater	Investigator
F. C. Wagner	"
J. L. Fisher	"
J. O. Mack	"
Marguerite Grymko	Research Assistant
Katherine Fisher	" "
Lary Ann Bishop	" "
Selma Krause	Drafting
Philip Vonada	Tech. Labor
Herman Colyer	" "
Torsten Bjalme	" "

STEELS

The steels investigated on this project are listed in Table 1. The chemical and spectrographic analyses of these steels were carried out in the laboratories of the Bethlehem Steel Company at the suggestion of Dr. C. H. Herty, Jr. The results of these analyses are presented in Table 2.

Oxygen and nitrogen determinations made at the Battelle Memorial Institute are presented in Table 3.

PART I

IMPACT TESTING

Resume of Testing Program: Impact specimens were oriented with respect to the plate, so that the long dimension was parallel to the rolling direction, while the notch was parallel to the thickness direction. These specimens have been designated LH specimens.

1. The methods of representing impact data, especially that for the standard Charpy keyhole-notch specimen, have been much controverted. To eliminate this controversy, insofar as possible, as it pertains to the steels investigated here, two sets of Charpy keyhole-notch specimens, 60 in each set, were tested in the transition range for two steels of considerably different energy absorption characteristics.
2. The program of impact testing was initiated with the determination of the energy absorption characteristics of the various steels, using test bars of standard dimensions; namely, .394 x .394 x 2.165 inches notched with the standard keyhole-and V-notches.
3. The results obtained with the standard Charpy specimens did not correlate well, quantitatively, with the results obtained with the large plate specimens. A third specimen was employed in an effort to obtain better agreement in the two cases. This specimen is an LH Charpy bar, of width equal to full plate thickness, by .394 x 2.165 inches. The notch was a 1/32-inch rectangular notch .197 inch deep.
4. Sections of the 72-inch wide plates, approximately 1 x 3 feet, and bounded on one edge by one-half the notch and fracture,

were received for testing. Standard LH Charpy keyhole-notch specimens were taken from these plates as indicated in Fig. E-3.

5. Test results (section 4) indicated that straining had a considerable effect on the transition from ductile to brittle failure, as revealed by the impact test used. It was deemed possible that some relationship between degree of strain and energy absorption could be used to correlate with the energy absorption characteristics of the large plate specimens. To examine this point, series of standard Charpy keyhole-notch bars were prepared from stock which had been strained in tension along the rolling direction to 2, 5 and 10% in elongation.

6. The metallographic examination of Steel N revealed that this steel had a grain size appreciably finer than that in the other project steels. Since grain size is known to effect the energy absorption characteristics of a given steel, it was deemed advisable to check sets of specimens that had been heat treated to develop different grain sizes, and which were then tested using standard Charpy keyhole-notch specimens.

7. Steel C has proven to be an especially interesting steel for the purposes of the related SR-92, -93 and -96. To be assured that the results hitherto obtained for impact testing of this steel were typical, test sections from three other plates were obtained and tested using the three types of test specimens.

8. Questions have arisen as to the differences inherent in plate of different thicknesses due to the rolling process. To clarify these questions, tests on steel C in plate thicknesses

7

of 1/2, 5/8, 1 and 1-1/8 inches have been conducted. The test specimen has been the standard LH Charpy keyhole- and V-notch specimen.

Testing Procedure: Impact testing was carried out to establish the relationship between energy absorption and temperature. With but one notable exception the testing consisted in placing a minimum of three specimens in an appropriate medium at the desired temperature, and holding for about 10 minutes to allow thermal equilibrium. The specimen was then rapidly transferred to the testing machine and broken. This transfer took place in a very short time so that no temperature change occurred in the specimen.

The exception to the procedure outlined above, consisted in cooling only one specimen to the desired temperature and testing. The same number of specimens were tested by shortening the interval between testing temperatures. This procedure was abandoned because of the difficulty in constructing average curves through the points obtained. No real average could be used, the average being drawn by means of the eye alone.

The Graphical Representation of Impact Test Data: There is need for clarification of the method of representing the impact test data, especially that obtained for the standard Charpy keyhole-notch specimen. The argument is offered that the data obtained for this test specimen are in general best represented by two curves, one at high energy absorption level and one at low energy absorption level. The two curves are understood to overlap for some temperature interval giving rise to a transition region as represented in Fig. A, -(A). The representation of the data in this manner is predicated on the contention that the large majority of tests yield either high or low numerical values for the energy absorbed. If this

predication were in truth correct, it would void the normal practice of representing such energy absorption data by means of one continuous curve as in Fig. A, -(B).

Now it is very convenient to be able to represent the impact properties of a given steel by means of a continuous curve, and while it is certainly correct that certain data can best be represented by curves similar to Fig. A-(A), it is desirable to know if the data, in general, require such representation for the steels investigated here. To answer this question, one set each of steels -Dr and -E (bars were taken from center of plate) consisting of 60 specimens each, were prepared. These specimens were standard keyhole-notch specimens, and were machined with no more nor less care than the other impact specimens received.

The 60 specimens of each steel were tested in what is considered to be the transition range for the respective steels. Testing conditions conformed to those in general obtaining when impact specimens are tested.

The test results are presented in Figs. A - 1 and A - 2. The solid lines have been drawn through the average points while the dotted lines are curves previously obtained for these two steels.

The data presented in Figs. A - 1 and A - 2, it is believed, are best represented by the continuous curve which is drawn through the mean values. It is believed that for these data a completely erroneous impression would be created, if representation were attempted using a discontinuous curve of two branches, one at high energy absorption, the other at low energy absorption.

An examination of Figs. A - 1 and A - 2 gives some notion as to the reproducibility of results. In both instances the curves have been displaced at extreme ends of the transition region while the temperature at

which 50% of maximum energy is absorbed is but slightly displaced. This leads to the impression that this temperature in general, is more easily determined accurately, than are other values of temperature at arbitrary energy absorption levels.

From the above, it will be gathered that nearly all energy absorption curves have been drawn as continuous curves. With but few exceptions this is true. In these excepted cases, the detail plots, only, have been drawn as discontinuous, while in summary curves, continuous curves, only, have been drawn. It is not possible to discuss the problem at length here, but it will be noted that those data represented by discontinuous curves have been obtained for specimens prestrained in some way. It is believed that this prestrain especially at low strain values lends materially to scatter of the test data.

The Tabulation of Impact Test Data: The desirability of using numerical values for indicating the results of a given impact test study is obvious. The numerical values which can be taken from impact curves and retain their significance, on the other hand, are not at all obvious.

Several factors must be considered in deciding this point. First, if a certain point is known to have physical significance it should be considered, if it can be represented numerically. Secondly, if the condition set down in the first instance does not recognizably exist; while a point, known from experience to be important does, this second point should be stated. Finally for an arbitrary representation, as it is believed holds here, that point which is subject to the least error in determination should be stated. From the foregoing section this would appear to be that temperature at which one-half maximum energy absorption is obtained. The transition temperature in this report is defined in this way.

In an earlier report (SR-94)⁴ a value of 15 ft. lbs. energy absorption was considered to be an important numerical value in classifying Charpy impact test data for standard specimens employing the V-notch. Further, energy absorption values in this range are commonly used in specifications. Now this range of energy absorption values roughly corresponds to one-fourth of maximum energy absorption. Therefore, the temperature at which these latter values are found also are reported for the steels.

Results of Impact Testing

A. V-notch specimens: The results of impact testing for the standard LH Charpy V-notch specimens are presented graphically in Fig. B-1. Detail plots of the data are found in Fig. B-2 to B-13. Numerical data taken from these curves are tabulated in Table B, along with the transition temperatures for the 72-inch wide plate tests. At first sight it appears that this test, with one exception, allows qualitative evaluation of the steels. Quantitatively, however, no such agreement exists; the low temperature coordinate being highly contracted, the high temperature coordinate being expanded.

Closer examination of the data reveals relationships which make doubtful the acceptance even, of the qualitative evaluation of these steels by this test. The transition temperatures for steels A, B and D for the 72-inch wide plates are all grouped in a 10°F temperature interval, (Table B). Considering the accuracy of the test results these steels should be considered as being identical in this respect. For the small scale tests, however, the transition temperatures range from 10° to 90°F with steel A being represented as inferior to both steels B and D.

Steels A and C were melted to have the same nominal chemistry; it

4 See Bibliography

being anticipated that they would then have the same physical properties. The impact results reported here indicate that this duplication has in all respects been successful. The steels seemingly have the same temperature - energy absorption properties. These results predict completely erroneous results to be obtained in the large plate tests. Steel A has a transition temperature in the large plate tests roughly 55°F less than that for steel C.

The analyses of these two steels reveal that steel C contains appreciably higher percentages of nitrogen than does steel A, and the impression has been formed that this difference in nitrogen content can account for the differences in the physical properties of the two steels. Whatever be the reason ultimately accepted to account for these differences in performance in the large plate tests, it is emphasized that these differences have not been suggested by the data obtained with the Charpy V-notch impact bar.

A final comparison of the data, for steels C and E, is made. By the large plate tests these two steels are revealed as having the same physical properties, in so far as their susceptibility to brittle failure is concerned. But for the impact test these two steels are revealed as being different from one another.

It is evident that the initial impression that this impact testing procedure evaluated the steels in the proper order qualitatively, is an unfortunate one, and cannot properly be retained. The question arises as to whether this is really a serious disagreement. It might be suggested that while certain minor disagreements are noted, differences in the order of magnitude are not. It is believed that any such suggestion should be discouraged. Actually the physical properties of the steel A and C appear to be very nearly extreme values normally obtained for merchant vessel plate

by the large plate test. Thus to materially improve the physical properties of steel A would require the usage of (at least) a fully killed steel. A slight decrease in carbon content with an increase in manganese content does not appreciably improve the physical properties as revealed by the large plate tests for the semi-killed grades of steel. At the same time the susceptibility to brittle failure in the large plate tests of steel C is fully as pronounced as that for steel E which is a rimming steel.

It would appear then that the impact test as conducted here is not capable of giving a clear impression as to the physical properties of a steel which may be anticipated when that steel is used in a large structure. This does not seemingly result from lack of sensitivity on the part of the impact test. There appears to be a basic difference in the two types of testing, in which instance a complete agreement for all tests could not be expected.

B. Keyhole-notch specimens: The results of impact testing for the standard LH Charpy keyhole-notch specimens are presented in Fig. C-1. Detail plots of the data are found in Figs. C-2 to C-13. Numerical data taken from these curves are found in Table C, with the data for the large plate tests.

By this test a better qualitative evaluation of the steels is obtained than for the V-notch specimen. Again there is a very serious distortion of the scale of transition temperatures. In addition there are qualitative disagreements between certain of the data obtained here and those obtained for the large plate tests. Again there has been no separation of the transition temperature for steels A and C.

The transition temperature for steel A is about 20-30°F higher than that for steel B, while for the large plate tests these steels are

nearly identical. (The transition temperature for steel E is indicated as being about 15°F higher than that for steel C, which is not in agreement with the large plate tests.)

The comparisons which have been made above are incomplete due to lack of data for the large plate tests. For the steels which have been tested, however, it may be concluded that the keyhole-notch Charpy impact test like the V-notch Charpy impact test is not capable of an unambiguous evaluation of the plate which might find usage in merchant vessel construction. Again two serious objections to the use of the impact test can be offered, namely, (1) excessive distortion of the scale of transition temperatures, necessitating the use of a complicated correction factor to predict accurately the transition temperature in the large plate tests, (2) for some of the steels an improper qualitative evaluation of the steels is obtained from the impact data.

C. In view of the objections to the conclusions arrived at in the discussion of the impact data for the standard Charpy bars, a third Charpy bar was employed. This bar was of standard length and thickness, but of width equal to full plate thickness and notched with a 1/32-inch wide .197" deep rectangular notch.

The results of impact testing using this test bar are presented graphically in Fig. D-1. Detail plots of the data are found in Figs. D-2 to D-13. Numerical data taken from these curves are tabulated in Table D with the data for the large plate tests.

Certain differences in the relative evaluation of the steels as compared to the evaluation by the standard Charpy bars are noted. These data, however, are subject to the same criticism which has been leveled at the test results for the standard Charpy bar. There is little other

than the decreased cost of specimen preparation then to recommend continued use of this test bar.

Discussion of Impact Data - Sections A, B and C: It is implicit in the foregoing discussion that the most important factor which prevents an intuitive approach at correlating the Charpy impact data with the large plate test data is the lack of a sharply defined transition temperature for the Charpy impact test. Because of this it is not possible to compare energy absorption curves of the same form (in the two tests) which leads to a sense of uncertainty in the validity of this comparison. For the present, this transition temperature shall be arbitrarily fixed to allow discussion, but it should be kept in mind that there is no justification on physical grounds for this selection. All transition temperatures in this section are taken as that temperature at which one-half the maximum energy absorption is observed. At higher temperatures the failure will be considered as essentially ductile while at lower temperatures the failure will be considered as essentially brittle.

The transition from ductile to brittle failure in a test section is visualized as depending on the steel and on the geometry of the test section and on testing conditions. The idealized results for a steel tested in the large plate sections and in the Charpy keyhole and V-notch impact tests are presented in Fig. D-a. The transition range for this steel is seen to lie at three different temperatures which are characteristic of the test sections employed.

In the discussion below ΔT_1 will designate the difference in transition temperatures for the large plate tests and for the Charpy keyhole-notch specimens. A second subscript designates the steel, as for example,

$\Delta T_{1,Br}$ is the difference in transition temperatures for steel Br between the large plate tests and the Charpy keyhole-notch tests. ΔT_2 in strict analogy will pertain to the Charpy V-notch test data.

For the purpose of a control test it must be assumed that the displacements ΔT_1 and ΔT_2 are functions of the geometry of the specimen only, if this test is to be properly employed. If this condition were correctly assumed, a change in the transition temperature for the large plate test would appear as a change of the same sign and of comparable order of magnitude for the transition temperatures of the keyhole and V-notch Charpy bars. The evaluation of the steel would then consist in the determination of the transition temperature for a standard test bar, in this case a standard Charpy bar, the addition thereto of ΔT_1 if the keyhole-notch specimen were used; or the subtraction therefrom of ΔT_2 if the V-notch specimen were used. This would give the transition temperature to be expected in the large plate test.

The question arises as to whether or not this treatment is adequate or not for practical use, as in the comparison tests carried out here. To better understand the significance of the data, idealized plots of the data for steels Dr, Br, A, C and E for the large plate test and for the Charpy keyhole and V-notch tests are presented in Fig. D-b. These idealized curves have been drawn parallel to one another with the value of temperature at 50% maximum energy absorption being taken from the data. If this simplification is not made, the relationships which exist are even more complicated than those indicated in Fig. D-b.

It is evident from Fig. D-b that the correction factor ΔT_1 is not constant for the various steels, nor is ΔT_2 . More serious than this,

however, is the fact that neither ΔT_1 nor ΔT_2 varies uniformly from one end of the series of steel to the other end. If this were true, ΔT_1 or ΔT_2 could be progressively changed from one steel to the next and the proper answer for the large plate test could be obtained. Since ΔT_1 and ΔT_2 change discontinuously, correction factors cannot be used properly and the means of correlating the control test are seriously weakened.

The numerical comparisons of ΔT_2 reveal that this value is a minimum for Steels B and C, but for Steel B, ΔT_2 must be added while for the remaining steels it must be subtracted. To a first approximation $\Delta T_{2,E} = 2 \Delta T_{2,C}$ while $\Delta T_{2,A} = 3 \Delta T_{2,C}$. The sign of ΔT_1 is plus in all instances but its magnitude varies erratically. Thus $\Delta T_{1,A}$ is the minimum value observed, but to a first approximation $\Delta T_{1,B} = T_{1,C} = 2 \Delta T_{1,A}$ while $\Delta T_{1,D} = 3 \Delta T_{1,A}$.

It is necessary to conclude that while the impact tests conducted as in sections A, B and C may afford some notion as to the behavior of the steel when it is used in a structure, this prediction very well may be incorrect. The test must at best be considered only partially reliable therefore.

D. Impact Specimens from large plate tests: Sections of the 72-inch wide test plates were received and were tested using standard LH Charpy keyhole-notch specimens taken from the plate as indicated in Fig. E-a. These tests were to be run to check the impact properties of the individual plates, but it soon became evident that the strain to which the section tested had been subjected, seriously affected the results.

Despite this effect the location of the impact specimens was not changed to the area under the notch, as it was deemed as more important to

preserve the strain-free material. This strain-free plate will ultimately be tested as a final check on the test method which is now under development. This point will be considered more fully in a later section.

The test results are summarized in Figs. E-1 to E-10. Detail plots of all curves are presented in Figs. E-11 to E-34. Numerical data are presented in Table E with data for the large plate tests. These results are extremely interesting.

Specimens taken from those plates tested at temperatures low as compared to the transition temperature by the large plate test, have a transition temperature to be expected from the results presented in Section C. This temperature is materially altered, however, for specimens taken from plates tested in the transition range and above. This change in transition temperature is positive in all instances, but the absolute value for each steel is different. The final consequences of these varied changes in transition temperatures are that specimens taken from plates tested at the highest temperatures give a transition temperature nearly equal to that observed in the large plate tests. Thus the straining and possible room temperature aging to which these steels have been subjected, has served to alter the energy absorption characteristics of the steels, but in a unique way.

These results indicated that the energy absorption characteristics of the steels determined as a function of the strain to which they had been subjected were important data to obtain. The results of such a study are the subject matter of the next section.

E. To determine quantitatively the effect of strain on the impact properties of the project steels, series of specimens strained in tension

in the rolling direction to 2%, 5% and 10% in elongation were prepared. The specimen selected was a standard LH Charpy keyhole-notch specimen. Steels A, B, C, D, E and H were investigated.

The results are summarized graphically in Figs. F-1 to F-8. Detail plots of these curves are presented in Figs. F-9 to F-32. Numerical data are presented in Table F.

As was anticipated from the results of the preceding section, the prestraining has altered the transition temperatures of the various steels. Prestrain values between 5% and 10% appear to give the most interesting changes. In Fig. F-8a are summarized the impact data for the steels studied for prestrains of 10%. The impact data now correlate very well with the energy absorption characteristics of the large plate tests if the transition temperature is taken at 50% maximum energy absorption, (See Table F-c). There are certain quantitative disparities but qualitatively the steels are properly evaluated. It is interesting to compare the effects of prestrain on the individual steels. These comparisons at 50% maximum energy absorption are contained in Table F. Rather unexpectedly it is seen that prestraining is much more potent in changing the transition temperature for the steels D, which are fully killed steels, than it is for any of the other steels, but steel C. It is also indicated that the normalized steels are not so drastically affected as are the as-rolled steels. This may possibly be due to cold work resulting either from low finishing temperature or straightening operations.

In the course of preparation specimens were held at room temperature for one month after straining. This gives rise to the possibility of room

temperature aging as causing the increase in the transition temperature. Now it has been shown that room temperature holding will cause appreciable aging in these steels. This is an important item and a program has been outlined to allow the investigation of the effect of straining followed by room temperature aging of various times on the impact properties of these steels.

F. In the course of the metallographic examination, it was observed that the ferrite grain size of steel N was very appreciably smaller than that for the other project steels. Since grain size is known to affect the impact properties of a steel to a very marked extent, it was deemed desirable to evaluate this factor for steel N.

To prosecute this investigation three sections from the large plate test section N-1-A⁷ were given the following heat treatments, respectively. N-1-A (1) was normalized from 1650°F; N-1-A (2) was normalized from 1750°F; N-1-A (3) was furnace cooled from 1850°F. This final treatment gave rise to a ferrite grain size comparable to that existing in the other project steels. Test results are summarized in Fig. G-1 to G-4. Photomicrographs of the sections are presented in Fig. G-5.

The two normalizing treatments have evoked no change in the impact properties of the steel, neither has there been a change in grain size. The furnace-cooled steel, on the other hand, while suffering a considerable growth in grain size has also suffered a very marked deterioration in impact properties. The change in grain size from < ASTM #10 (extrapolated to #10 to #12) to ASTM #6 has displaced the transition temperature measured at 50% of maximum energy absorption by +140°F. This is a rather startling increase in the transition temperature.

⁷ See Bibliography

G. Due to the great dissimilarity of steels A and C in the 72-inch wide plate tests and due to the failure of the impact test to establish this difference, it was felt desirable that further plates of steel C should be examined to make certain that the results initially obtained were representative of all the plates in this heat. For this purpose small sections from three additional 6' x 10' x 3/4" plates were obtained and tested using each of the three test bars. The results are presented in Figs. H-1 to H-12. The test results initially obtained are denoted by the dotted lines. It is evident that while some variations are observed, these variations are not important ones. The steel C is still evaluated as at first indicated.

H. Plate of various thicknesses is required in the construction of various structures making up a merchant vessel. For the construction of hatch corner sections, plates of steel C were furnished in the following thicknesses: 1/2", 5/8", 3/4", 1" and 1-1/8". It was felt that sections of these different thickness plates should be tested to determine the possible variation in impact properties due to differences in fabrication processes by which these different thicknesses are achieved. In the thicker plates there also exists a possible variation in properties from the rim to the core of the plate. The testing program consisted in the determination of the energy absorption - temperature relationships existing in the center section of plates 1/2", 5/8", 1" and 1-1/8" thick using standard LH Charpy specimens with the standard keyhole- and V-notches. In addition the energy absorption - temperature relationships for the rims of the 1" and 1-1/8" plates were determined using the two Charpy test bars.

The data obtained are summarized graphically in Figs. K-1 and K-2. Detail graphs are presented in Fig. K-3 to K-14. Numerical data are presented in Table K.

The transition temperature is very greatly altered by changing plate thickness from 1-1/8" to 1/2". The rate of change of the transition temperature with change in plate thickness from 1-1/8" to smaller thicknesses is slow at first, there being but a moderate decrease in the transition temperature as the thickness is decreased to 3/4", when the impact specimen is the standard Charpy V-notch specimen. When the thickness is decreased to 1/2", however, there is a large decrease in the transition temperature.

For the standard Charpy keyhole-notch specimen the reduction of plate thickness from 1-1/8" to 3/4" lowers the transition temperature by about 40°F. The reduction in the transition temperature resulting from the change of thickness from 1-1/8" to 1/2" is nearly 80°F.

In the 1" and 1-1/8" plates the rim is found to have slightly better properties than the core. This condition is not especially pronounced, however.

DISCUSSION AND CONCLUSIONS

In the foregoing pages data have been presented to show that the standard impact test as normally conducted does not yield a reliable prediction of the fracture characteristics (brittle or ductile fracture) of the steel when it is to be used in a full scale structure. A test has been developed which, with no serious exception, properly predicts the transition temperature of the steels for which data are available. This test consists in straining the steel in tension to 10% in elongation followed by holding at room temperature for about one month after which time it is tested by the standard Charpy keyhole-notch impact test.

The effect of grain size on the energy absorption - temperature characteristics of steel N have been studied to a limited degree. It has

been shown that one of the reasons for the excellent low temperature impact properties of this steel lies in its highly refined ferrite grain structure. The treatment of this steel to develop a grain size comparable with that found in the remaining project steels raises the transition temperature by approximately 140°F.

The testing of additional 3/4" plates of steel C has shown that the initial relationships established between energy absorption and temperature are correct.

It has been shown that a change in plate thickness may seriously modify the transition temperature in a given steel, as determined by the notched impact tests.

This briefly reiterates those points of importance which have been emphasized in the presentation of the experimental data. It would appear that the foregoing experimental work to a satisfactory degree explores the possibility of the use of a standard impact testing procedure to predict the behavior of a given steel when it is to be used in a large structure. This investigation has revealed the possibilities of using a specimen prestrained to a given degree to give the numerical data required. However, it has not led to a rationalization of the reasons why this prestrained specimen will give the correct answer when used as specified. Until such rationalization is achieved or until further tests for comparison of the two types of test data (strained Charpy bars vs. large plate results) are available, this test should be used only with some reservation. In the meantime further steps to rationalize the impact test are being pursued. These additional steps are the out-growth of the following line of reasoning.

The breaking of an impact specimen can be considered as taking

place by a similar process to that that leads to the fracture of a large plate specimen. The differences in results (transition temperature for the large plate section and the small test sections), then must result from quantitative differences in the factors active in the fracturing process, - thus take on the guise of the so-called "size-effect". In this manner of thinking the "size-effect" would appear to be composited of several factors interrelated in some mathematically complicated way. One of these factors, which comes to mind immediately, is the geometry of the test section. The change in geometry if it does not lead to extremely small specimens and too severe notching should not introduce variables seriously dependent on the grain size of the steel, but should lead to changes in stress conditions only. These changes in stress conditions could, however, be anticipated usually within reasonable limits, and test conditions could be adjusted to reduce differences, insofar as desired. Thus there does not appear to be any reason why the "size-effect" cannot be eliminated as a variable thus making possible the use of a small scale test to predict the properties of the full size plate.

After these considerations a more close comparison of the test conditions obtaining in the impact test and in the large plate tension test is evidently needed. A first difference arises in the consideration of the type of test. The impact test is a notch-bend test while the plate test is a notch-tensile test. The stress conditions in the two test sections are very much different if the overall stress systems are compared. But if the stress conditions at the bases of the stress raisers are considered it is found that these are roughly comparable at the start of cracking. (cf ⁵ H. Neuber: "Theory of Notch Stresses". Translated by F. A. Raven, Navy Department, David Taylor Model Basin, Washington, D. C., 1945.) Due to the

5 See Bibliography

drastic changes in testing conditions arising in the impact test bar, as it is bent and as the crack progresses, the stress conditions in the test bar depart very seriously from those obtained in the notched tension test.

[Thus in the notched tension test the entire section is loaded in tension.

This means that in the instance of a crack being propagated at sufficiently high velocity the section has no chance to unload, even if the physical

surroundings were modified enough by the initial cracking to allow this to take place. The entire section then fails. In the bend test this situation

does not obtain. In the notched bend impact specimens at the start of cracking,

more than one-half of the cross section is a zone of compression into which

the crack is being propagated. It is evident that as the crack is propagated

unless the stress concentration should increase (which does not happen cf.

H. Neuber, supra) the maximum stress at the base of the effective notch de-

creases. (This results from the fact that the crack moves at a rate much

higher than the rate at which the hammer in the impact machine moves.) In

order to maintain the stress at the base of the notch to a level producing

failure it is necessary that the specimen be bent more. In the upper temper-

ature range it is actually physically impossible to maintain this stress so that

the two halves of the test bar do not part completely but are bent back

along the top and carried through with the hammer.] These changes are such

that they expand the range of temperature in which the fracture changes from

an entirely ductile to an entirely brittle failure. It would appear from

this that the intermediate values of energy absorption do not exhibit a

fundamental aspect of the metal, but merely reflect a change in geometry

in the test specimen.

If this change in geometry could in effect be eliminated it would

appear that the transition range would be shortened and would become

extremely abrupt in most cases. This argument, while interesting, cannot be developed until considerable data have been accumulated. But despite this limitation it allows the fixing of certain points on the various energy absorption curves as being roughly comparable and thus points the way to the development of a laboratory test procedure which can effectively predict the cracking characteristics of a given steel if the service conditions are known. It is evident that the test specimen should be notched so that the stress conditions simulate those anticipated in service.

Assuming that the stress conditions in the test bar at the start of test simulate those found in the large plate, it is necessary to consider those points on the energy absorption curve which are equivalent for the two different modes of testing. Now to a first approximation, the transition temperature range for the large plate tests can be considered as being negligibly narrow, i.e., intermediate values of energy absorption can be obtained only with appreciable difficulty, and only within a temperature interval of 10-15^oF. On the other hand, the transition temperature range for the impact test is very large. In the discussion above it has been indicated that this spread in transition temperature range is due essentially to changes in geometry of the test bar. If this were correct, the point on the energy absorption curve which could possibly best reveal the changes taking place in the metal to give a brittle failure is that lowest temperature at which maximum energy absorption is obtained. This point should correlate directly with the corresponding point obtained in the large plate tests. Data for the project steels taken in this way are presented in Table L. These data do not agree with the large plate results. Therefore, either the reasoning employed above is wrong or an additional variable, which has not been

anticipated, is operative.

A factor which has not been considered above as determining, in any way, the transition-temperature of the various steels is the rate at which the test is conducted for the rates of straining. The large plate tests are static tests which are conducted at rates of straining even less than those that might be encountered under service conditions in vessels. On the other hand, the impact test is conducted at rates of straining an order of magnitude greater. Possibly the differences in the rates of straining can account for the non-agreement of the two tests.

The data presented in Fig. L-a serve to enhance this notion. These data are taken from Davidenkov and Wittmann.⁶

The change from a dynamic bend test to a static bend test using in both instances the same test bar has altered the temperature at point A, Fig. L-a, by more than 60°F for a steel which is roughly comparable to the ship plate being investigated under these related projects. This reduction in the lowest temperature at which maximum energy absorption is obtained is of the right order of magnitude to bring this point into direct correspondence in the small scale test and in the large plate test. This change in the energy absorption curve as a function of the rate of straining is now being investigated for the project steels.

⁶ See Bibliography

PART II

METALLOGRAPHIC STUDY

One of the specified objectives of Research Project SR-96 was the metallographic examination of the project steels. While it was doubtful that such an examination could furnish the key to a laboratory test whereby the steels could be evaluated, it was felt that it should be conducted nonetheless.

Specimens were selected from the impact test bars and were subjected to a routine examination. All specimens were sectioned parallel and perpendicular to the rolling direction. After polishing, the surface was examined in order to reveal any peculiarities associated with the structure of inclusions. Following this examination the specimen was etched with picral and nital for photographing at 600 diameters. Subsequently it was re-etched with nital and photographed at 50- and 100- diameters.

Due to the highly subjective character of the analysis of metallographic data, little would be gained by an attempted description of the structures obtained. In preference to such a description, the photomicrographs are presented while salient features of the various structures are pointed out.

An effort has been made to correlate a so-called ferrite grain size with transition temperature for these steels. There is scarcely any satisfactory procedure whereby this comparison can be made for, first of all, there is pearlite, which plays a most important role in determining tensile properties, present in the structure; and secondly, the amount of pearlite in the structures of the

various steels is not constant. To a first approximation the action of pearlite in altering the tensile properties of the various steels has been eliminated as a variable by stating the number of ferrite grains per square inch of ferrite. This is effective in giving a correct statement of the ferrite grain size. The number of ferrite grains per square inch has been plotted against the transition temperature taken at 50% maximum energy absorption. This manner of plotting is not equivalent to the plotting of an A.S.T.M. grain size number against the transition temperature and has been used as it is slightly more sensitive to grain size change than would be a plot of A.S.T.M. grain size.

Experimental Results: The photomicrographs of the steels are presented in Figs. M-1 to M-12. The steels are presented in the order of decreasing transition temperature. The plot of transition temperature from brittle to ductile failure versus grain size is contained in Fig. M-13.

The photomicrographs of steel E presented in Fig. M-1 and M-1a reveal the structures found in the core and rim of this rimming steel. The decarburized rim is plainly evident in the longitudinal section at 50- and 100- diameters. Little of this rim was left on the specimens after the machining operation as is evident from an examination of the transverse sections. The typical structure of this steel is best revealed in the photomicrographs of Fig. M-1a.

This structure is characterized by a lack of banding, a larger proportion of pearlite than might be expected, and an extremely coarse structure over all. A faintly developed Widmanstätten structure is discernible and leads to the impression that the finishing temperature for this steel may have been too high. The ratio of pearlite to ferrite for

of the project steels is greatest for this steel, while the ferrite grain size of this is greatest for this steel. In Fig. M-2 are presented the photomicrographs of steel C. The behavior of this steel in the large plate tests places it with steel E as having the maximum transition temperature of the project steels. This behavior finds a parallel in the respective microstructures. Steel C is very similar, microstructurally, to steel E. As for steel E, there is little tendency toward banding; the ratio of pearlite to ferrite is relatively high, and the ferrite grain size is relatively large. Again there is a faint tendency for the steel to form a Widmanstätten structure which again may be interpreted as resulting from too high a finishing temperature in rolling.

For steel A, Fig. M-3, there is a tendency toward banding, although this is not pronounced. At first sight the ratio of pearlite to ferrite appears to be less than was true for steels E and C; however, measurements do not bear this observation out. The relative amounts of pearlite for the three steels are about the same (see Table M). The ferrite grain size is not appreciably smaller than that for steels E and C. It would appear that the essential difference between the microstructure for steel A and that for steels E and C lies in the absence of the Widmanstätten structure in steel A.

In Figs. M-4 and -5 are presented the microstructures for steels Br and Bn. These structures differ little from one another so may be discussed together. The structures are banded and definitely finer than any discussed above. The percentage pearlite in the structure is decreased as would be expected from the reduction in carbon content. However, despite this reduction in percentage of pearlite the rolling process has been such that the pearlite

zones are nearly continuous. Thus the structure approximates a condition of alternate ferrite and pearlite regions. This condition obtains throughout the plane of the plate as is evident from a consideration of the transverse sections. The ferrite grain size is somewhat smaller than that found in the previously discussed steels.

The microstructures of steels Dr and Dn, Figs. M-6 and M-7 may also be considered together. Again the steel is banded, however, in this case in the longitudinal direction only. Banding in the transverse direction does exist but is not so pronounced as in the longitudinal direction. Thus the pearlite zones are more nearly lath shaped than planar as was true for steels Br and Bn. Further the pearlite zones are distributed more uniformly throughout the structure than was true for steels Br and Bn. The ratio of pearlite to ferrite has increased due to the increase in the percentage of carbon in the steel. The ferrite grain size for the as-rolled steel is about the same as that for steel Bn; that for steel Dn is somewhat reduced.

In Fig. M-8 are presented photomicrographs of steel Q. This steel is structurally entirely different from the remaining project steels. For this reason it would be unwise to attempt a discussion of this structure in terms analogous to those used for the other steels. It is probably sufficient to state that this structure is tempered bainite. This bainite is high temperature bainite, a structure which was not desired, and a structure which normally does not have especially desirable properties. A structure of this type has been referred to in some instances as a "Slack-quenched" structure.

Steels F, -G and -H are all high manganese low carbon steels which have been fully killed. The respective microstructures of these steels are presented in Figs. -9, M-10 and M-11. The structures of steels F and H are identical and differ from that of steel G. This situation might have been

anticipated from a consideration of the impact properties for these steels. Steel G has the least desirable structure of the three steels as it is characterized by regions of high pearlite concentration.

There is little tendency toward banding in steels F and H. This effect is most noticeable in steel G. The total amount of pearlite is the same in each of the three structures.

The ferrite grain size is larger than that found in all steels but steels C and E.

In Fig.12 are presented the photomicrographs of steel N. As previously indicated the outstanding characteristic of this structure is the highly refined ferrite grain size. There is a tendency toward banding while the pearlite structure is poorly formed.

of the steel. The results of the study are discussed in the following sections.

DISCUSSION AND CONCLUSION

The examination of the inclusions revealed them to be the expected sulphides and oxides. Since the distribution of these non-metallics cannot be ascertained from a photomicrograph, no photomicrographs of inclusions are presented. However an attempt has been made to contain in the field at 600 diameters a large inclusion. It is pointed out that this may not be a typical inclusion in all instances.

The study of microstructures has allowed no satisfactory correlation of this factor with the energy absorption characteristics of the steels. Thus the alteration of ferrite grain size in a given steel produces a considerable change in transition temperature for that steel, as measured by the standard impact test. But the effect of a change in ferrite grain size from steel to steel may be completely concealed in so far as the energy absorption characteristics are concerned. The data, here as elsewhere, indicate indirectly that one of the most important factors in the determination of the energy absorption characteristics of the steel is the deoxidation practice employed in the melting process.

BIBLIOGRAPHY

1. Research Project NRC-92, "Cleavage Fracture of Ship Plate as Influenced by Design and Metallurgical Factors NS-336, Part II - Flat Plate Tests", OSRD No. 6452, Serial No. M-608, dated January 1946.
2. Research Project NRC-93, "Cleavage Fracture of Ship Plates as Influenced by Size Effect," NS-336, OSRD No. 6457, Serial No. L-614, dated January 1946.
3. Research Project NRC-96, "Correlation of Laboratory Tests with Full Scale Ship Plate Fracture Tests," OSRD No. 6204, Serial No. L-613, dated October 1945.
4. Research Project NRC-94, "Correlation of Laboratory Tests with Full Scale Ship Plate Fracture Tests," NS-336, OSRD No. 5380, Serial No. L-526, dated July 1945.
5. H. Neuber. "Kerbspannungslehre" Berlin, Julius Springer 1947. The David Taylor Model Basin Translation 74. November 1945.
6. N. Davidenkov and F. Wittmann: Techn. Phys. USSR, Vol. 4 (1937) p.308.
7. Research Project SR-92, "Causes of Cleavage Fracture in Ship Plate: Flat Plate Tests," Serial No. SSC-2, Contract NObs-31222, dated August 1946.
8. Research Project SR-93, "Cleavage Fracture of Ship Plate as Influenced by Size Effect," Serial No. SSC-3, Contract NObs-31224, dated August 1946.

TABLE 1

STEELS INVESTIGATED ON PROJECTS SR-92, -93 AND -96

<u>Designation</u>	<u>Description</u>	<u>Use</u>
A	Carnegie-Illinois "Chattanooga" Normal Carbon and Manganese, Semi-killed	NRC-75 & SR-92
Br Bn	Bethlehem, Low Carbon and High Manganese Semi-killed; Br = as rolled; Bn = normalized	SR-92
C	Carnegie-Illinois, Normal Carbon and Manganese Semi-killed	SR-92
Dr Dn	Lukens Fully-killed Steel; Dr = as rolled; Dn = normalized	SR-93
E	Lukens Rimmed Steel	SR-93 and David Taylor Model Basin
F	Bethlehem Low Carbon and High Manganese, Fully-killed	SR-93
G	Bethlehem Low Carbon and High Manganese, Fully-killed	SR-93
H	Bethlehem Fully-killed steel .16 C and .85 Mn.	SR-92
N	Lukens 3 $\frac{1}{4}$ Nickel, .15% C Steel 60,000 Psi Yield Point, as rolled	SR-92
Q	Republic .23% C and 1.05% Mn Steel Water Quenched and Drawn to 70,000 Psi Tensile strength	SR-92

TABLE 2

CHEMICAL ANALYSES OF THE STEELS*

<u>Code</u>	<u>C %</u>	<u>Mn %</u>	<u>P %</u>	<u>S %</u>	<u>Si %</u>	<u>Al %</u>	<u>Ni %</u>	<u>Cu %</u>	<u>Cr %</u>	<u>Mo %</u>	<u>Sn %</u>	<u>Nb %</u>
A	.26	.50	.012	.039	.03	.012	.02	.03	.03	.006	.003	.004
Br	.18	.73	.008	.030	.07	.015	.05	.07	.03	.006	.012	.005
Bn	.18	.73	.011	.030	.04	.013	.06	.08	.03	.006	.015	.006
C	.24	.48	.012	.026	.05	.016	.02	.03	.03	.005	.003	.009
Dr	.22	.55	.013	.024	.21	.020	.16	.22	.12	.022	.023	.006
Dn	.19	.54	.011	.024	.19	.019	.15	.22	.12	.021	.025	.006
E	.20	.33	.013	.020	.01	.009	.15	.18	.09	.018	.024	.005
F	.18	.82	.012	.031	.15	.054	.04	.05	.03	.008	.021	.006
G	.20	.86	.020	.020	.19	.045	.08	.15	.04	.018	.012	.006
H	.18	.76	.012	.019	.16	.053	.05	.09	.04	.006	.004	.004
N	.17	.53	.011	.020	.25	.077	3.39	.19	.06	.025	.017	.005
Q	.22	1.13	.011	.030	.05	.008	.05	.13	.03	.006	.018	.006

V % < .02; AS % < .01 in each steel.

*Supplied by the Bethlehem Steel Corporation

TABLE 3

GAS ANALYSES BY BATTELLE MEMORIAL INSTITUTE

<u>STEEL</u>	<u>COMPOSITION IN WEIGHT PERCENTAGE</u>		
	<u>Oxygen Vacuum Fusion</u>	<u>Nitrogen Vacuum Fusion</u>	<u>Nitrogen Kjeldahl</u>
E	0.012	0.002	0.005
Dn	0.002	0.003	0.005
Dr	0.002	0.004	0.005
A	0.012	0.004	0.004
C	0.011	0.007	0.010
Br	0.010	0.003	0.004
Bn	0.009	0.004	0.005

TABLE B

THE TEMPERATURE OF TRANSITION IN DEGREES FAHRENHEIT AT 25% AND AT 50% OF MAXIMUM ENERGY ABSORPTION FOR THE STANDARD LH CHARPY V-NOTCH SPECIMEN

<u>Steel</u>	<u>25%</u>	<u>50%</u>	<u>72" Wide Plate Results (Ref.) *</u>
A	55	90	35 (7)
Br	-20	+10	30 (7)
Bn	+10	30	45 (7)
C	65	100	95 (7)
Dr	0	45	30 (8)
Dn (1)	-5	30	30 (8)
E (2)	100	150	92 (8)
F	-10	-40	-
G	20	40	-
H	-10	0	-
N	-130	-50	-40 (7)
Q	-30	-5	-

(1) Max. E.A. = 100'# (Assumed)
(Energy Absorption)

(2) " E.A. = 80'# (Assumed)
(Energy Absorption)

*
See Bibliography

TABLE C

THE TEMPERATURE OF TRANSITION IN DEGREES FAHRENHEIT AT 25%
 AND AT 50% OF MAXIMUM ENERGY ABSORPTION FOR THE STANDARD
 LH CHARPY KEYHOLE NOTCH SPECIMEN.

<u>Steel</u>	<u>25%</u>	<u>50%</u>	<u>72" Wide Plate Results (Ref.)*</u>
A	-20	0	35 (7)
Br	-40	-30	30 (7)
Bn	-40	-20	45 (7)
C	0	15	95 (7)
Dr	-80	-60	30 (8)
Dn	-70	-60	30 (8)
E	5	30	92 (8)
F	-85	-65	-
G	-55	-40	-
H	-80	-50	-
N	-230	-220	-40 (7)
Q	-100	-55	-

* See Bibliography

TABLE D

THE TEMPERATURE OF TRANSITION IN DEGREES FAHRENHEIT AT 25% AND
AT 50% OF MAXIMUM ENERGY ABSORPTION FOR THE LH RECTANGULAR NOTCH,
FULL PLATE THICKNESS SPECIMENS

<u>Steel</u>	<u>25%</u>	<u>50%</u>	<u>72" Wide Plate Results (Ref.)*</u>
A	40	60	35 (7)
Br	-5	10	30 (7)
Bn	15	35	45 (7)
C	35	50	95 (7)
Dr	-45	-20	30 (8)
Dn	-40	-30	30 (8)
E	45	75	92 (8)
F	-50	-30	-
G	-15	10	-
H	-30	0	-
N	-140	-100	-40 (7)
Q	-30	15	-

* See Bibliography

TABLE E

THE TEMPERATURE OF TRANSITION IN DEGREES FAHRENHEIT AT 25% AND AT 50% OF MAXIMUM ENERGY ABSORPTION FOR THE STANDARD LH CHARPY KEYHOLE NOTCH SPECIMEN. SPECIMENS TAKEN FROM 72-INCH WIDE TEST PLATES.

Steel	72" Wide Plate Tested at °F.	25%	50%	72" Wide Plate Results (Ref.) *
A	30-35	10	35	35 (7)
A	75	40	45	35 (7)
Br	30-35	-20	-15	30 (7)
Br	72	15	35	30 (7)
Bn	29-32	-45	25	45 (7)
Bn	72	5	20	45 (7)
C	30-33	-15	0	95 (7)
C	75-78	50	70	95 (7)
Dr	0	-85	-60	30 (8)
Dr	15	-55	-50	30 (8)
Dr	31	-20	-15	30 (8)
Dn	-38	-85	-70	30 (8)
Dn	0	-85	-70	30 (8)
Dn	15	-65	-60	30 (8)
Dn	32	-20	-15	30 (8)
E	38	0	35	92 (8)
E	74	65	95	92 (8)
E	110	80	95	92 (8)

* See Bibliography

TABLE F

THE TEMPERATURE OF TRANSITION IN DEGREES FAHRENHEIT AT 25% AND
AT 50% MAXIMUM ENERGY ABSORPTION FOR THE STANDARD LH CHARPY
KEYHOLE-NOTCH SPECIMEN

A PRESTRAIN = 2% IN ELONGATION

<u>Steel</u>	<u>25%</u>	<u>50%</u>	<u>72" Wide Plate Results (Ref.)*</u>
A	20	40	35 (7)
Br	-20	-5	30 (7)
Bn	-20	0	45 (7)
C	40	55	95 (7)
Dr	-60	-30	30 (8)
Dn	-75	-55	30 (8)
E	50	70	92 (8)
H	-90	-55	-

B PRESTRAIN = 5% IN ELONGATION

<u>Steel</u>	<u>25%</u>	<u>50%</u>	<u>72" Wide Plate Results (Ref.)*</u>
A	35	45	35 (7)
Br	+5	10	30 (7)
Bn	-10	0	45 (7)
C	55	65	95 (7)
Dr	-35	0	30 (8)
Dn	-45	-25	30 (8)
E	45	60	92 (8)
H	-55	-35	-

* See Bibliography

TABLE F (CONT'D)

C PRESTRAIN = 10% IN ELONGATION

<u>Steel</u>	<u>25%</u>	<u>50%</u>	<u>72" Wide Plate Results (Ref.)</u>	<u>T.*</u>
A	40	60	35 (7)	60
Br	10	20	30 (7)	50
Bn	15	30	45 (7)	50
C	70	95	95 (7)	80
Dr	-5	20	30 (8)	80
Dn	-30	0	30 (8)	60
E	60	85	92 (8)	55
H	-40	-20	-	30

* The increase in the transition temperature resulting from 10% Strain in Tension at 50% Max. E. A. (energy absorption)

TABLE K

THE TEMPERATURE OF TRANSITION IN DEGREES FAHRENHEIT AT 25%
AND AT 50% OF MAXIMUM ENERGY ABSORPTION FOR PLATES OF STEEL
C OF VARIOUS THICKNESSES

A. - STANDARD LH CHARPY KEYHOLE-NOTCH SPECIMEN.

<u>Plate Gage</u>	<u>25%</u>	<u>50%</u>
1/2"	-45	-25
5/8"	-10	- 5
3/4"	0	15
1" (rim)	10	30
1" (core)	5	25
1-1/8" (rim)	10	30
1-1/8" (core)	25	45

B. - STANDARD LH CHARPY V-NOTCH SPECIMEN.

<u>Plate Gage</u>	<u>25%</u>	<u>50%</u>
1/2"	30	70
5/8"	55	95
3/4"	70	100
1" (rim)	80	105
1" (core)	70	100
1-1/8" (rim)	70	110
1-1/8" (core)	70	105

TABLE L

THE LOWEST TEMPERATURE FOR MAXIMUM ENERGY ABSORPTION FOR
 THE IMPACT TEST SPECIMENS FOR THE PROJECT STEELS.

	<u>V-Notch</u> <u>Test Data</u>	<u>Keyhole-Notch</u> <u>Test Data</u>	<u>Full Width</u> <u>Specimen Data</u>
A	170	95	140
Br	95	35	75
Bn	165	110	105
C	200	90	160
Dr	130	100	85
Dn	-	105	85
E	> 200	110	155
F	30	45	85
G	90	40	70
H	50	40	55
N	25	25	15
Q	90	55	65

TABLE M - RESULTS OF MEASUREMENTS ON MICROSTRUCTURES

Steel Section		G/in. ²	% Ferrite	% Pearlite	$\frac{\% P}{\% Fe}$
A	T	41	86	14	.163
	L	47	85.9	14.1	.165
Br	T	32	90.3	9.7	.107
	L	40	90.8	9.2	.101
Bn	T	60	87.3	12.7	.145
	L	82	85.9	14.1	.164
C	T	34	85.5	14.5	.170
	L	40	83.8	16.2	.195
Dr	T	60	85	15	.177
	L	75	83.1	16.9	.202
Dn	T	87	86.1	13.9	.162
	L	117	89.8	15.2	.179
E	T	30	79.1	20.9	.264
	L	31	83.6	16.4	.197
F	T	30.5	87.7	12.3	.141
	L	29	88.1	11.9	.136
G	T	24	82.0	18.0	.219
	L	30	85.3	14.7	.172
H	T	26	81.8	18.2	.222
	L	27	84.1	15.9	.189
N	T	202	90.4	9.6	.106
	L	185	92.9	7.1	.0765
Q	T	-	-	-	-
	L	-	-	-	-

APPENDIX A

MILL DATAA Steel

Heat Number 72L122

Yield Point 37,900 psi

Ultimate Strength 59,900 psi

Elongation in 2 inches 33.5%

Finishing Temperature 1900 F.

Deoxidation

1-1/3 lb. of silicon per ton in the ladle and

1/3 lb. of aluminum in the mold

Chemical Analysis

.23 C, .47 Mn, .042 S, .02 Si, .011 P.

B Steel

Heat No. 60-E-796

	<u>C</u>	<u>Mn.</u>	<u>P.</u>	<u>S.</u>	<u>Si.</u>
Ladle	.15	.77	.010	.029	.05
Check 98062.16	.16	.74	.011	.030	.03

Total Charge 380,840

Percent Hot Metal 49.0

Percent Scrap 45.0

Percent Ore 4.7

Percent Limestone 6.4

Furnace Addition: Fe Mn - 3,000 lbs. 8 minutes

Ladle Addition: Fe Mn - 1,500 lbs.

Fe Si - 200 lbs.

Al Si - 450 lbs.

B. Steel (Cont'd)

Mold Addition: Small amount of Al to cap.

The normalizing temperature of the plates which were furnished in the normalized condition were 1650° F.

The physical tests on the plates on which the check analysis was made are as follows:

<u>Serial</u>	<u>Gauge</u>	<u>Yield Point</u>	<u>Ultimate</u>	<u>Elong. 8"</u>	<u>Treatment</u>
98062	3/4"	35800	59600	26.0	As Rolled
98062	3/4"	34800	58900	32.0	Normalized

C Steel

Heat No. 572367

Deoxidation Practice

Bath Addition: 6-1/2 lb. per ton of 80% Ferromanganese

Ladle Addition: 6 lb. per ton of 80% Ferro-manganese

2.6 lb. per ton of 50% Ferro-silicon

Mold Addition: 1/3 lb. per ton of Aluminum

Ladle Analysis

<u>C</u>	<u>Mn</u>	<u>P</u>	<u>S</u>	<u>Si</u>
.24	.49	.015	.033	.043

Mold Size 31 in. x 66 in.Slab Size 4-3/4 in. to 6-1/4 in. x 62 in. x 5951 lb. to 11851 lb.Plate Gage 1/2 in. to 1-1/8 in.

No finishing temperature recorded.

The following are the mill test results on the as-rolled plate:

C Steel (Cont'd)

<u>Gage</u>	<u>Y.P.</u> <u>(psi)</u>	<u>T.S.</u> <u>(psi)</u>	<u>Along.</u>
1/2 in.	41,200	68,400	26.5
5/8 in.	40,410	68,900	25.00
3/4 in.	39,780	67,760	25.5
	38,930	67,340	25.5
	38,200	67,240	25.0
1 in.	40,780	69,900	24.75
1-1/8 in.	38,720	68,720	24.0

D Steel

Heat No. 20340

Silicon Killed Steel

Chemical Composition (Ladle Analysis)

<u>C</u>	<u>Mn</u>	<u>P</u>	<u>S</u>	<u>Si</u>	<u>Cu</u>
<u>%</u>	<u>%</u>	<u>%</u>	<u>%</u>	<u>%</u>	<u>%</u>
.18	.55	.015	.028	.23	.20

Dimensions & Weight of the Ingots

<u>Size</u>	<u>Wt. with Hot Top</u>	<u>Wt. under Hot Top</u>
42 x 16#	9,300#	7,700#

Deoxidation Practice (Furnace) Details of Melting Practice

Spiegel	1,575#
Ferro Manganese 80%	1,365#
Ferro Silicon 15%	2,625#

D Steel (Cont'd)

Deoxidation Practice (Ladle)

Ferro Silicon 50%	1,365#
Aluminum - Shot	100#
Aluminum - Bar	100#

Tensile Properties (As Rolled)

<u>Yield Point</u> Lb. per Sq. inch	<u>Tensile Strength</u> Lb. per Sq. inch	<u>Elongation</u> in 8 inch percent	<u>Reduction</u> in Area. Percent
40500	67200	27.0	50.1

Tensile Properties (Normalized)

<u>Yield Point</u> Lb. per Sq. inch	<u>Tensile Strength</u> Lb. per Sq. inch	<u>Elongation</u> in 8 inch percent	<u>Reduction</u> in Area. Percent
45300	69300	32.0	57.3

E Steel

Heat No. 20279

Rimming Steel

Chemical Composition (Ladle Analysis)

<u>C</u> <u>%</u>	<u>Mn</u> <u>%</u>	<u>P</u> <u>%</u>	<u>S</u> <u>%</u>	<u>Si</u> <u>%</u>	<u>Cu</u> <u>%</u>
.23	.39	.019	.032	.008	.19

Dimensions & Weight of the Ingots.

<u>Size</u>	<u>Wt. with Hot Top</u>	<u>Wt. under Hot Top</u>
42 x 16 #	10,200#	-----

Furnace Additions:Details of Melting Practice

Ferro Manganese 80% 840#

E Steel (Cont'd)Ladle Additions:

Aluminum - Bar20#

Ferro Silicon 50%.....30#

Tensile Properties

<u>Yield Point</u> Lb. per Sq. inch	<u>Tensile Strength</u> Lb. per Sq. inch	<u>Elongation</u> in 8 inch percent	<u>Reduction</u> in Area. percent
38000	62500	28.0	52.3

H Steel

Heat No. 75H017

Chemical Composition

<u>C</u> <u>%</u>	<u>Mn</u> <u>%</u>	<u>P</u> <u>%</u>	<u>S</u> <u>%</u>	<u>Si</u> <u>%</u>	<u>Al</u> <u>%</u>
.17	.82	.022	.024	.15	.056

Fully Al Killed

Tensile Properties (As Rolled)

<u>Yield Point</u> psi	<u>Tensile Strength</u> psi	<u>Elongation in</u> 8" %	<u>Reduction of</u> Area %
42,800	63,800	24	46.8

Impact Resistance (As Rolled)

Charpy Keyhole Notch specimens perpendicular to the rolled surface.

Energy Absorbed, Ft. Lbs. at

<u>76°F.</u>	<u>0°F.</u>	<u>-50°F.</u>	<u>-80°F.</u>	<u>-98°F.</u>
55	38.8	25.5	10.4	5.5

N Steel

Heat No. 20572

Chemical Composition

<u>Ni</u> %	<u>Si</u> %	<u>C</u> %	<u>Mn</u> %	<u>P</u> %	<u>S</u> %
3.34	0.22	0.13	0.49	0.018	0.027

Yield Point 49,800 psi

Ultimate Strength 79,400-77,200 psi

Elongation 25.5%

Q Steel

Heat No. 1-15749

Chemical Composition

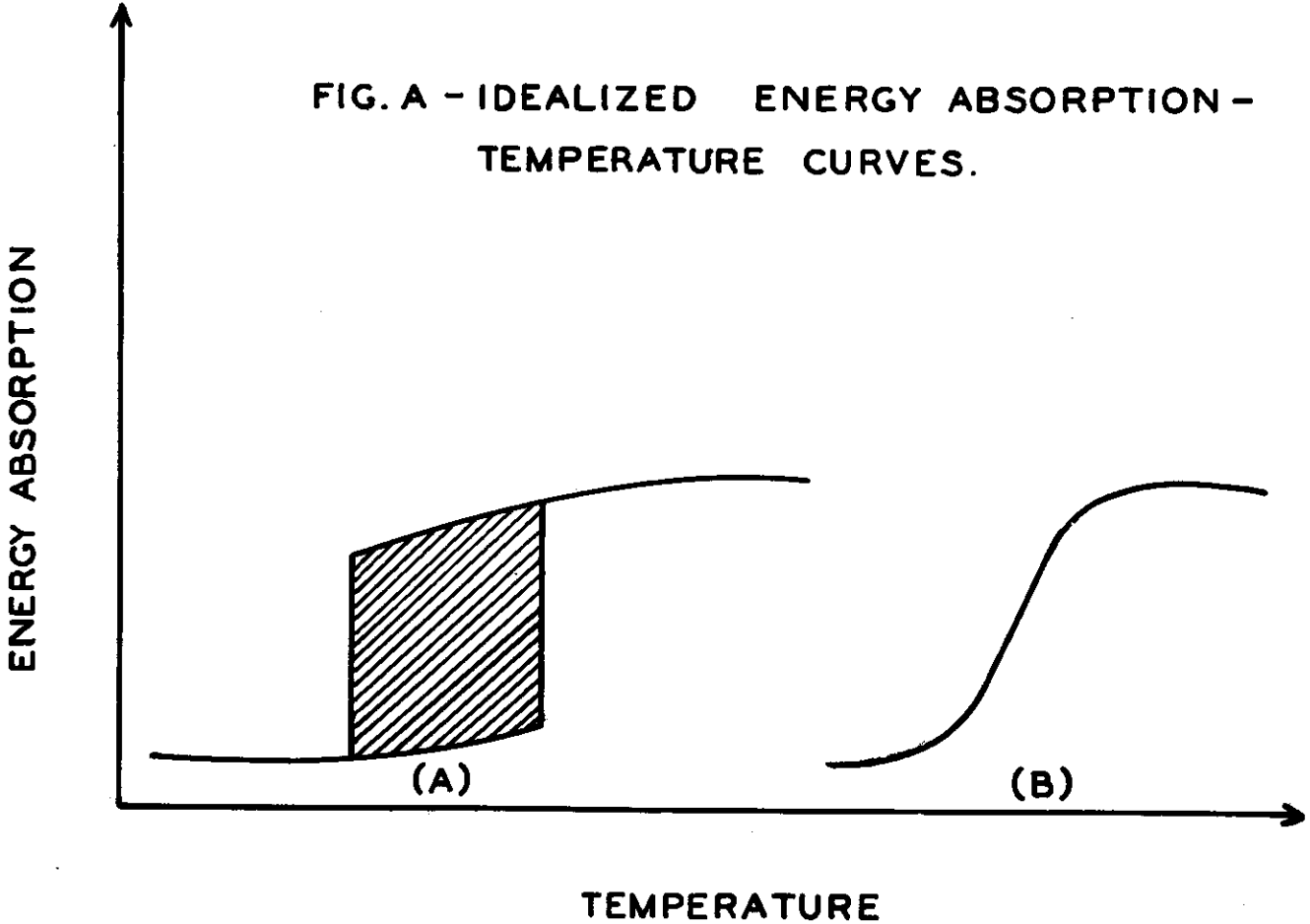
<u>C</u> %	<u>Mn</u> %	<u>P</u> %	<u>S</u> %
.21	1.05	.011	.030

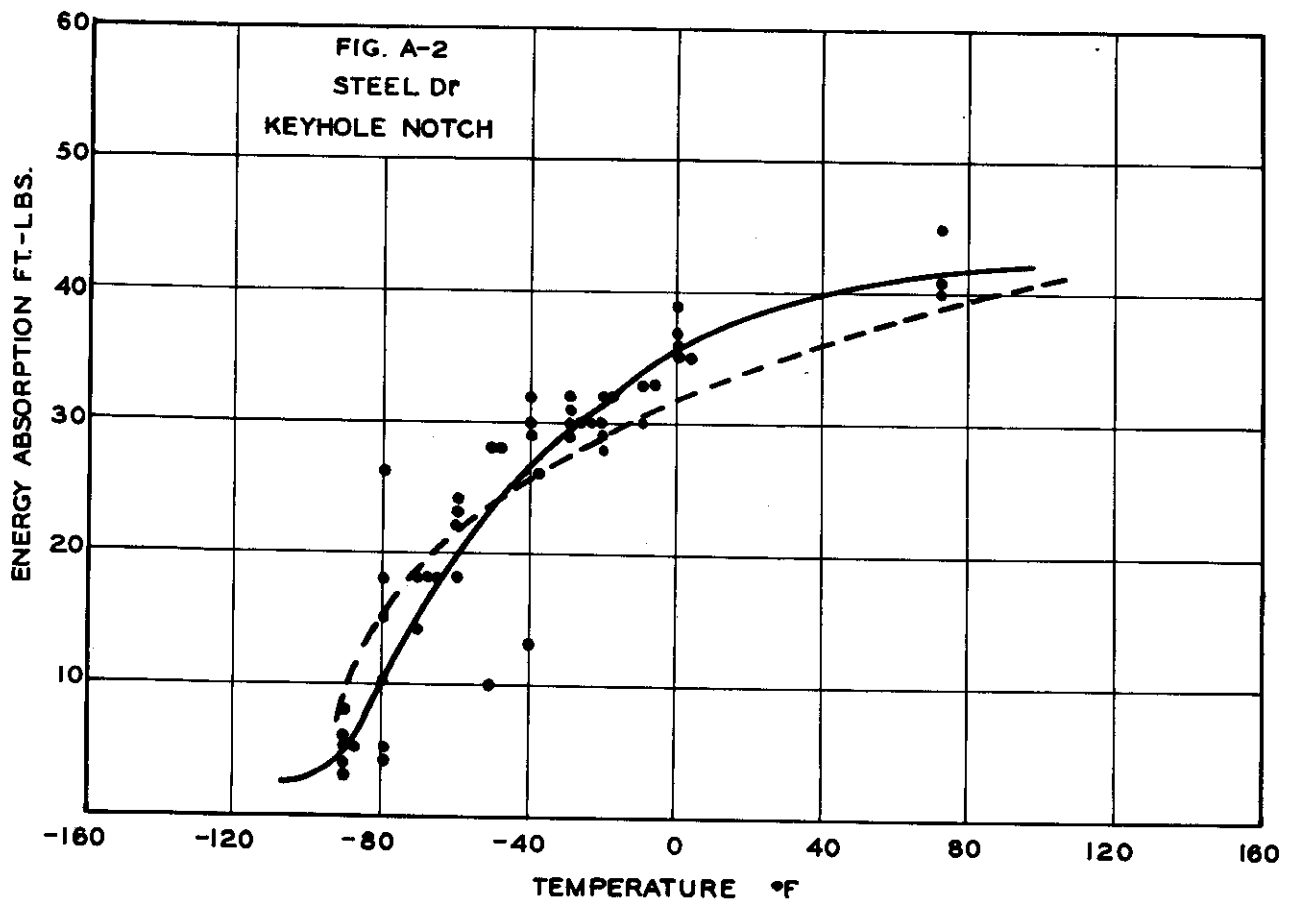
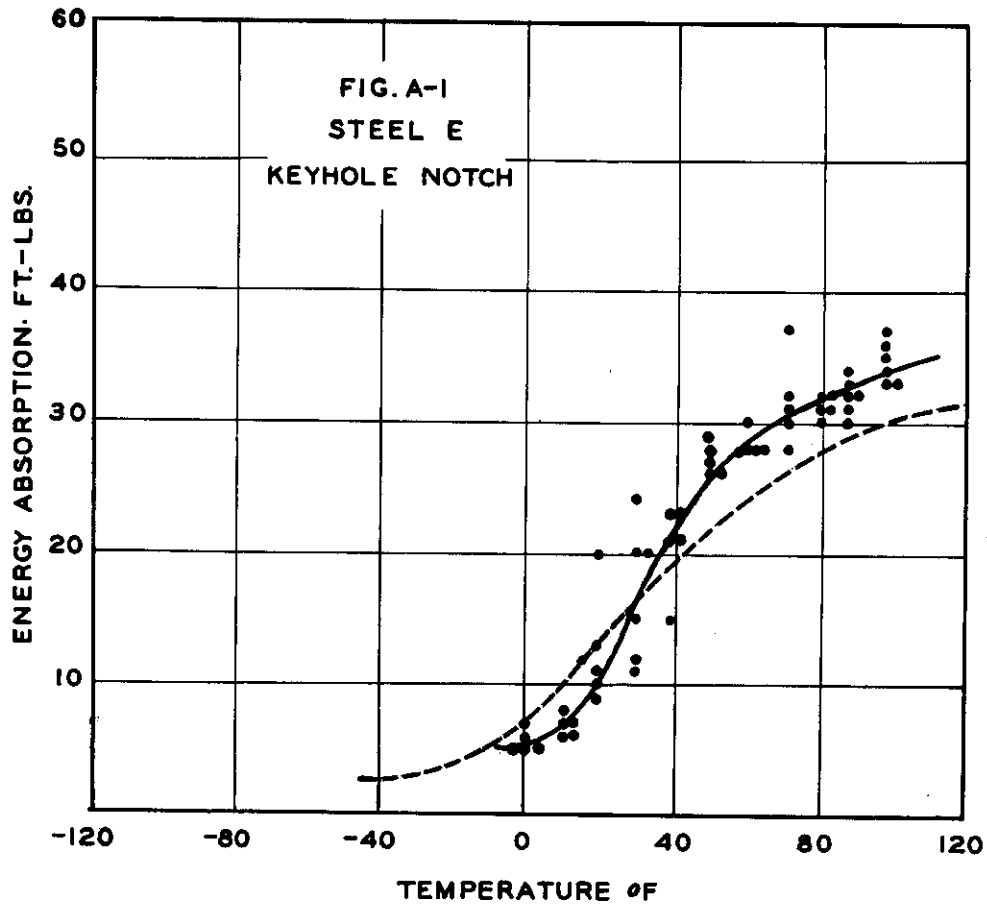
Heat Treatment

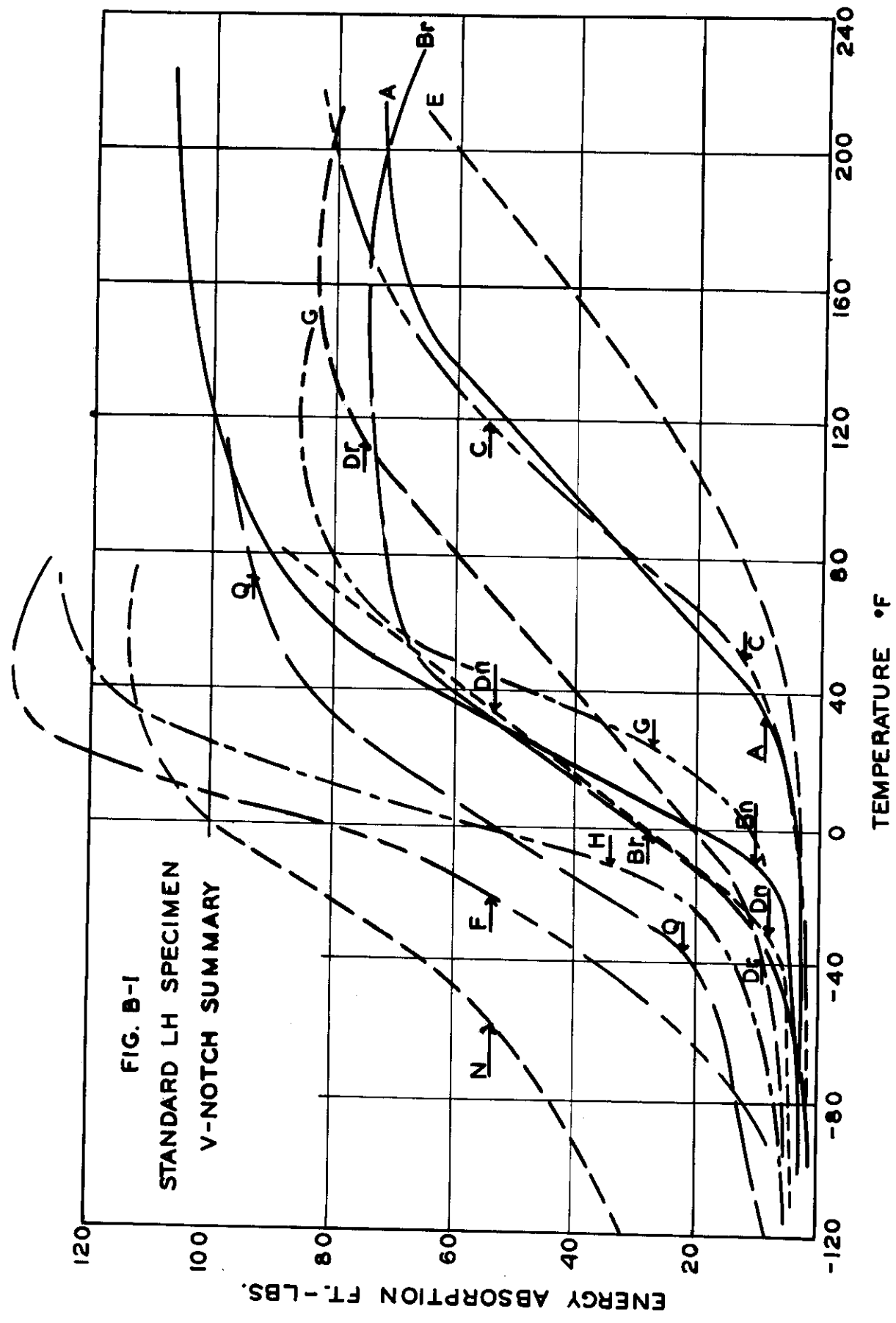
Quench in water from 1625 Fahr. (drastic quench)

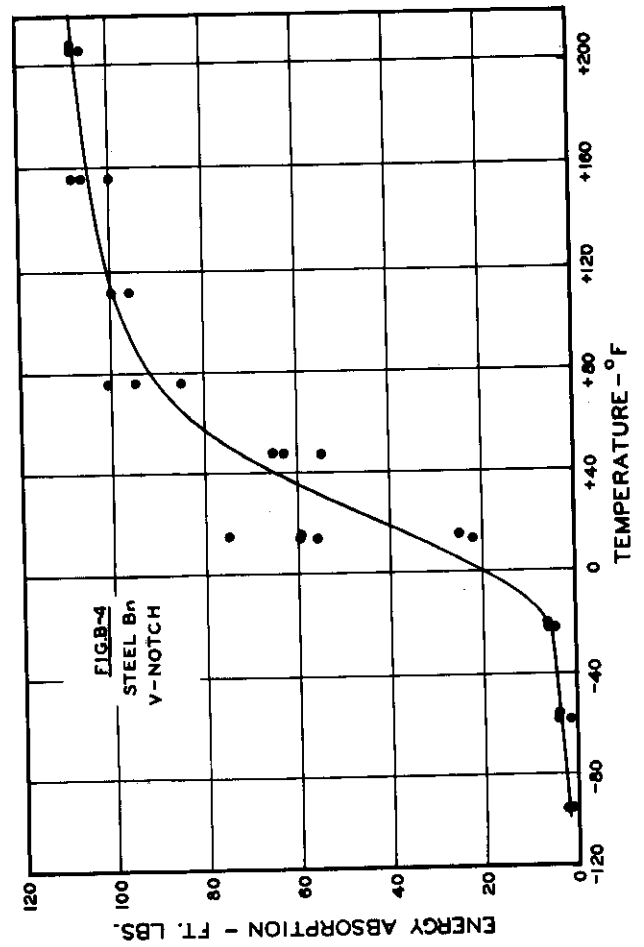
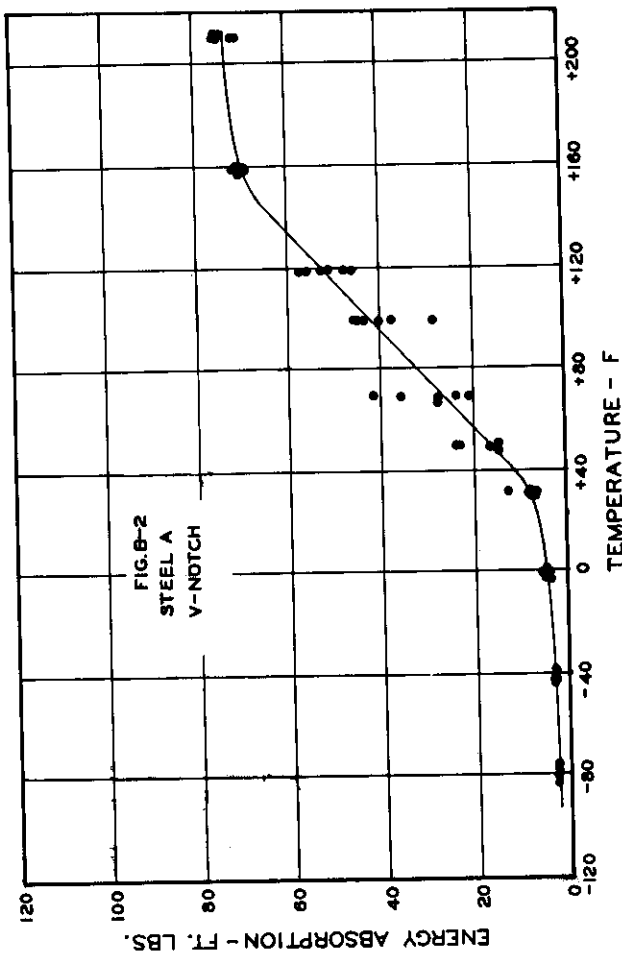
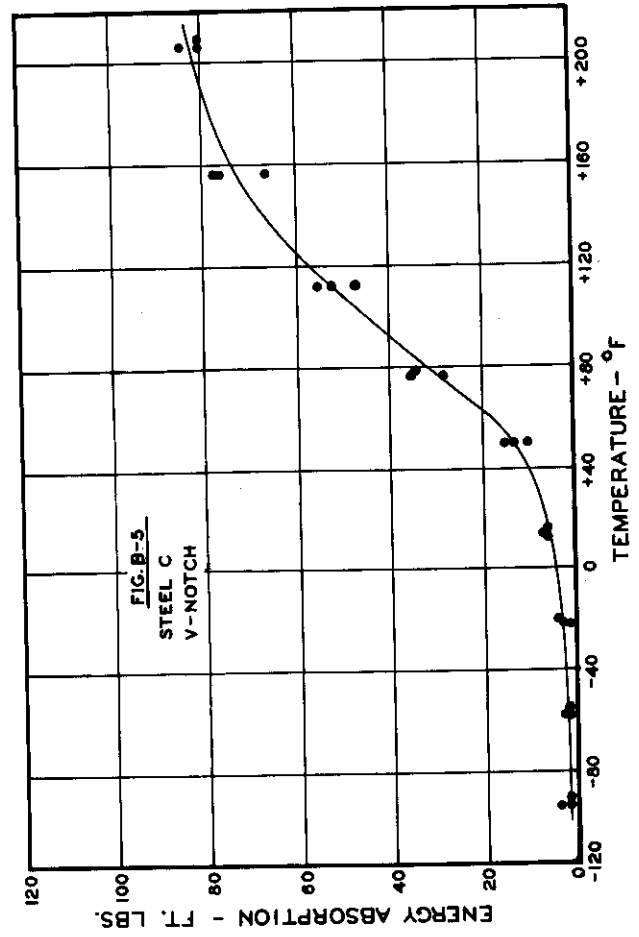
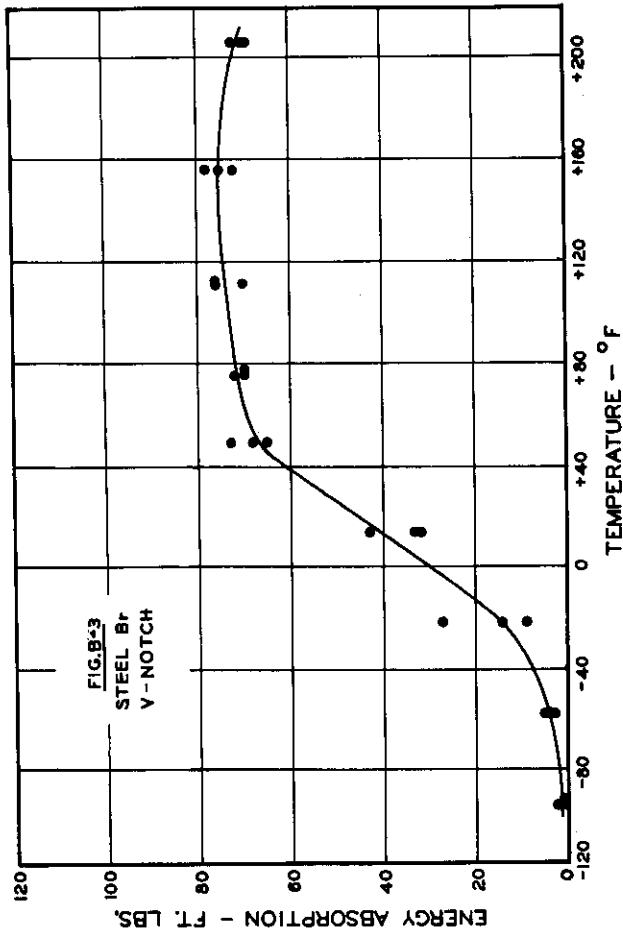
Draw two (2) hours at 1300 Fahr.

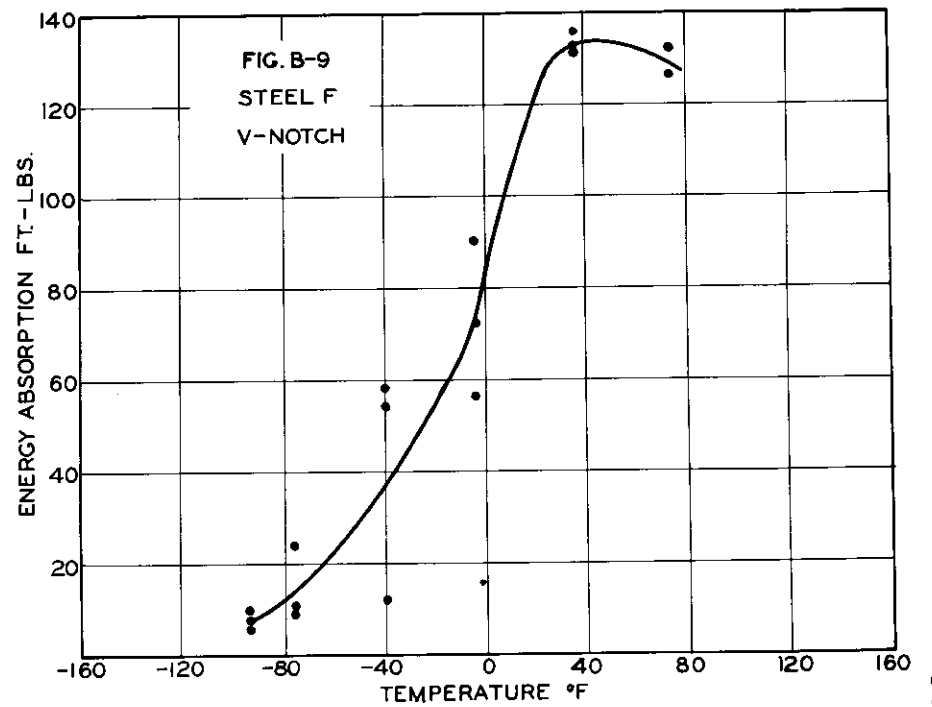
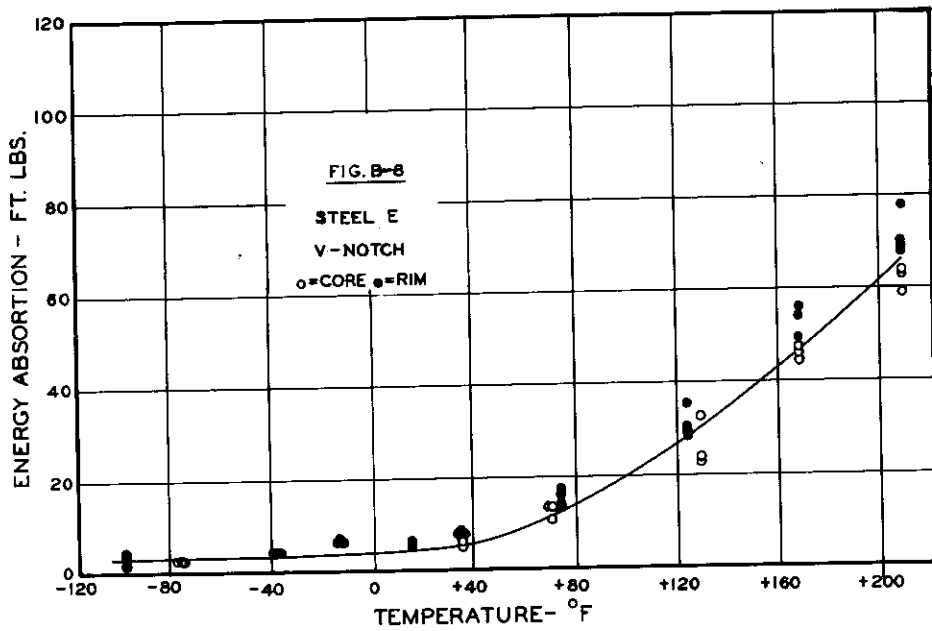
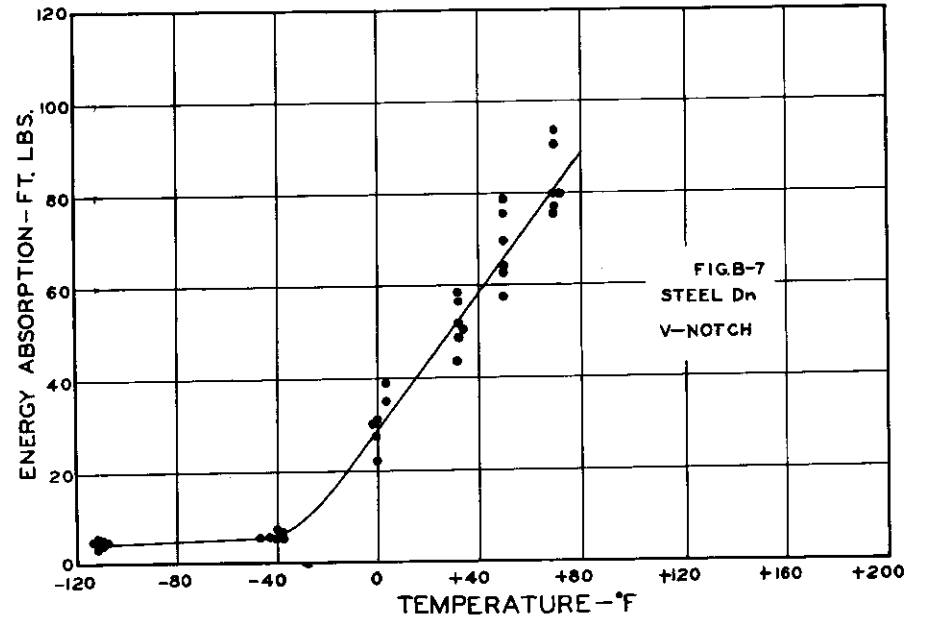
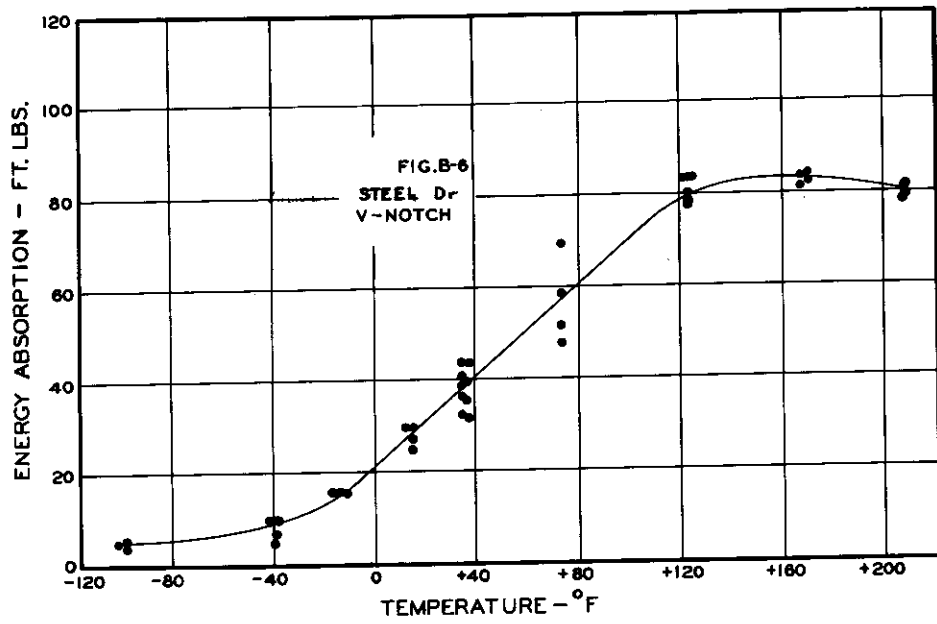
FIG. A - IDEALIZED ENERGY ABSORPTION -
TEMPERATURE CURVES.

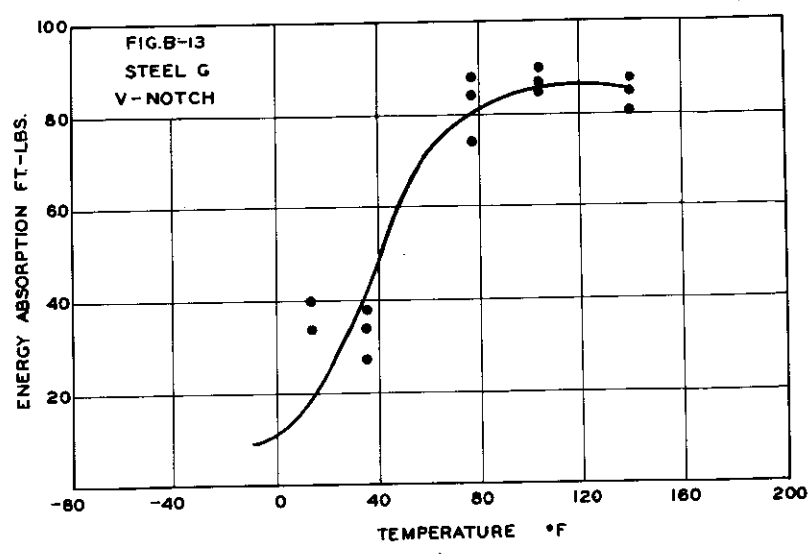
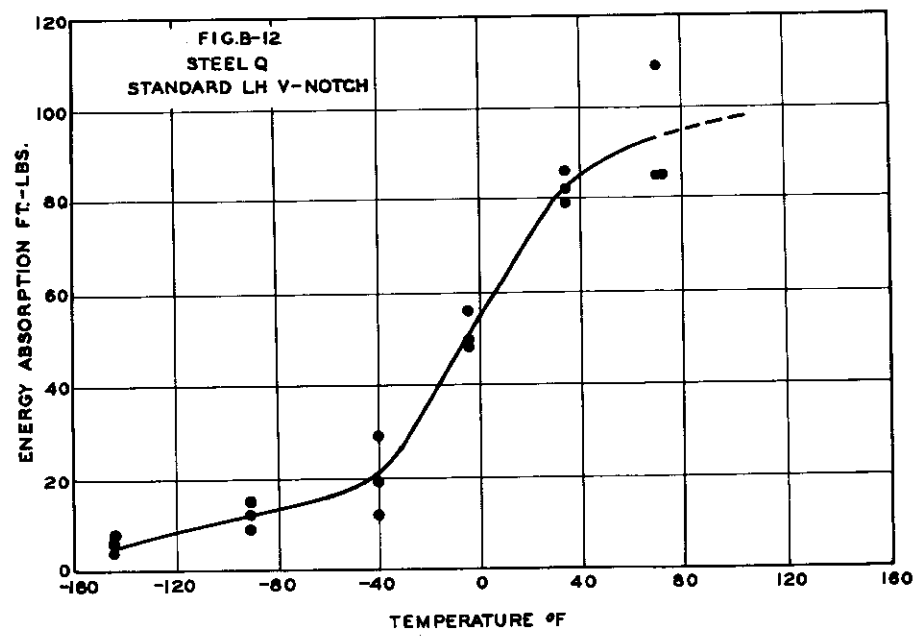
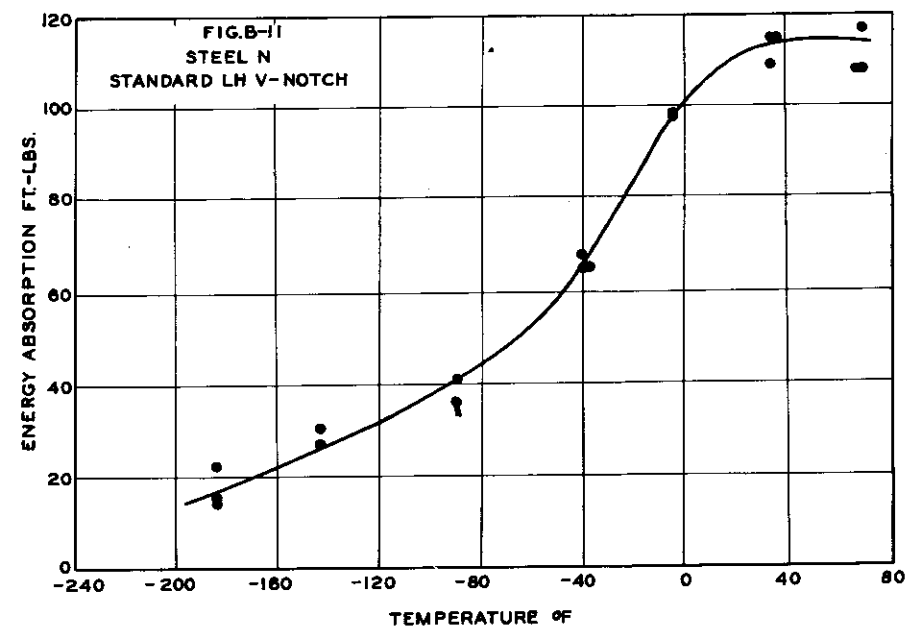
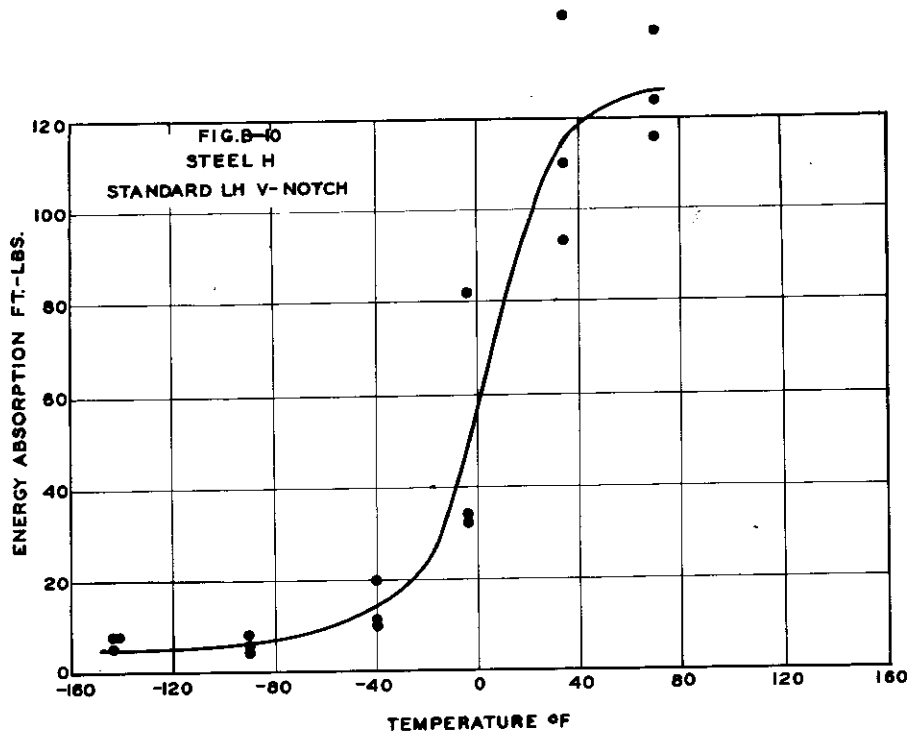


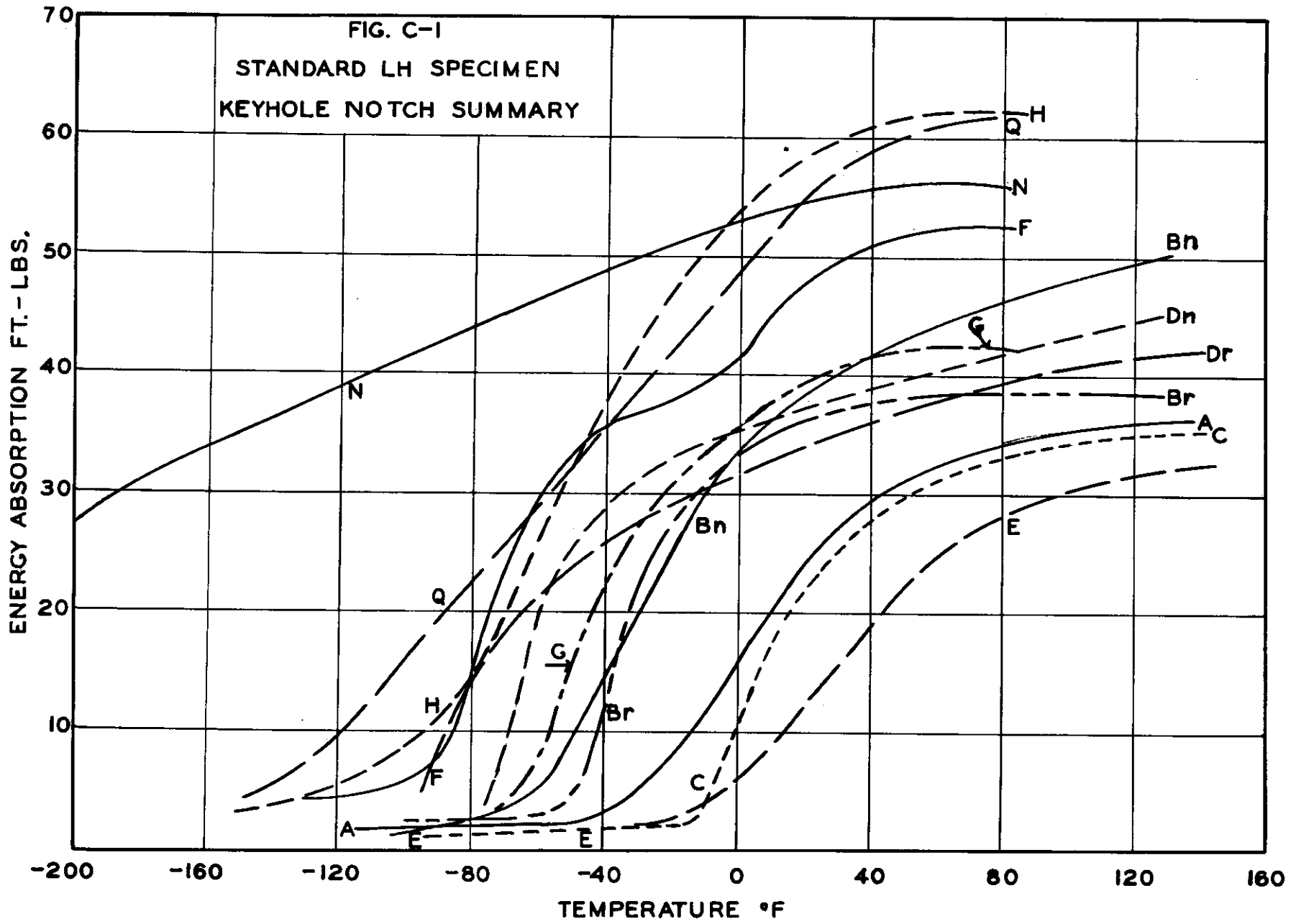


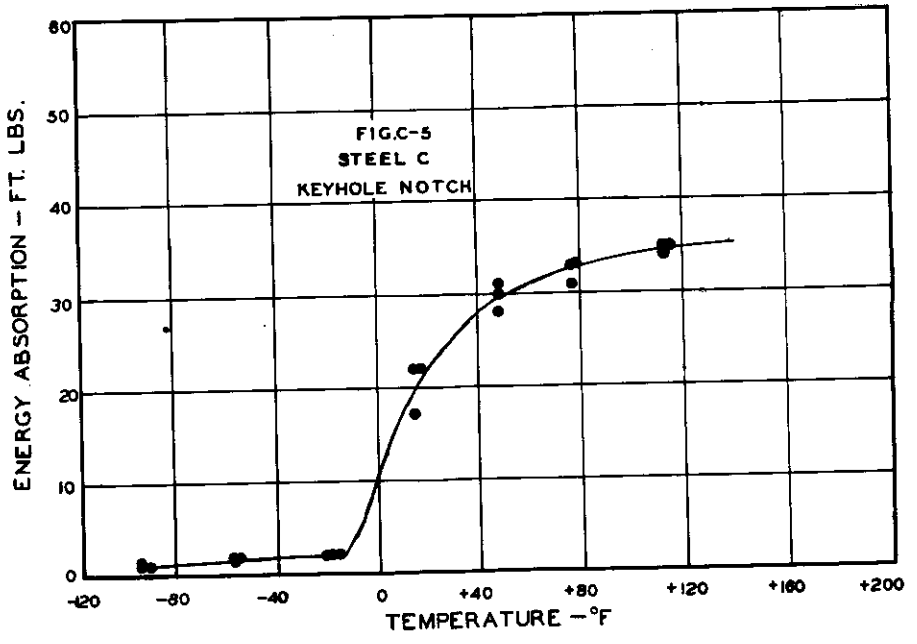
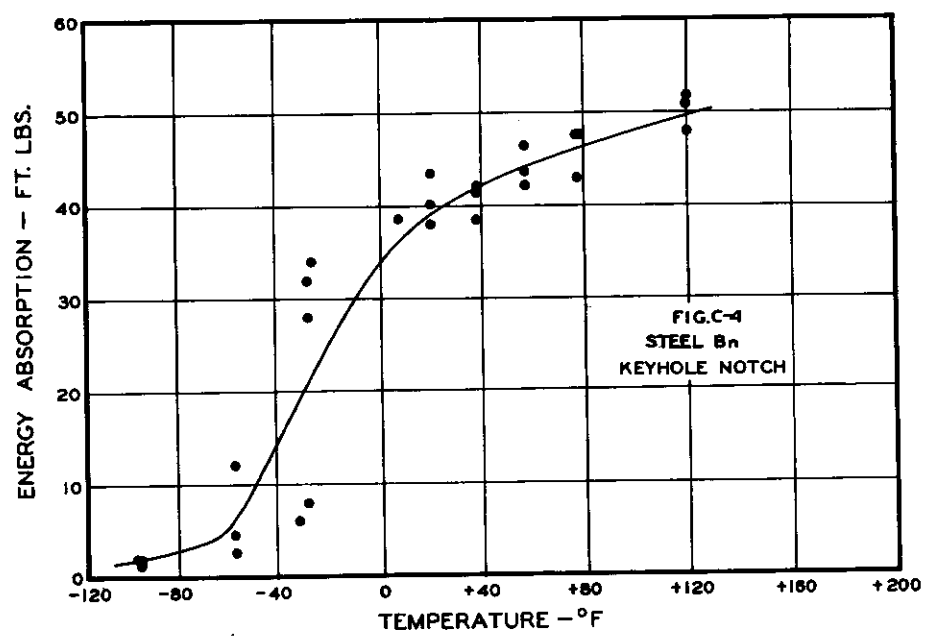
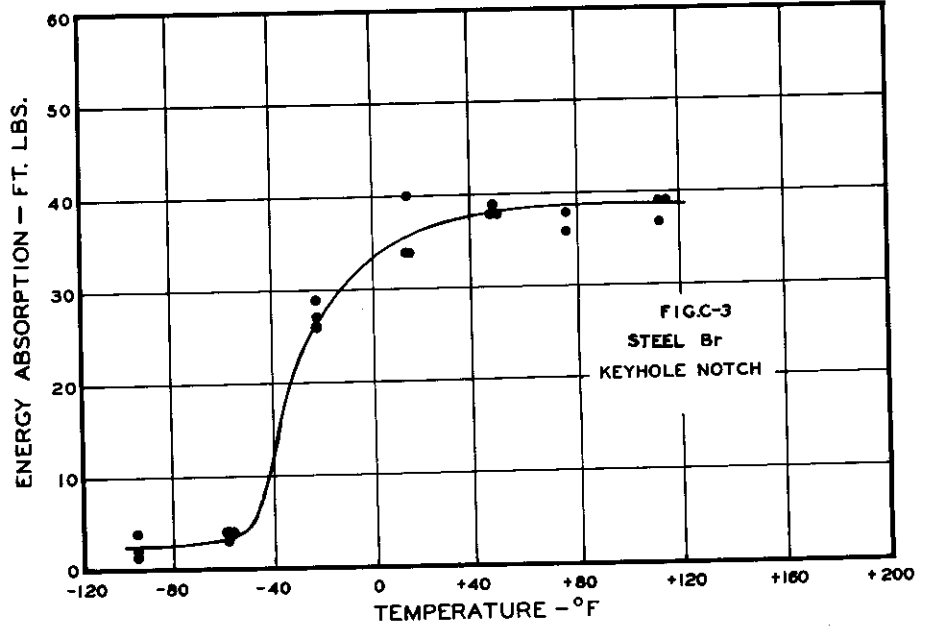
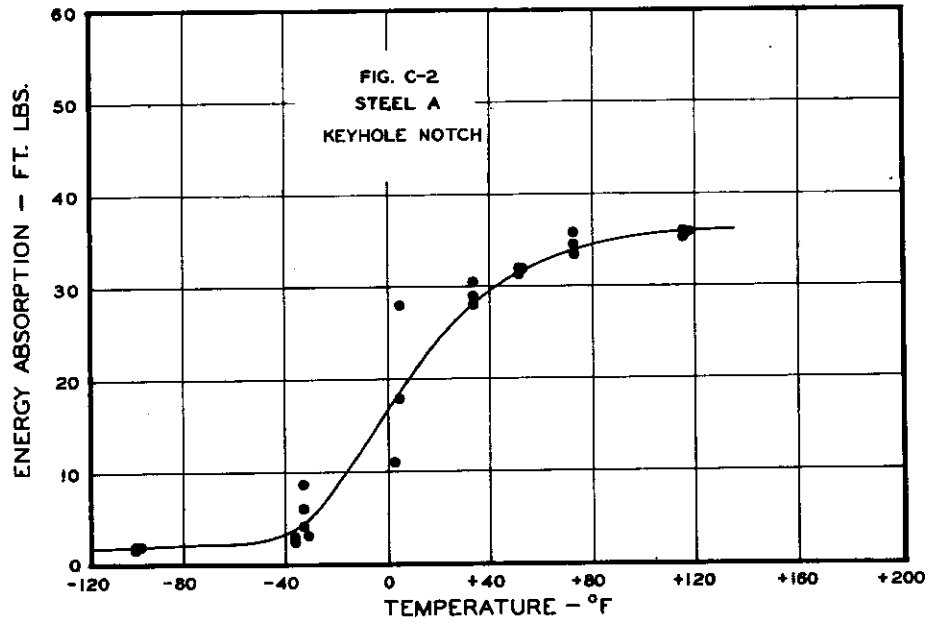


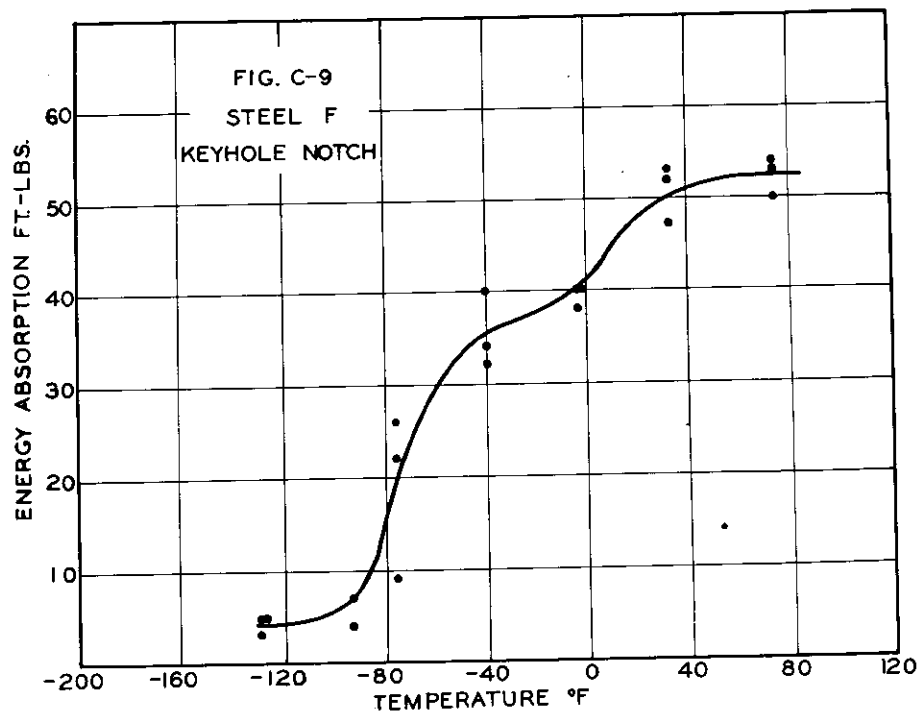
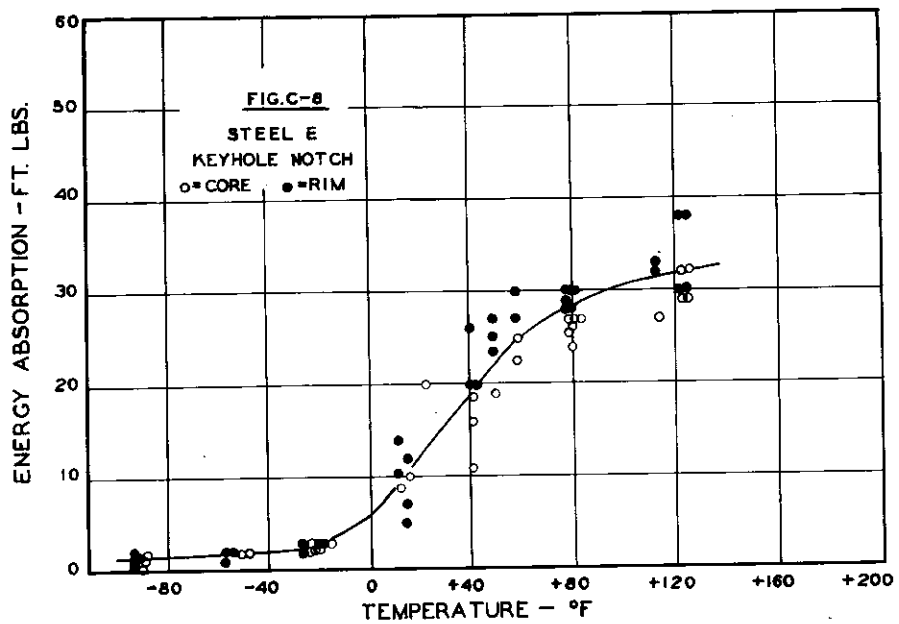
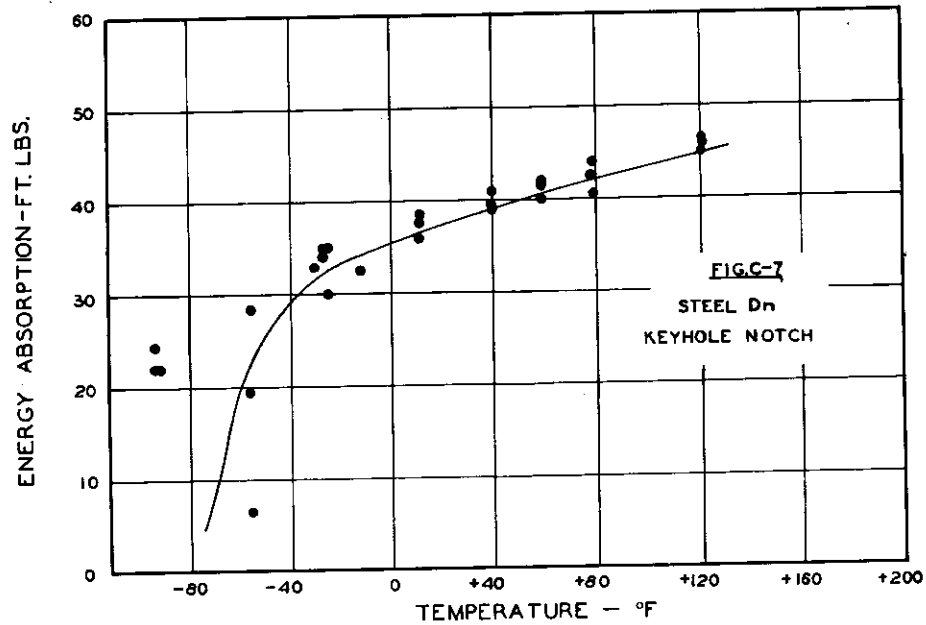
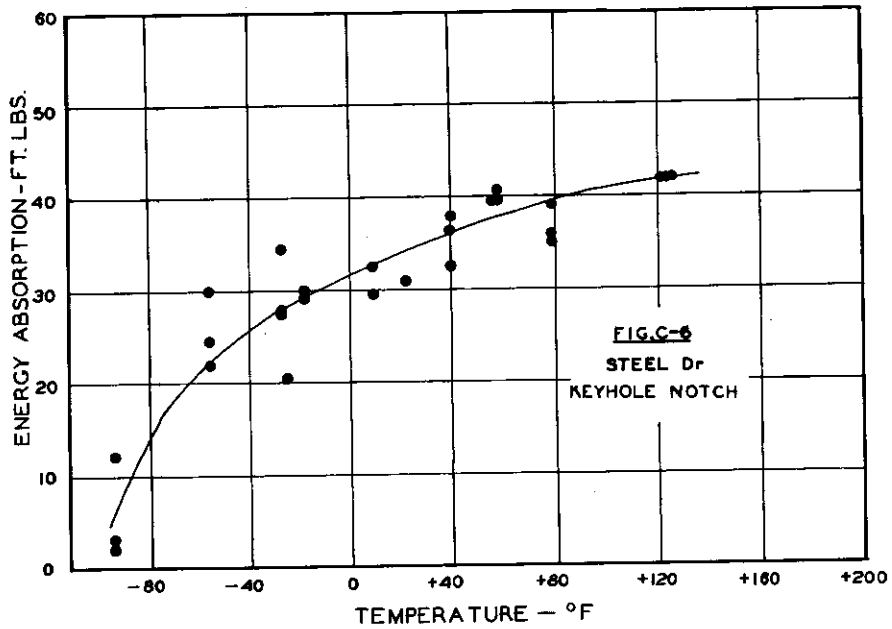


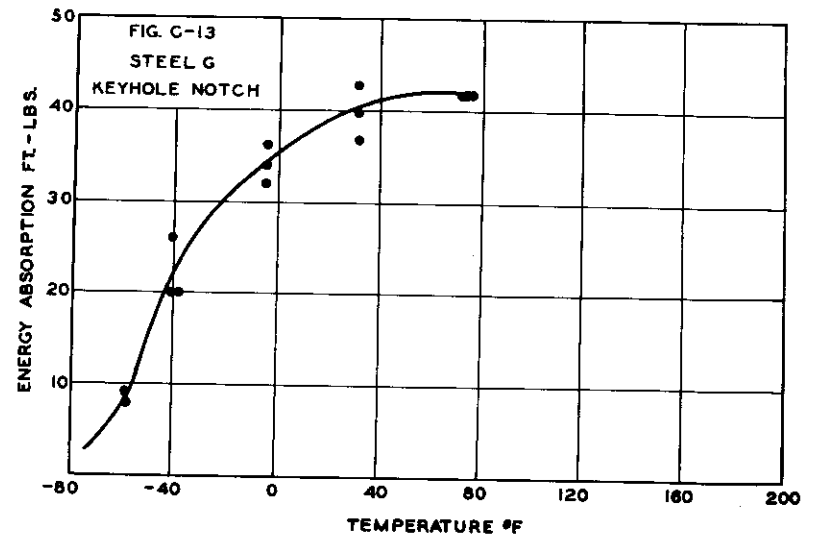
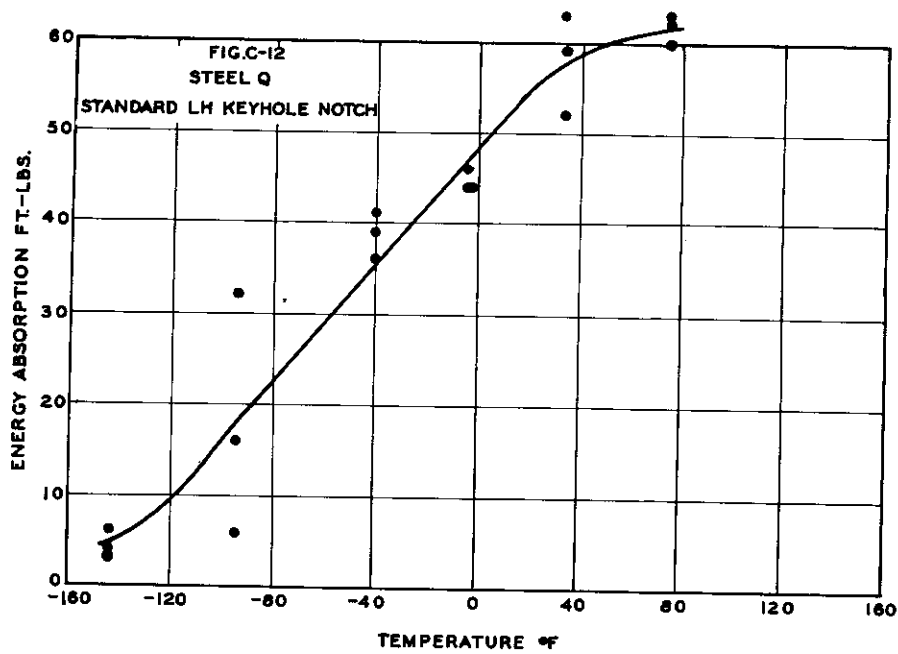
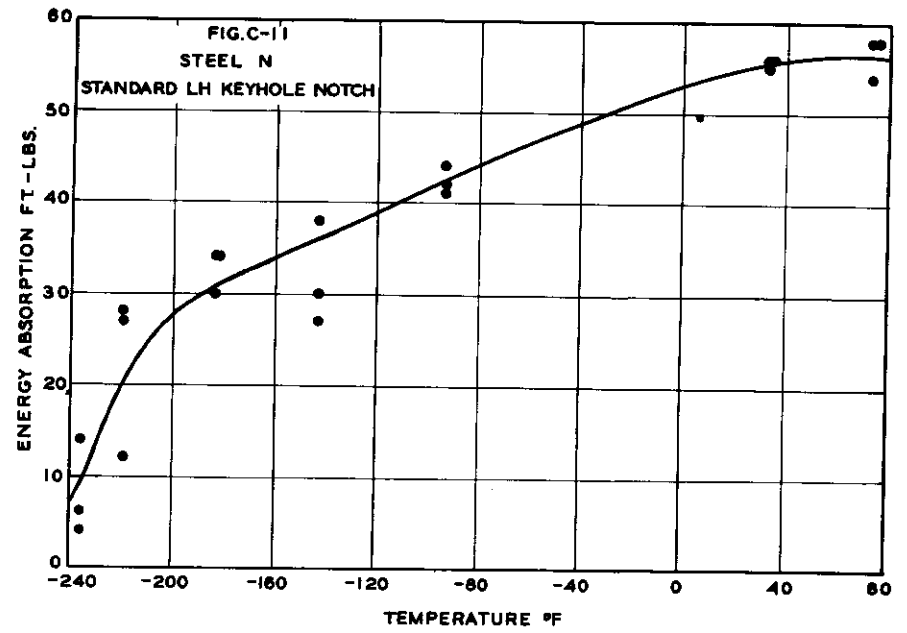
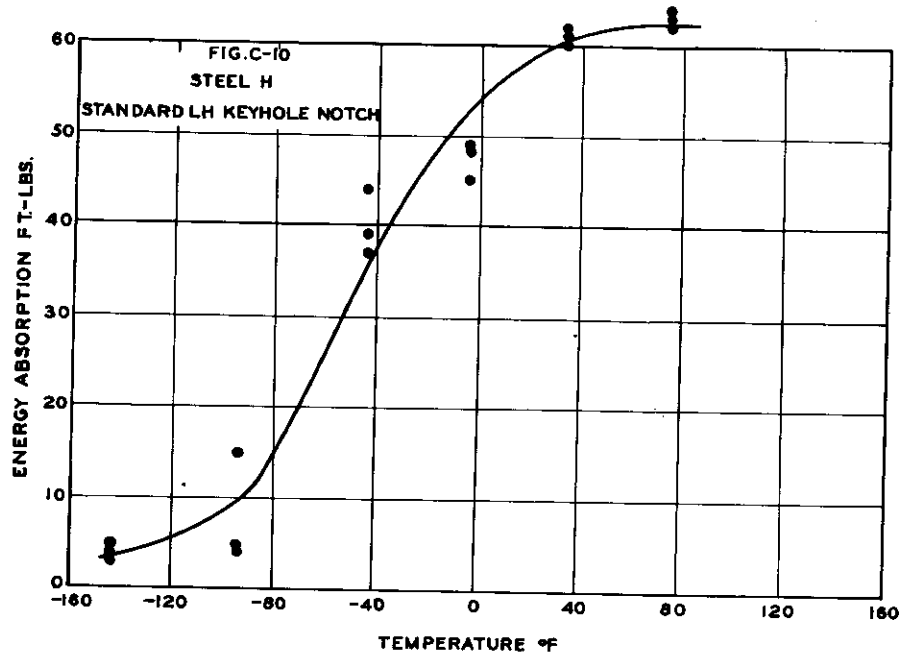


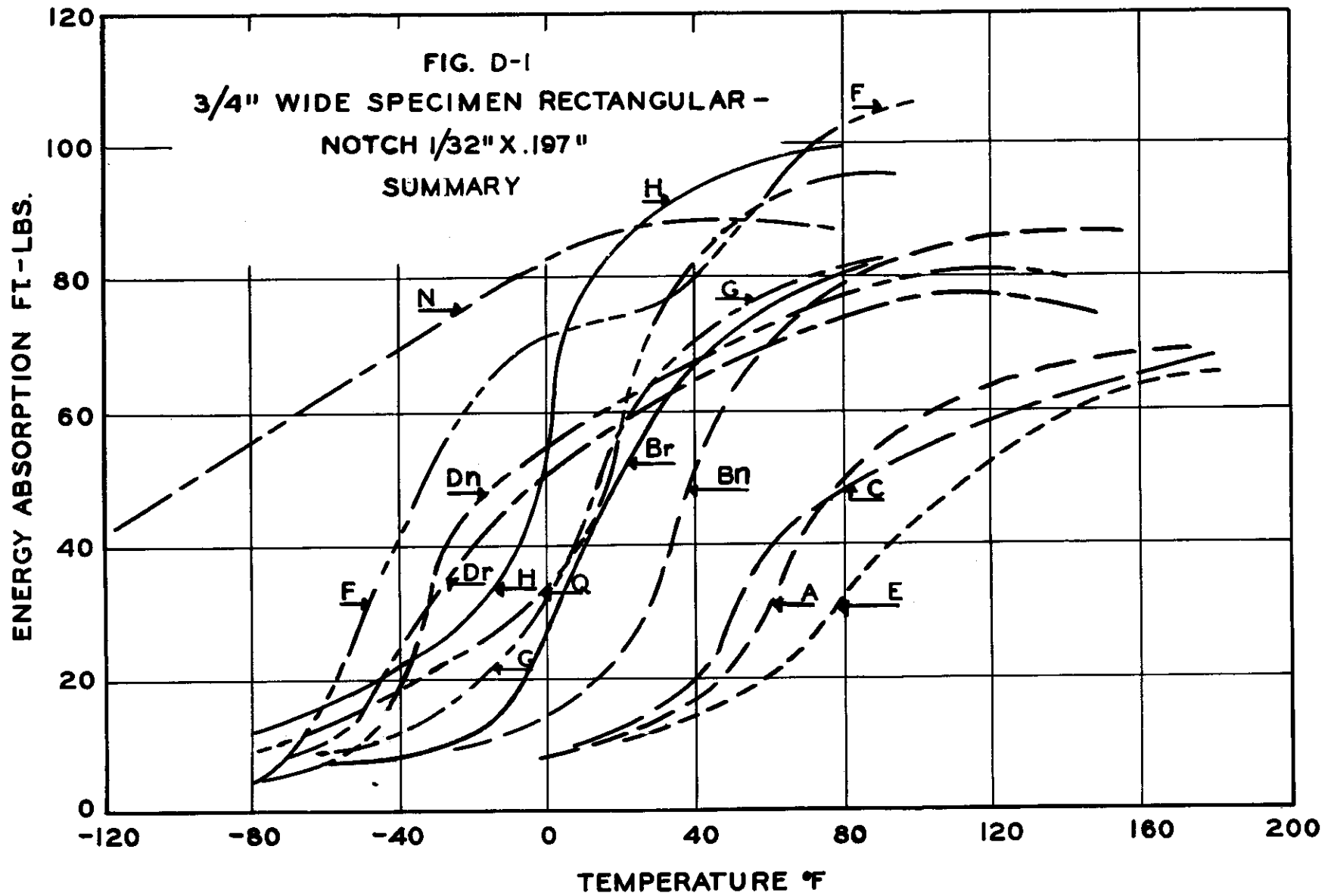


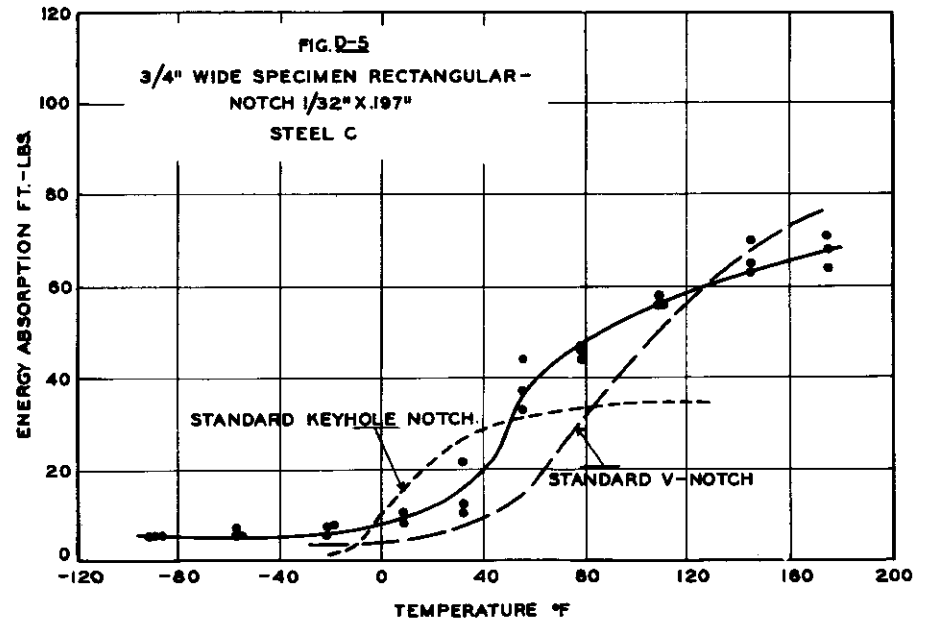
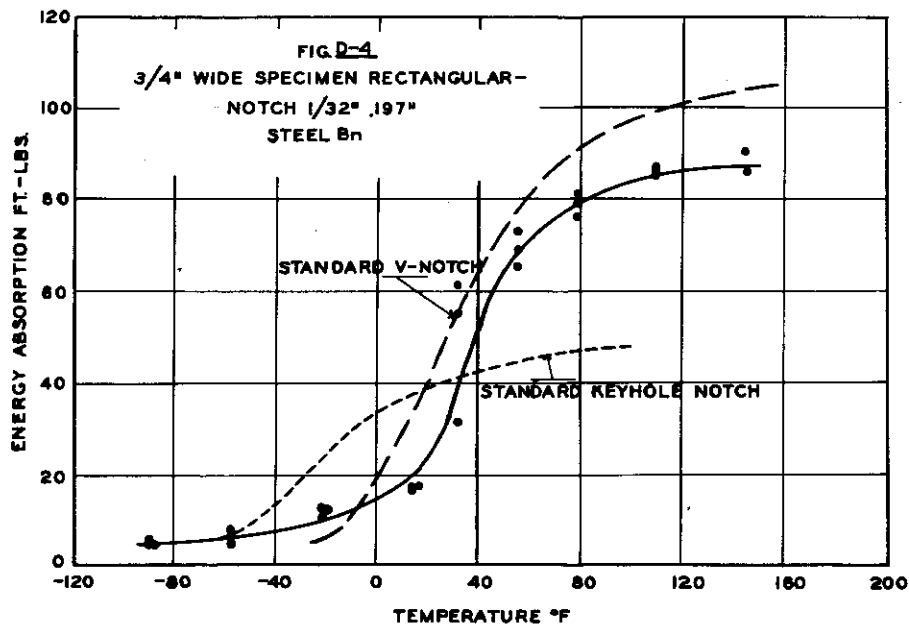
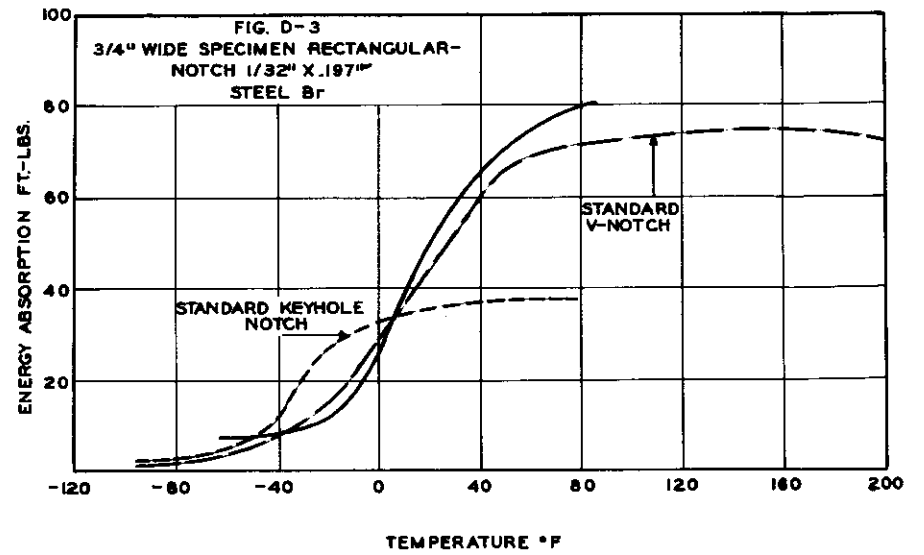
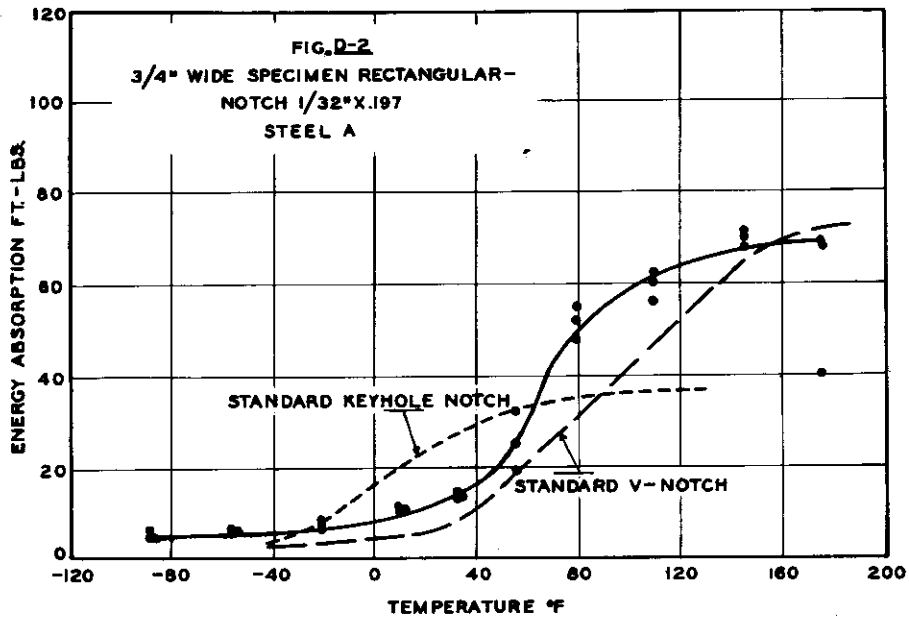


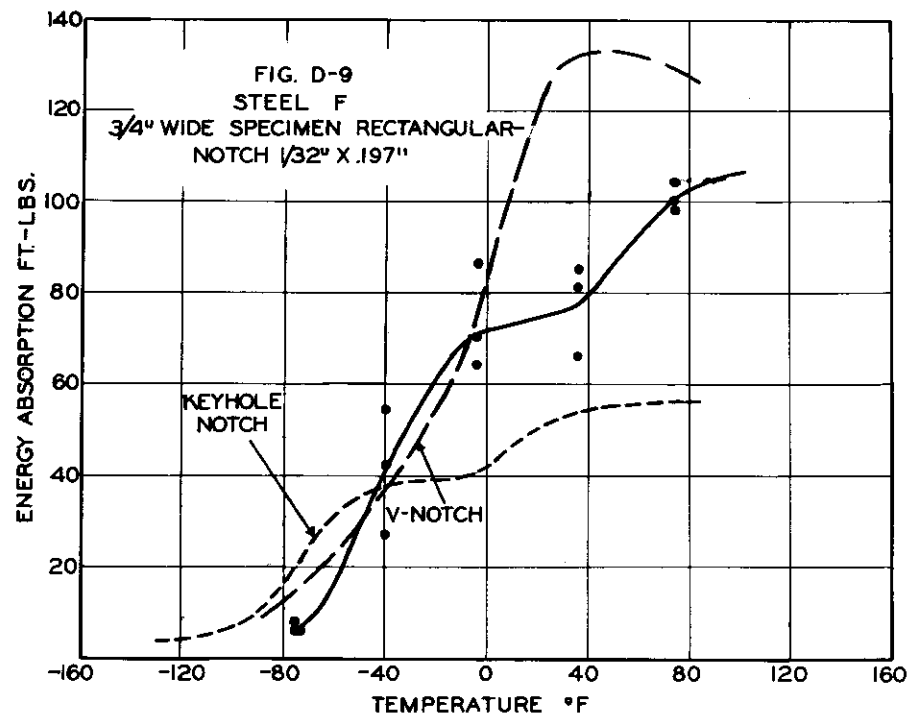
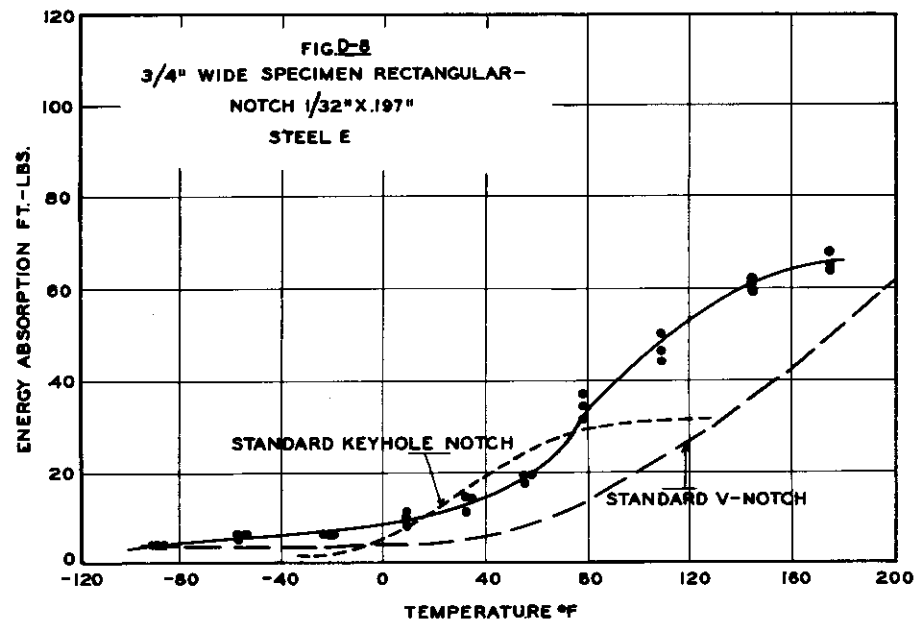
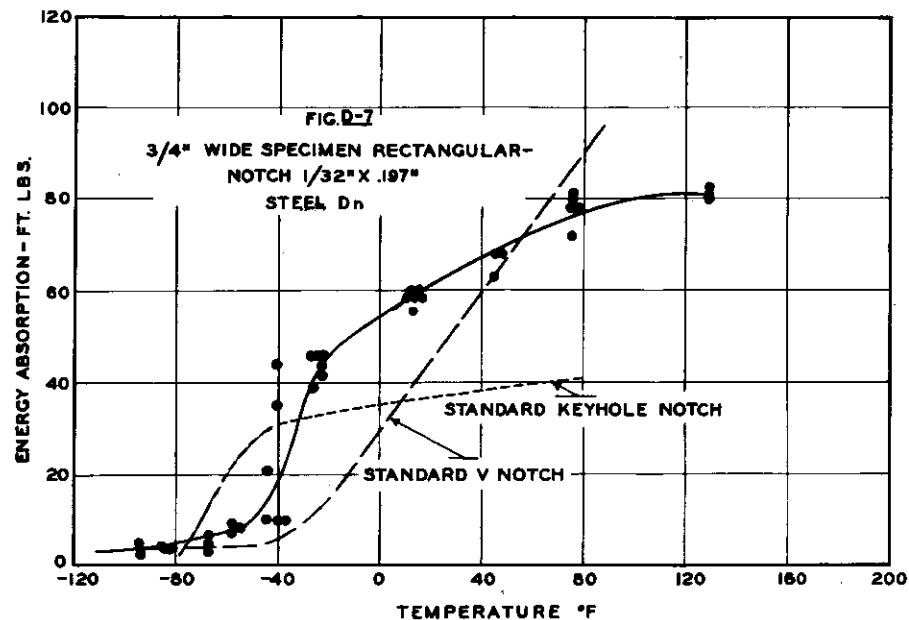
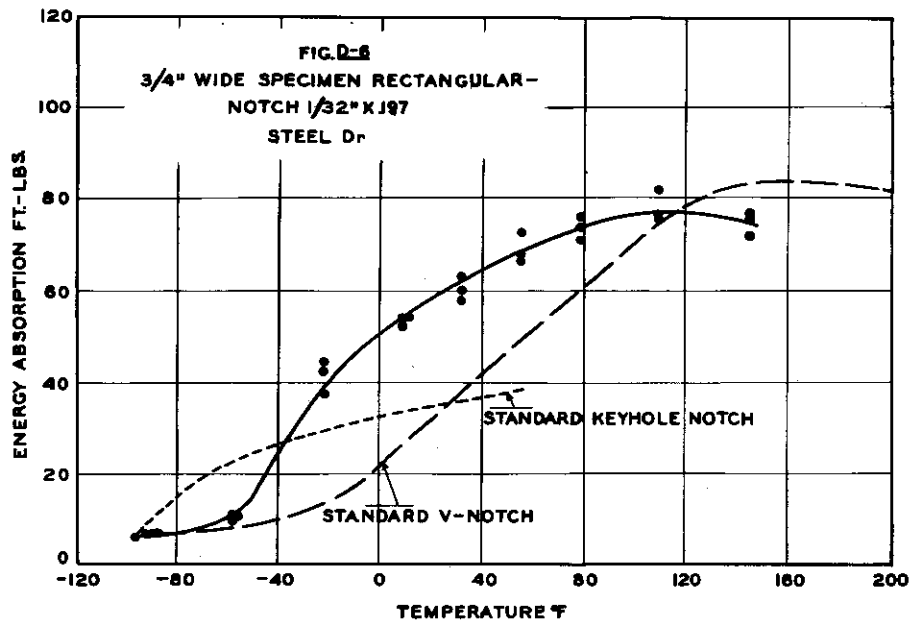












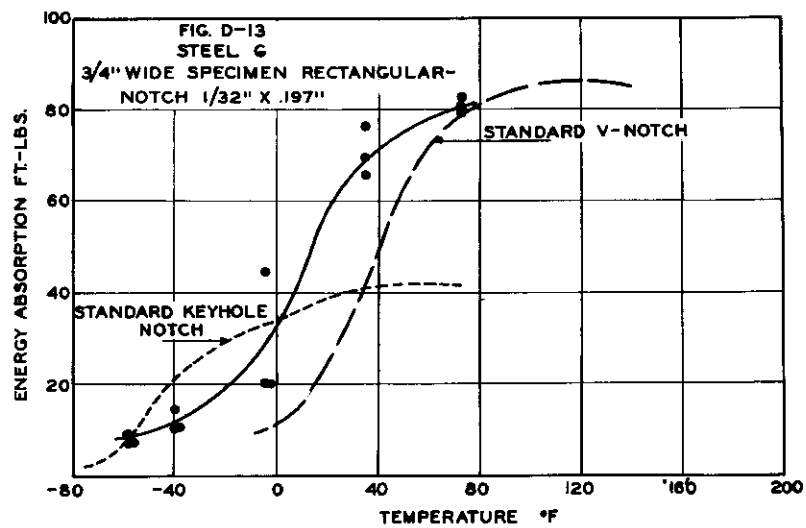
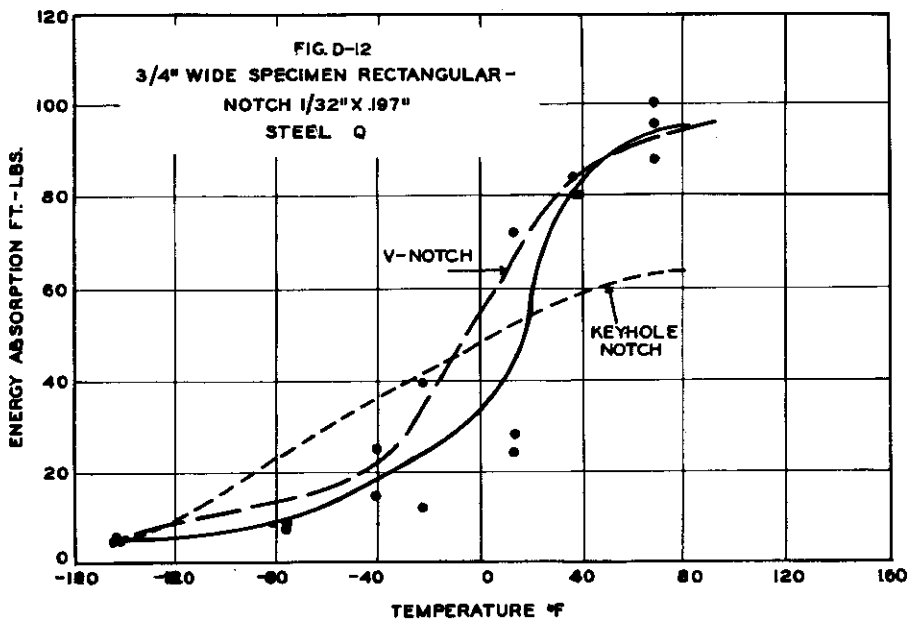
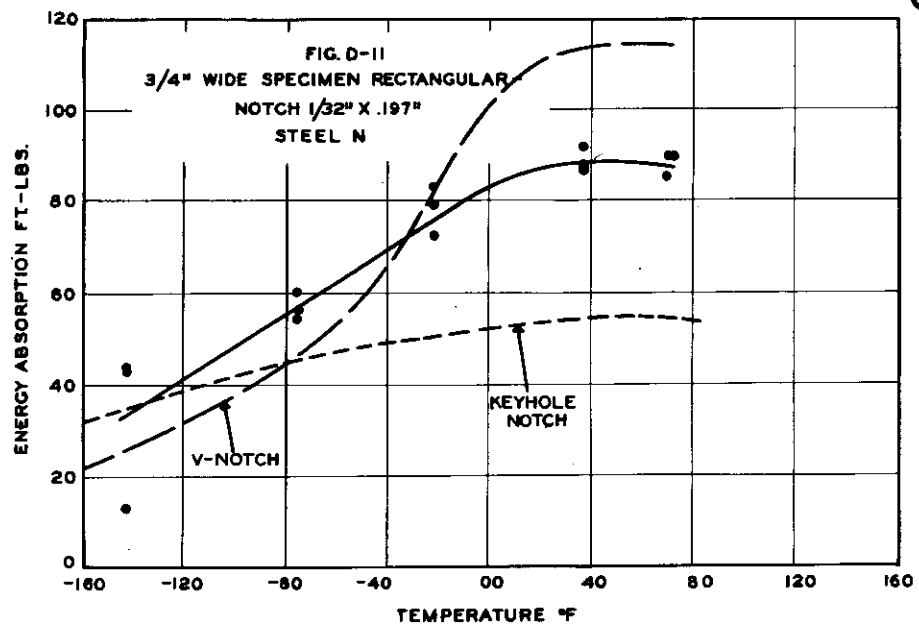
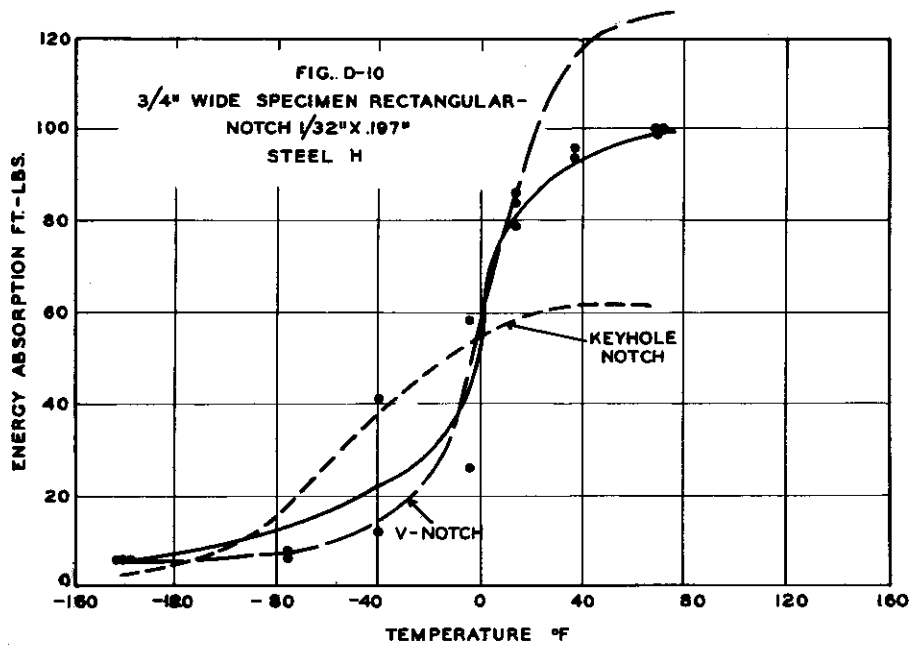


FIG. D-a

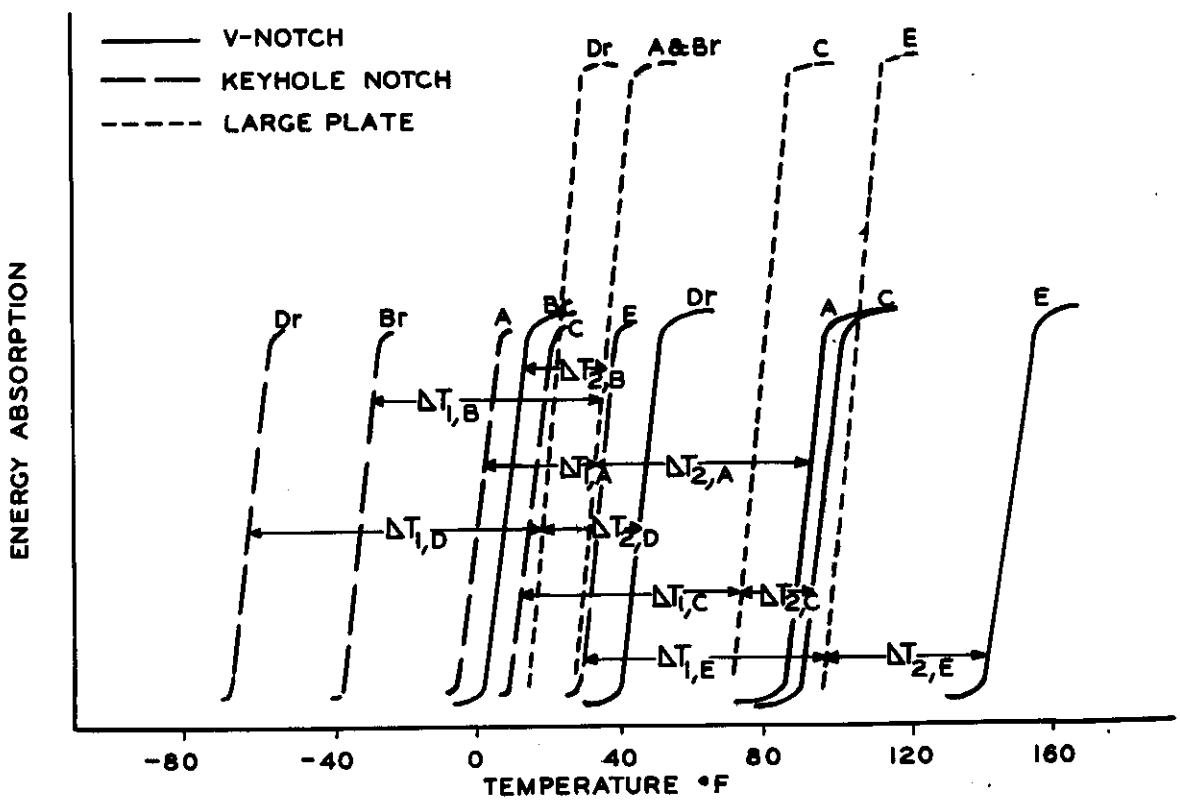
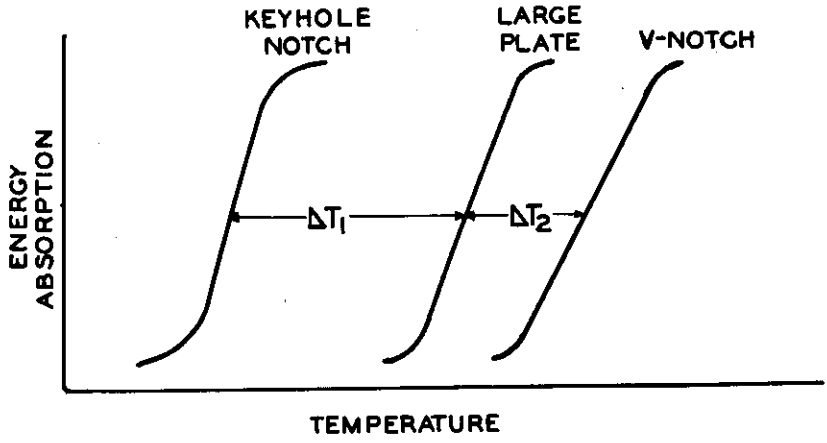
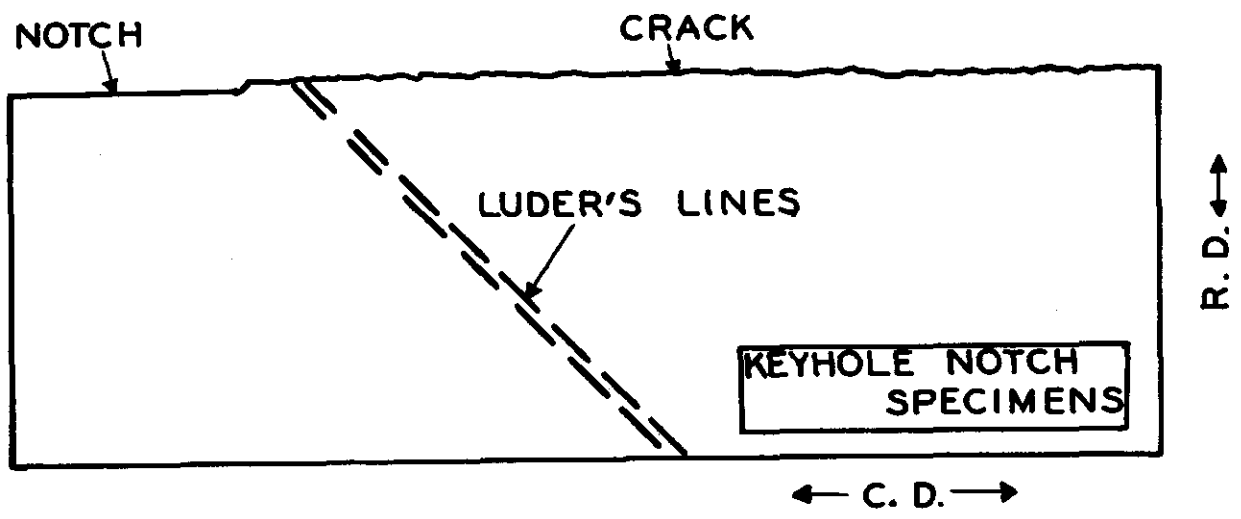
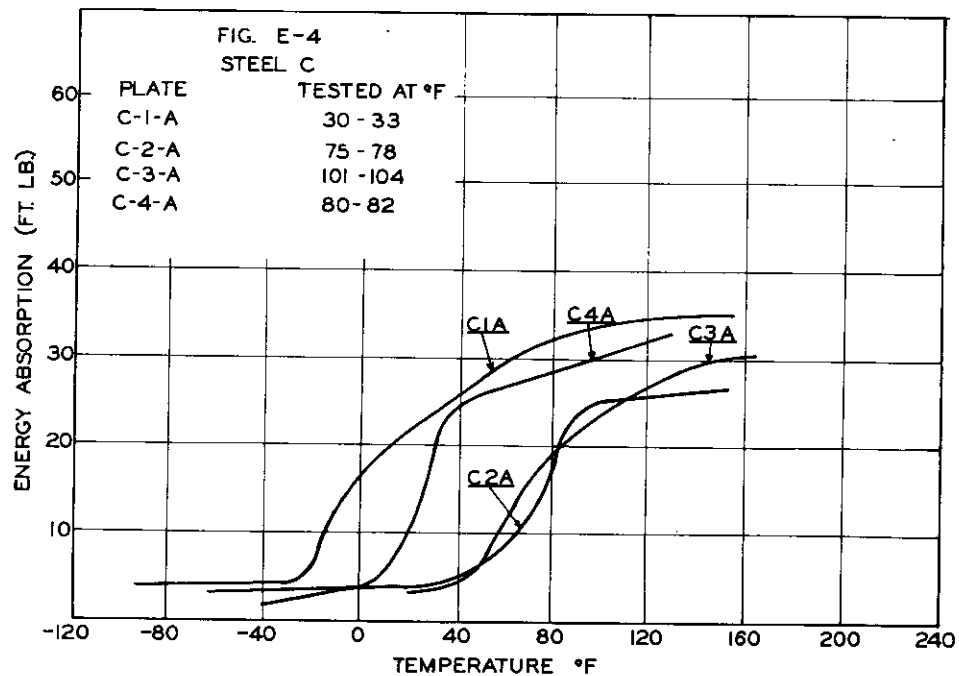
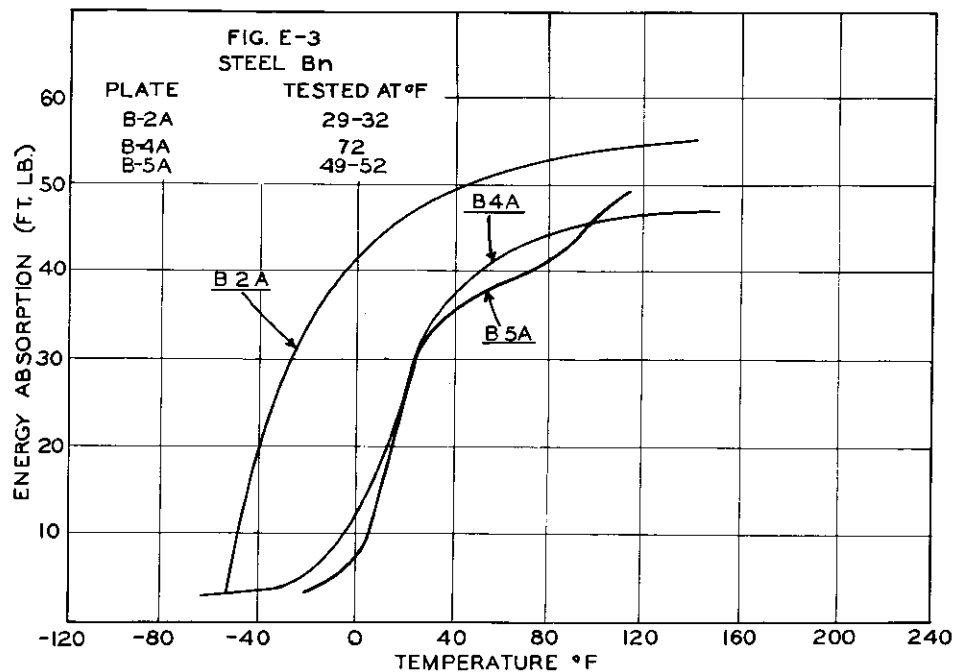
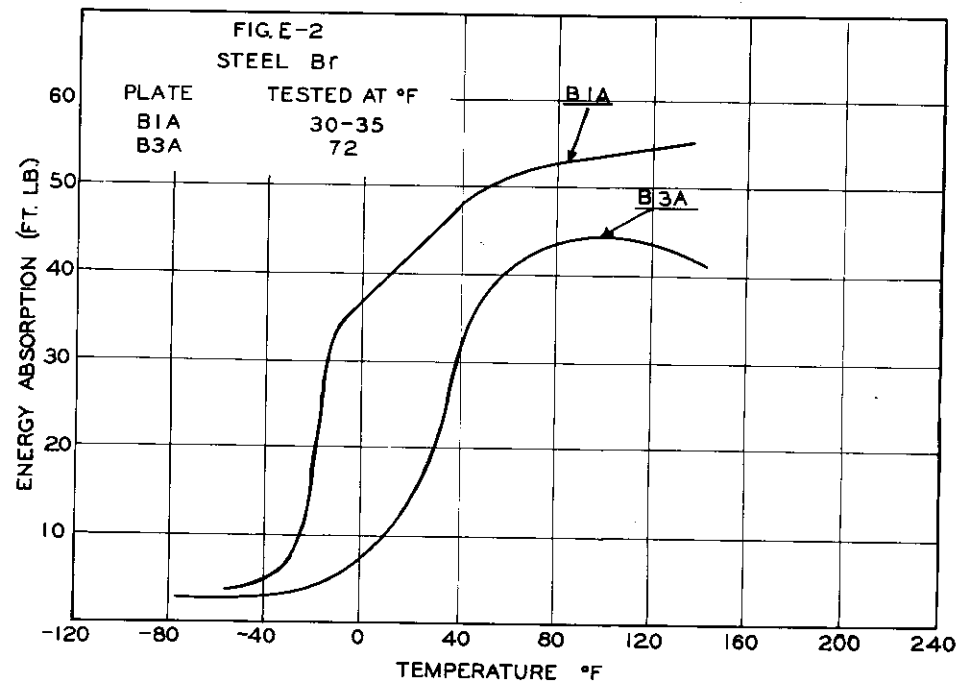
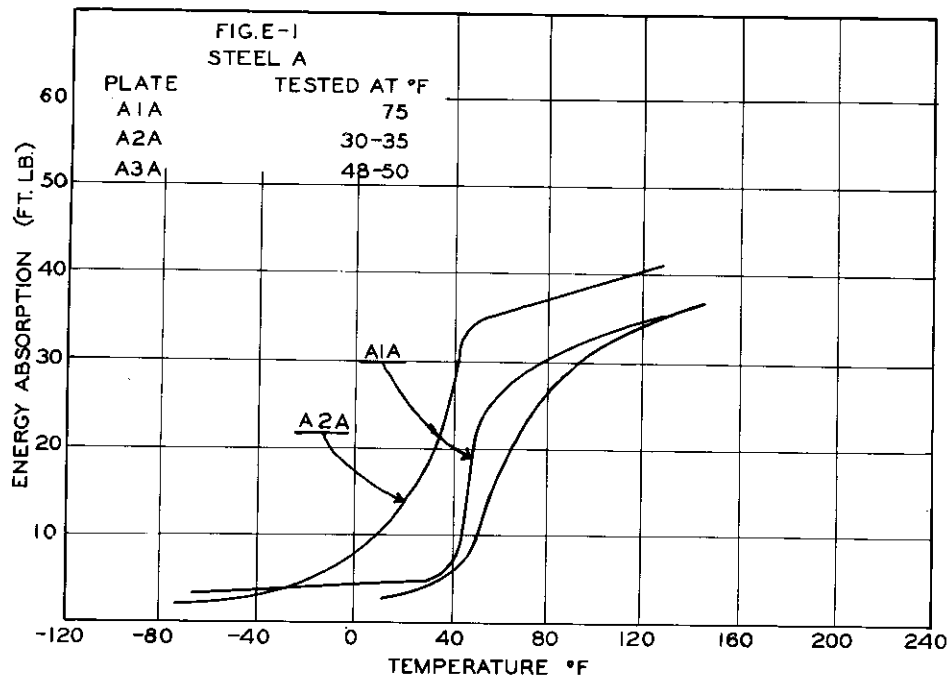
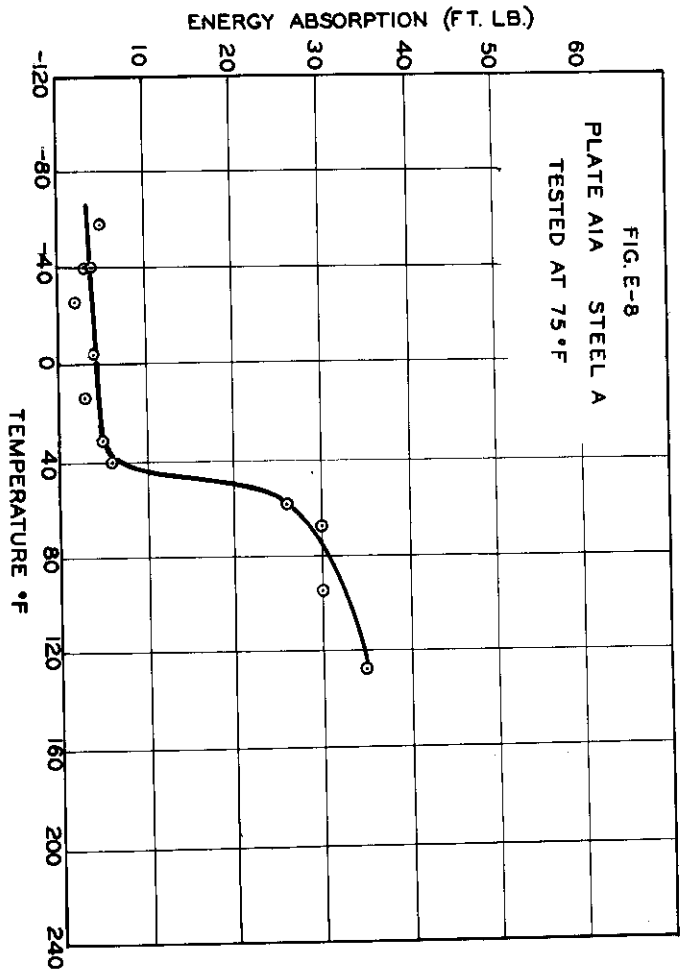
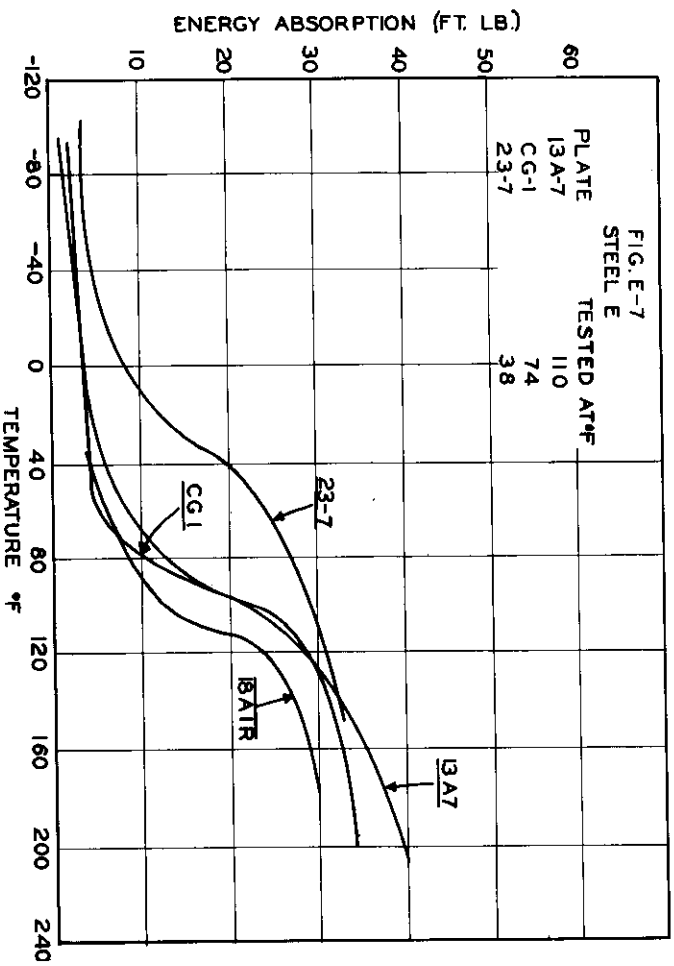
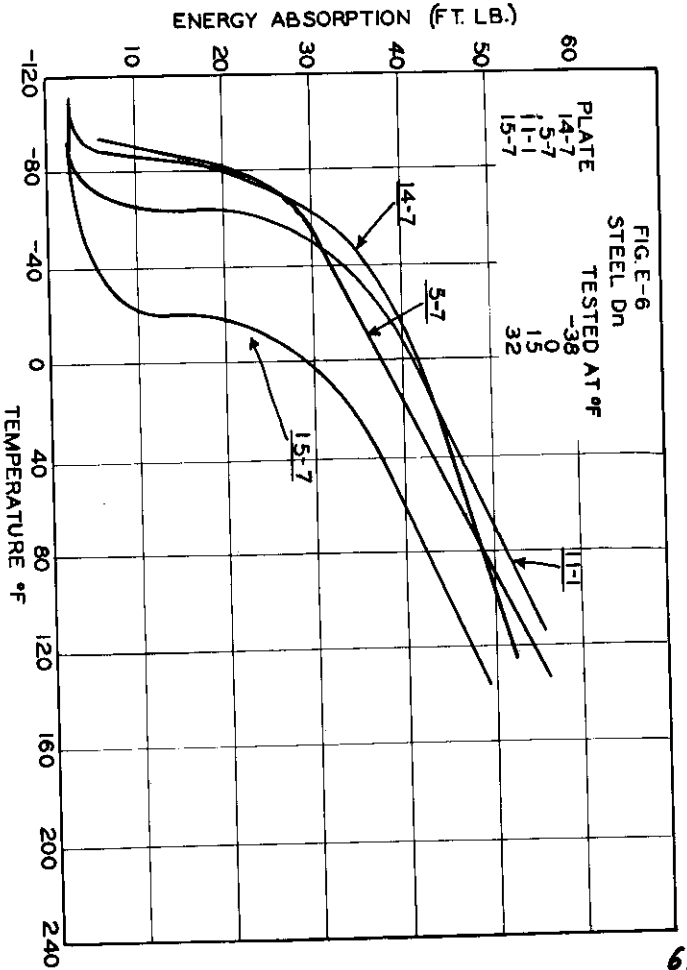
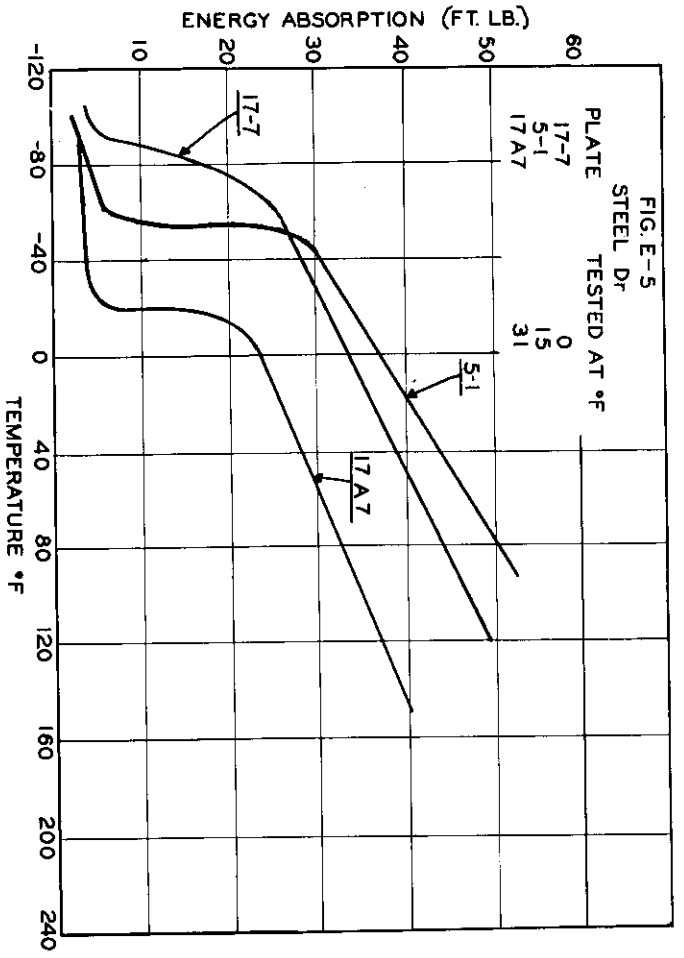


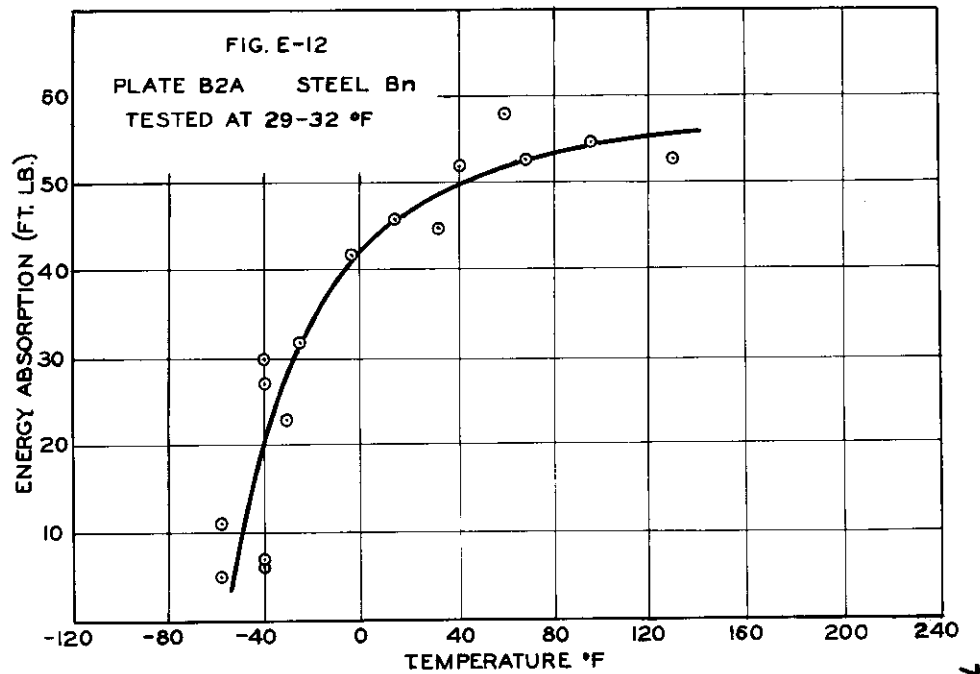
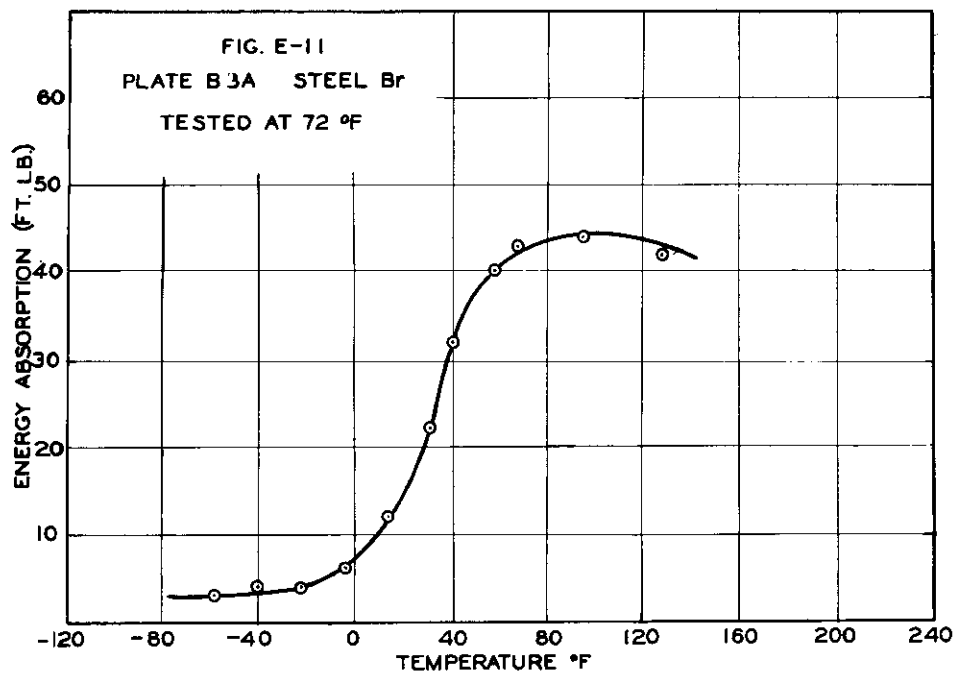
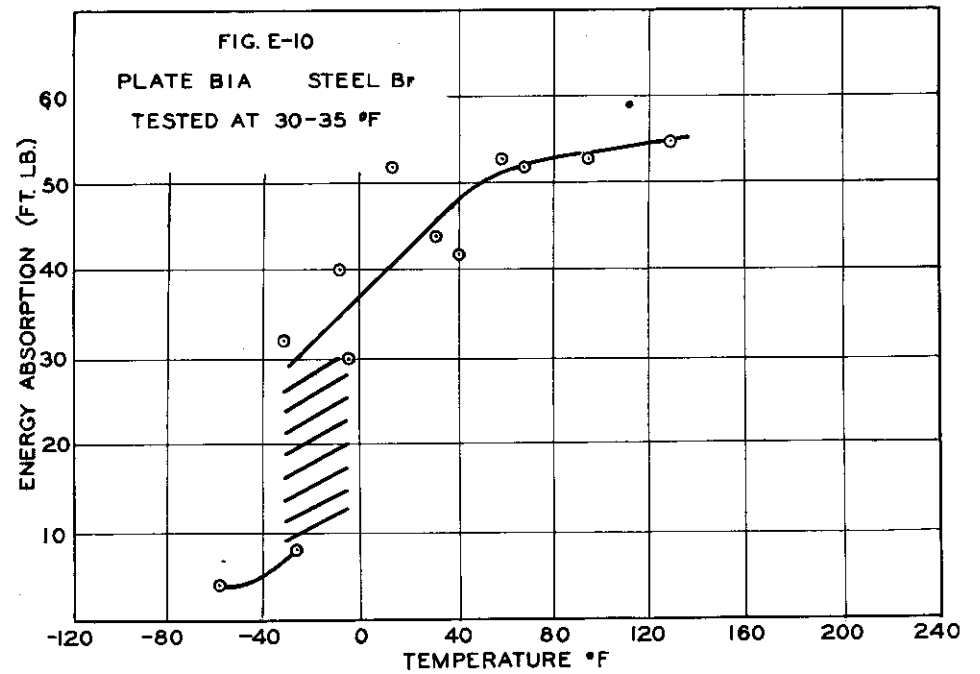
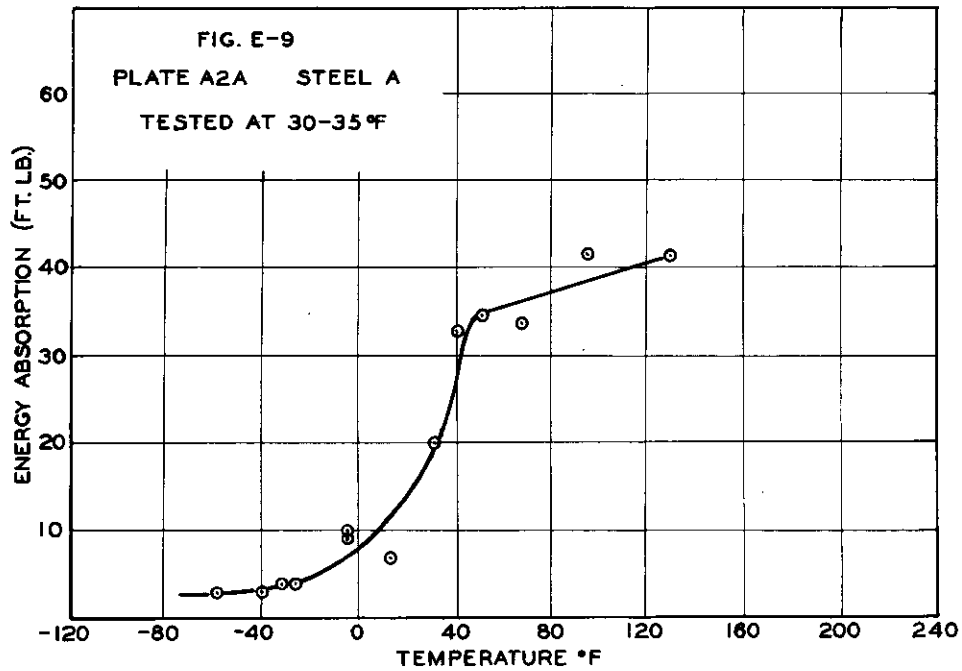
FIG. D-b - COMPARISON OF ENERGY ABSORPTION DATA FOR STEELS OBTAINED IN LARGE PLATE AND STANDARD CHARPY TESTS.

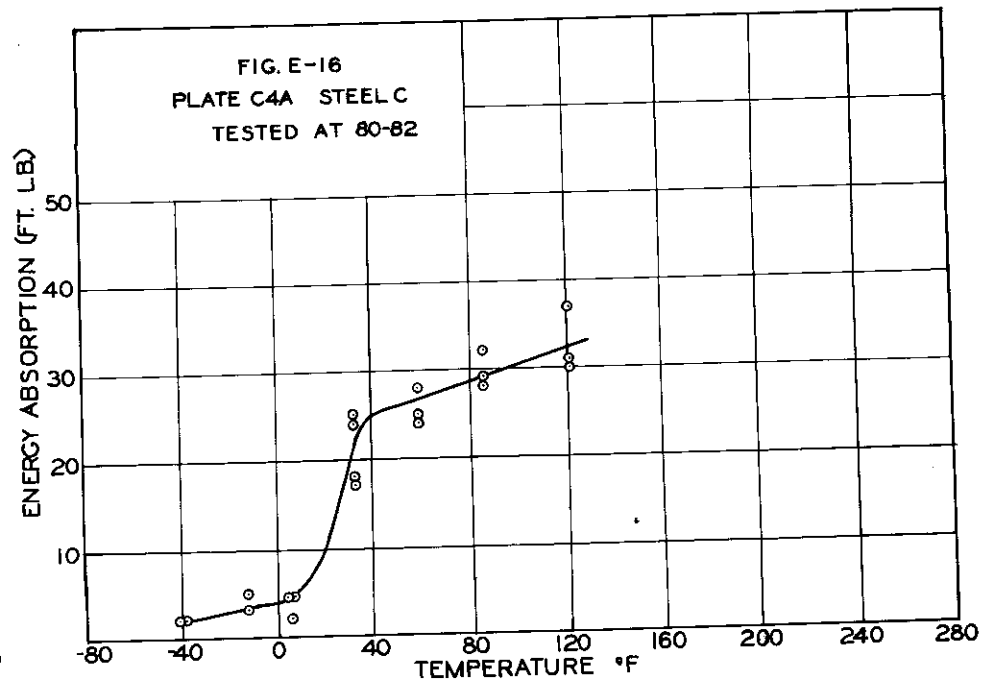
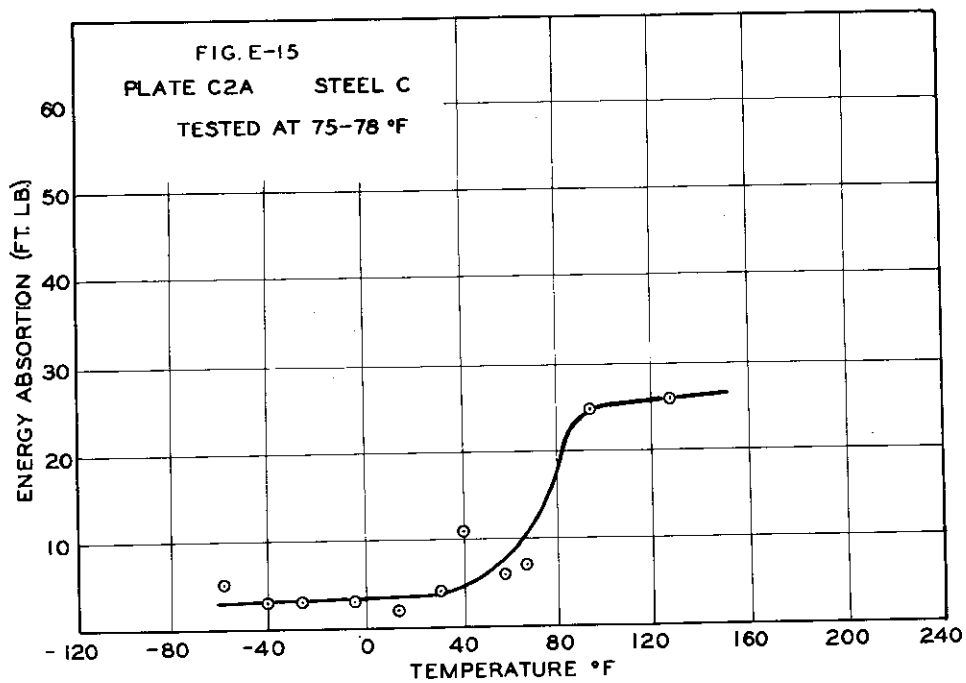
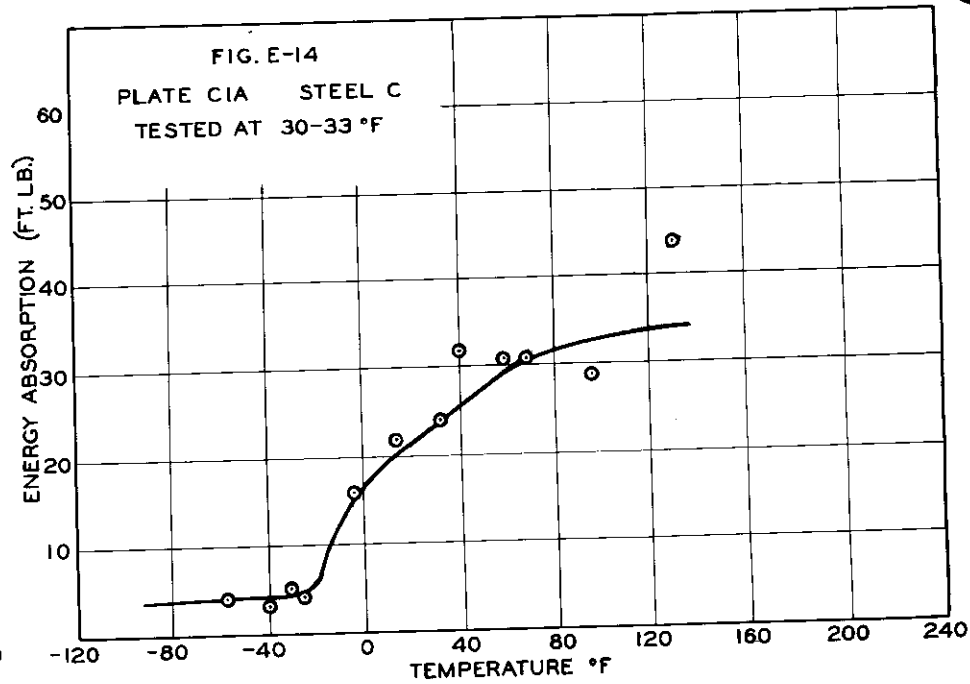
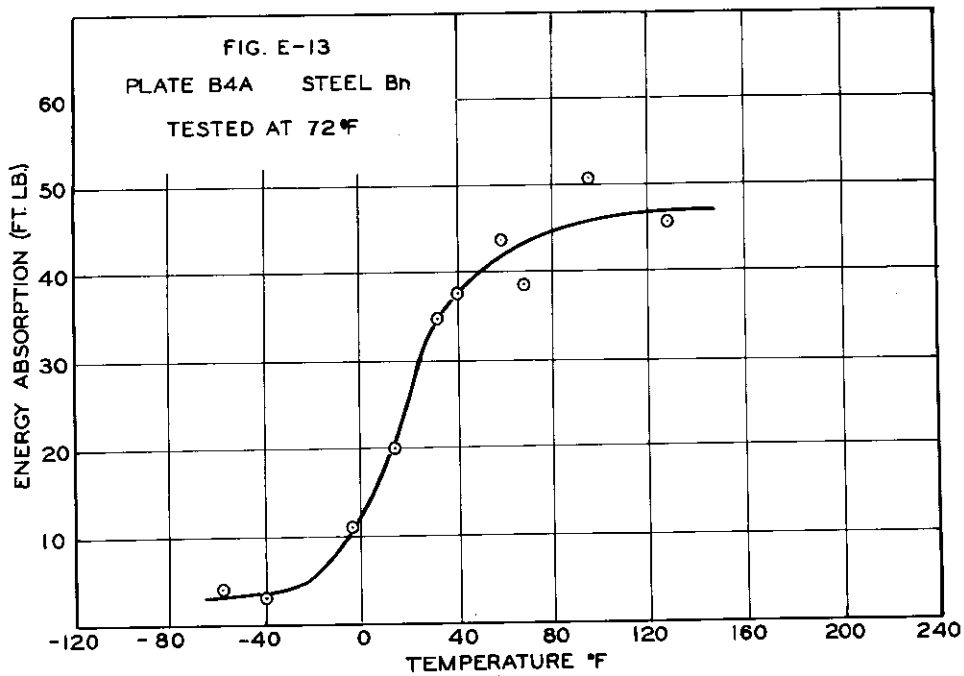
FIG. E-Δ LOCATION OF IMPACT SPECIMENS
IN LARGE PLATE SECTIONS.

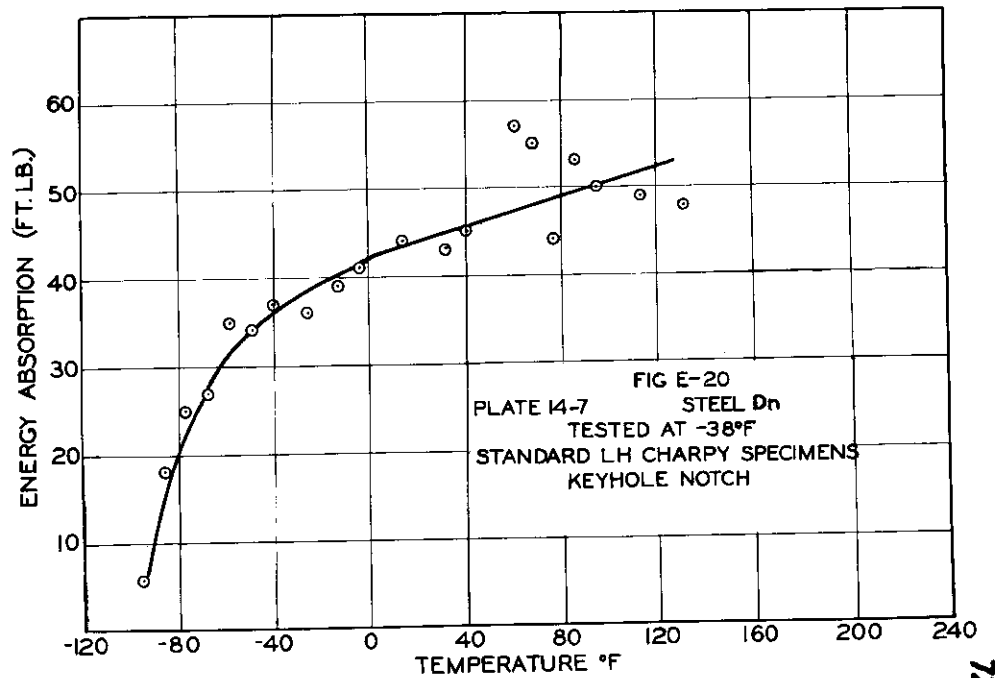
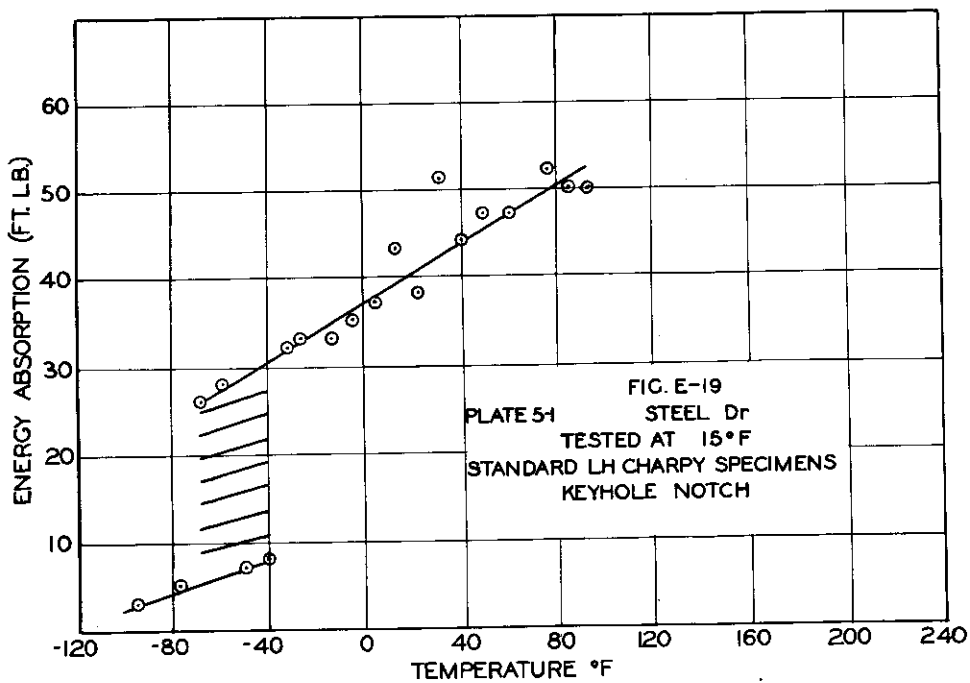
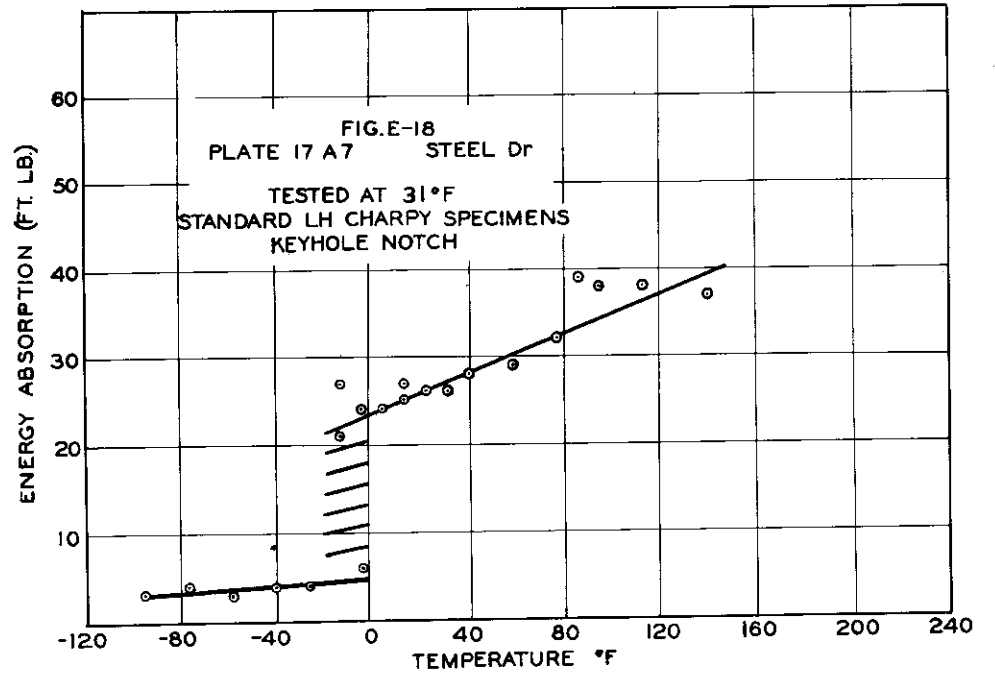
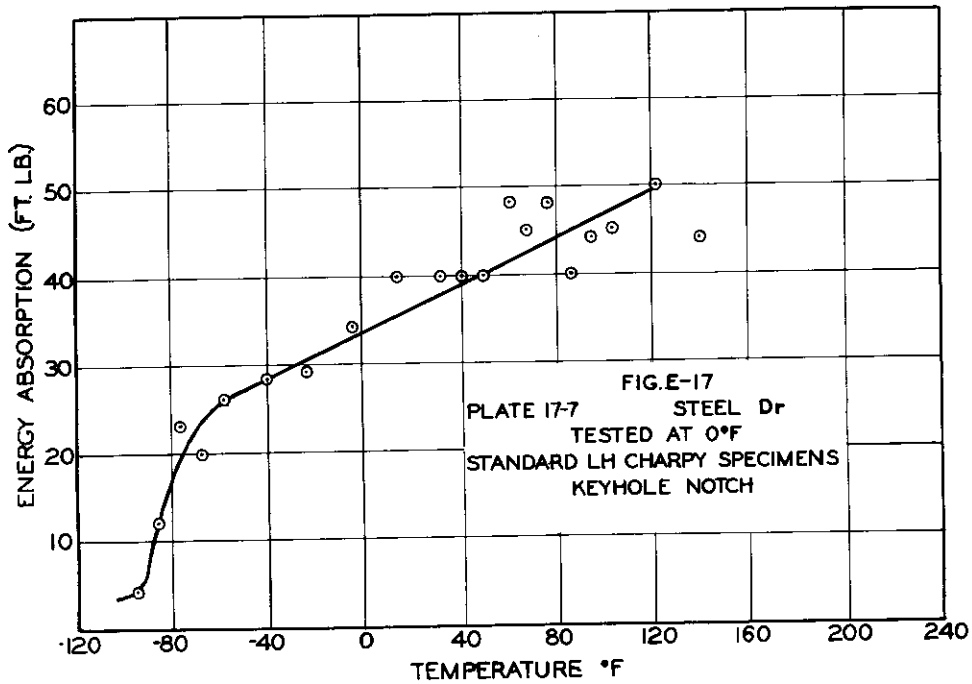


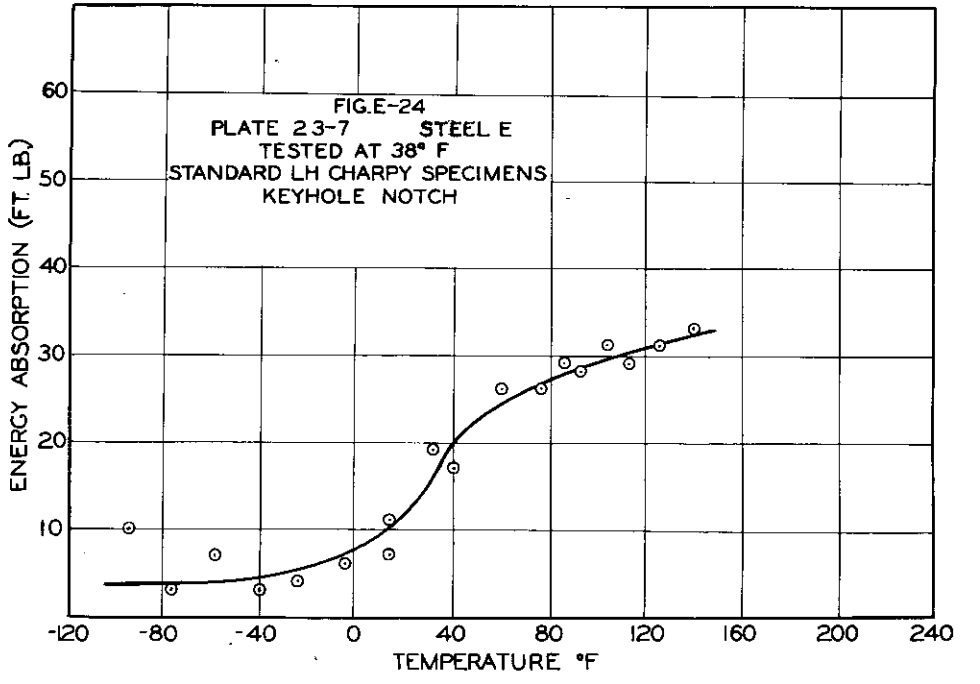
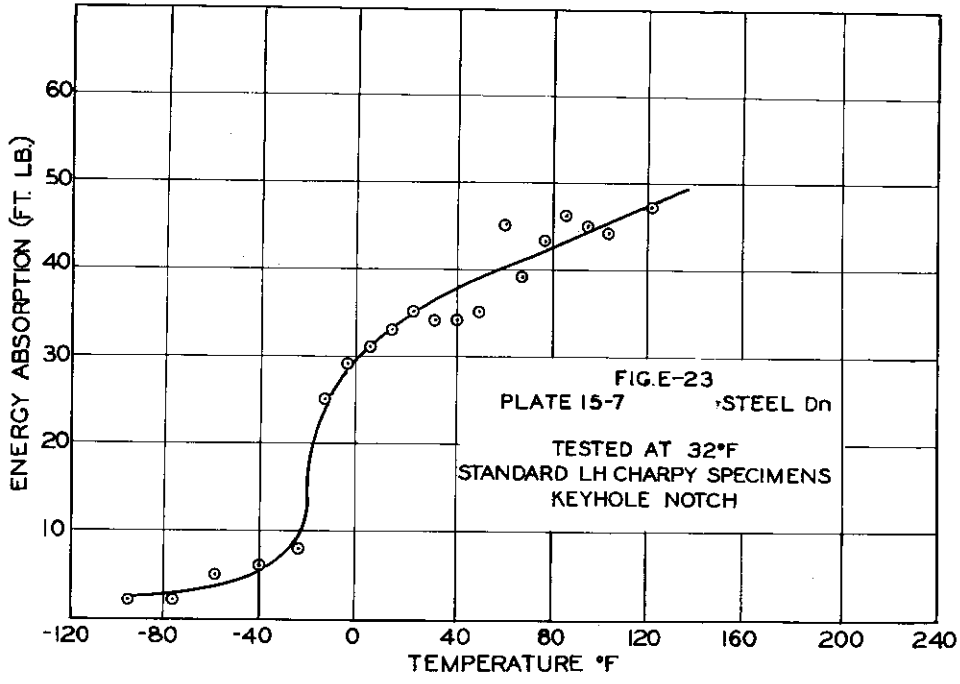
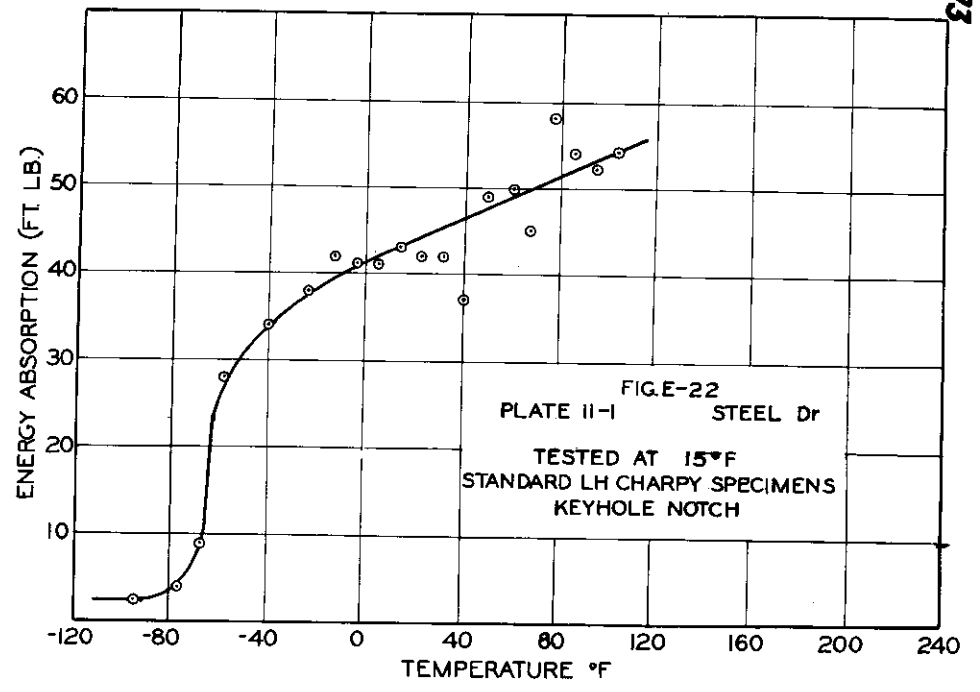
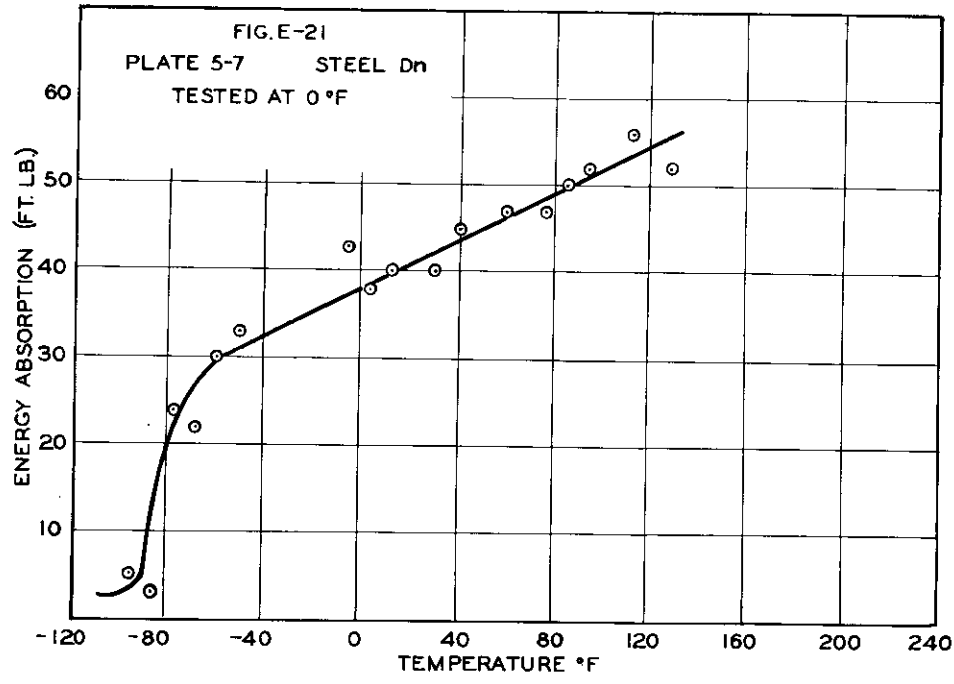


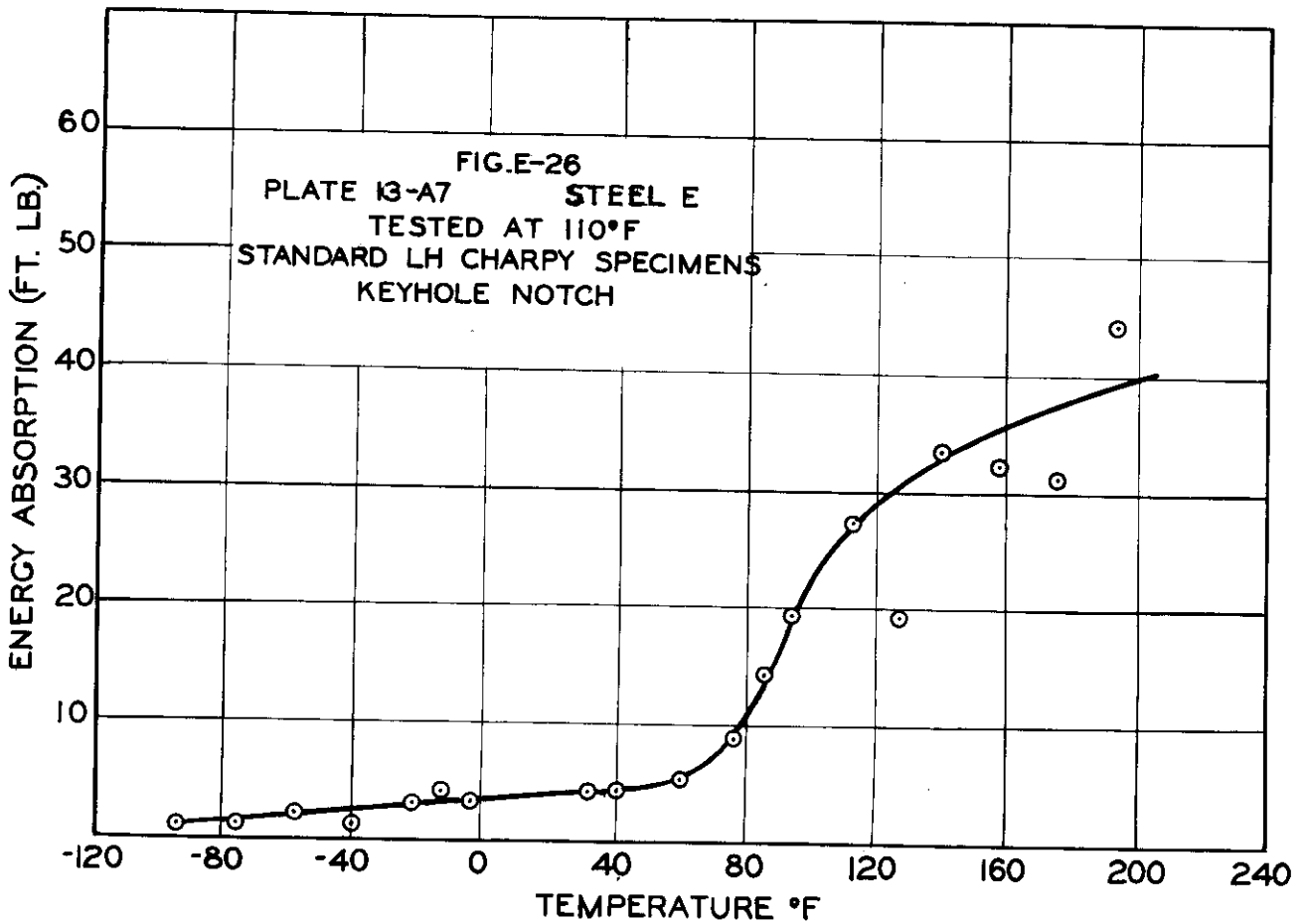
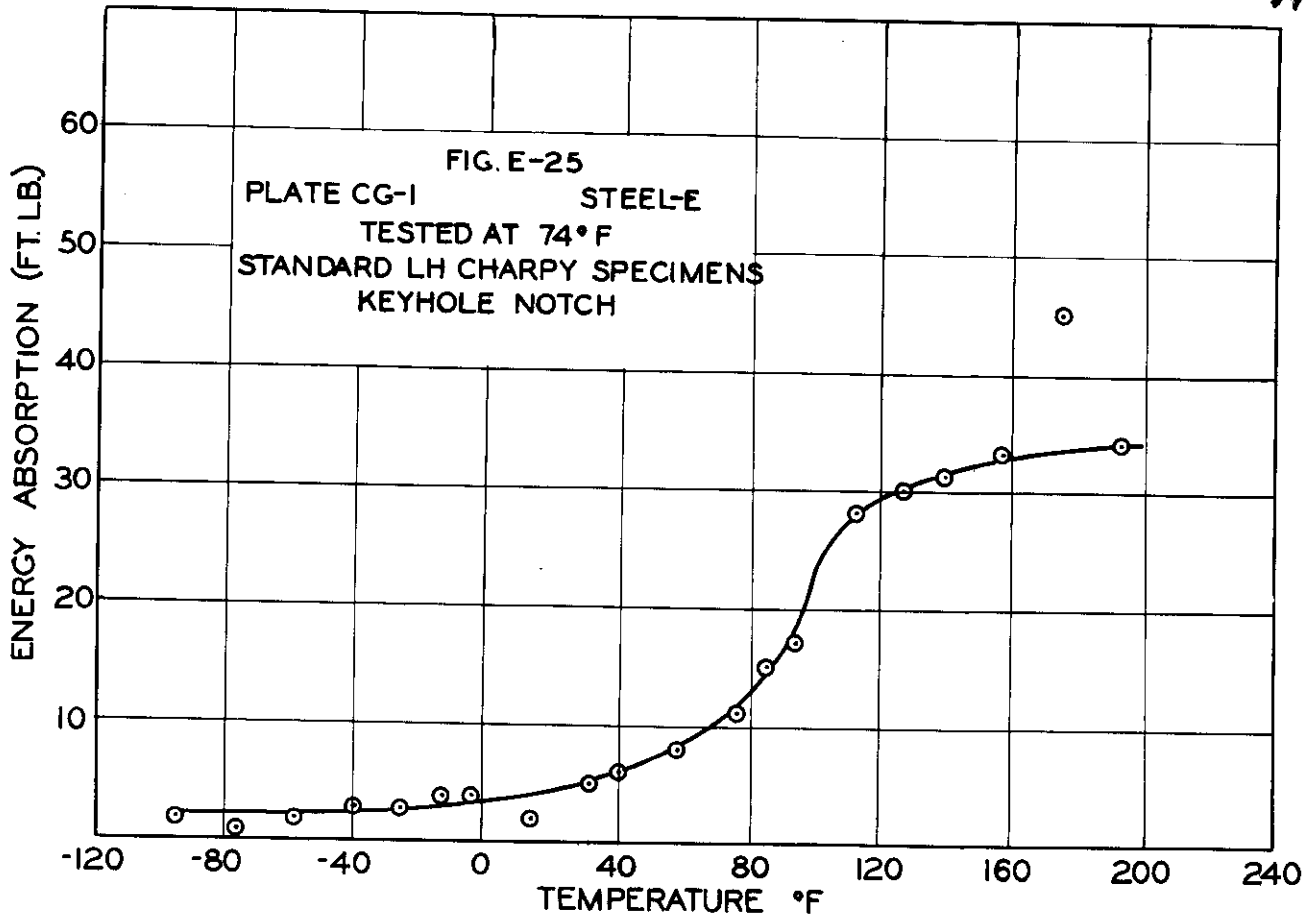


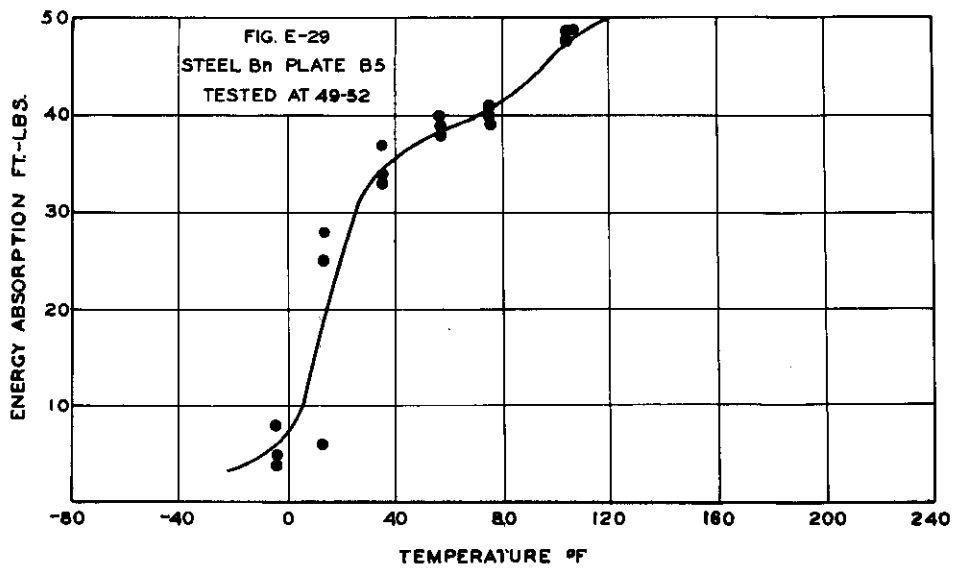
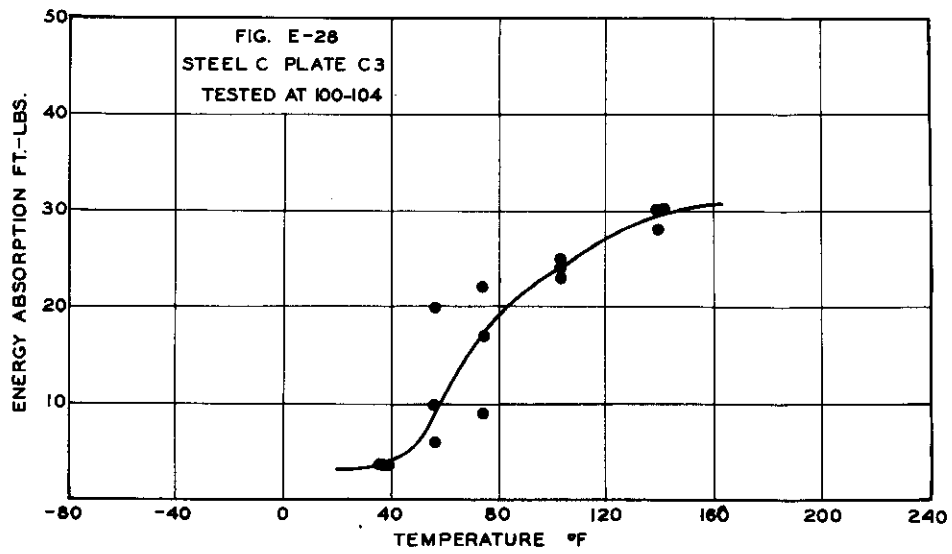
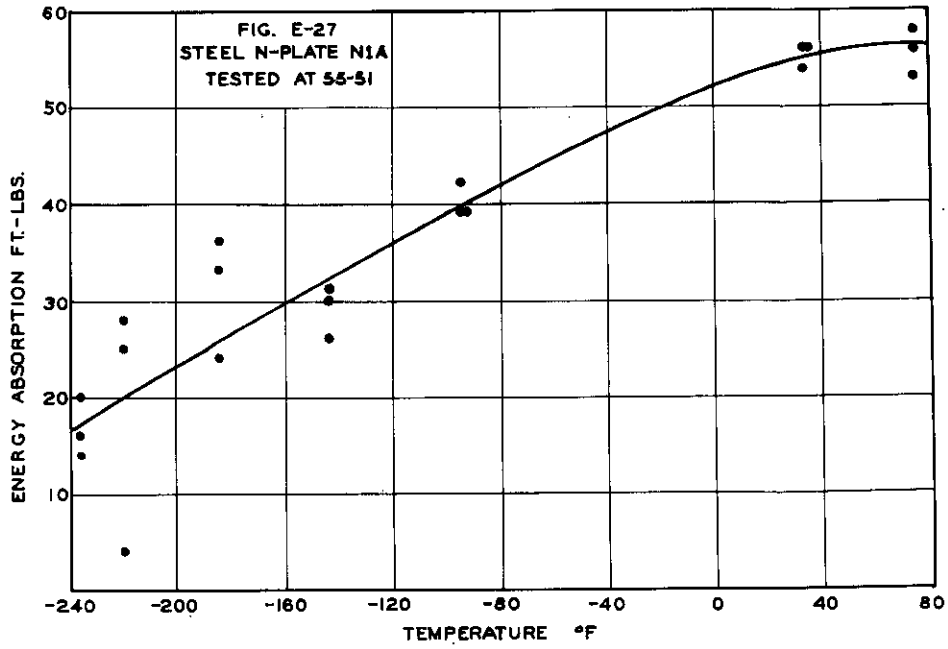


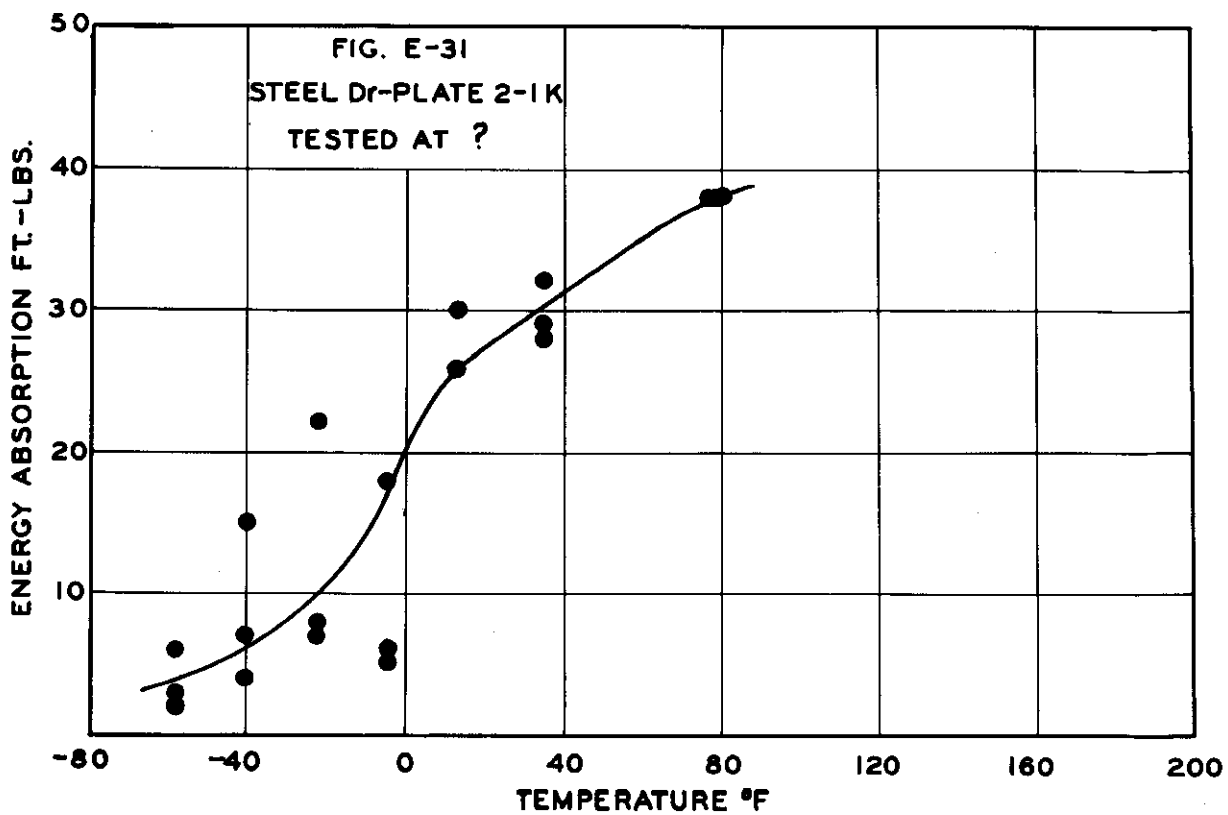
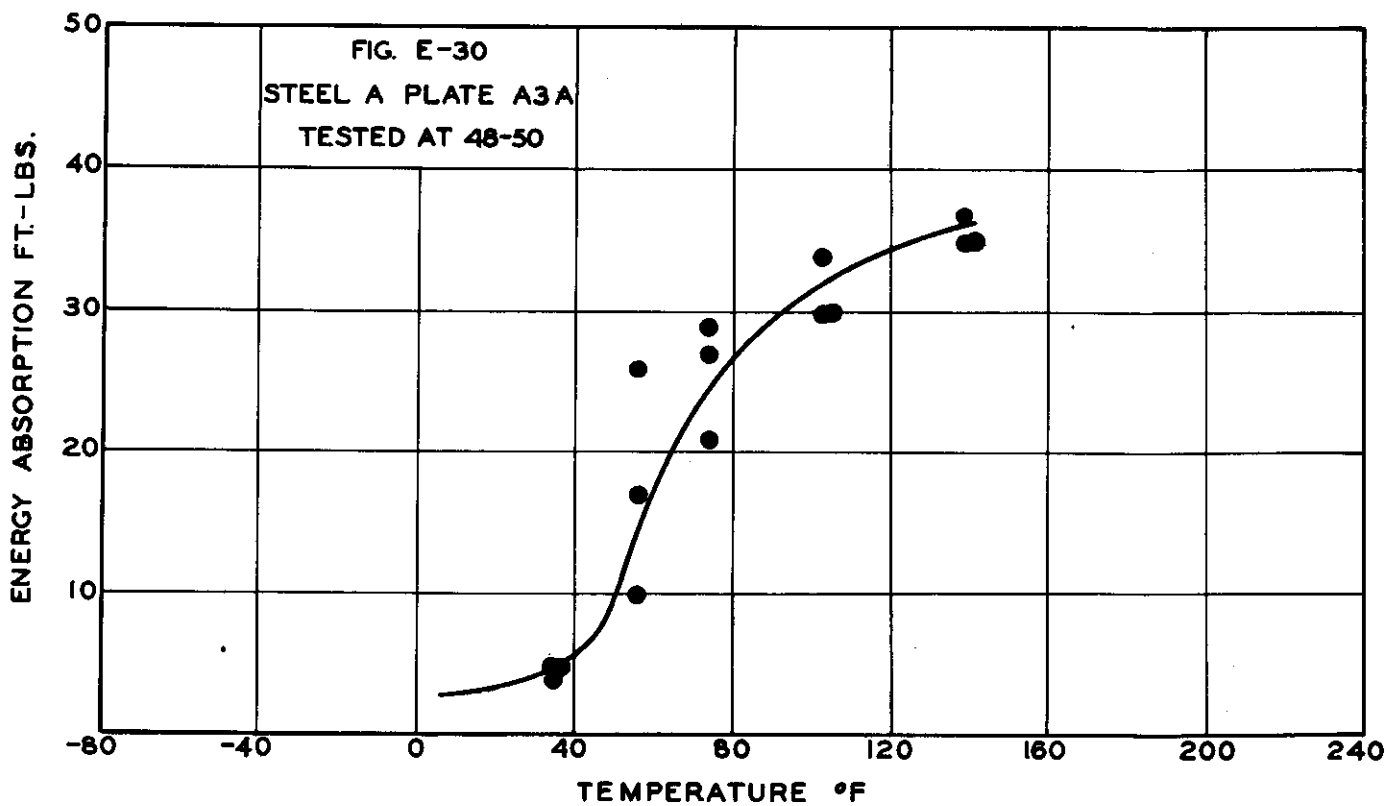


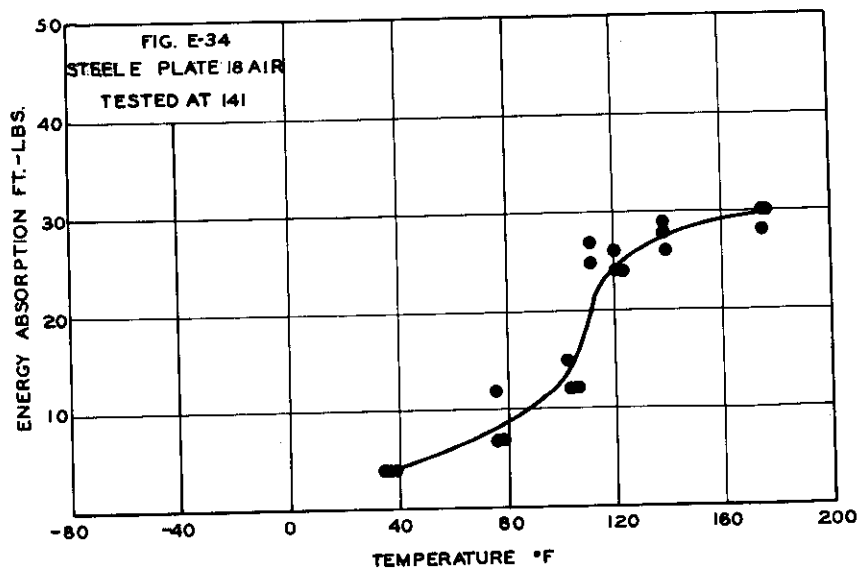
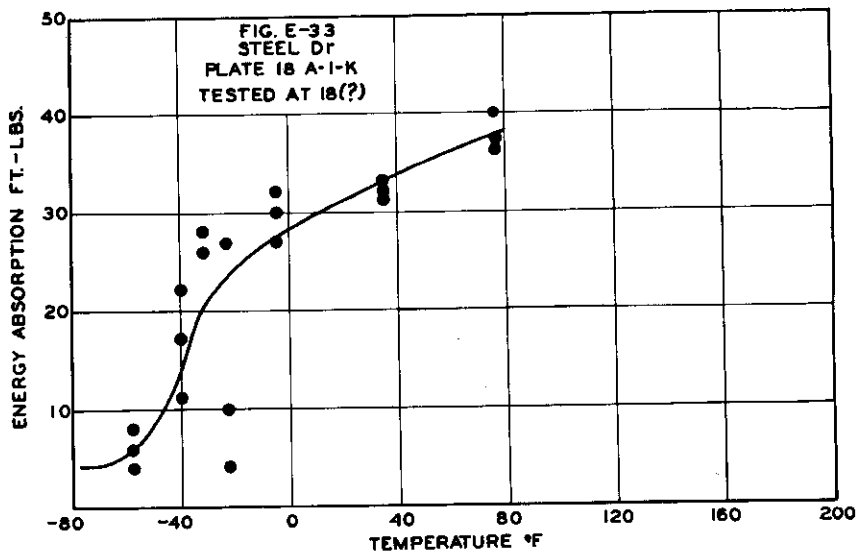
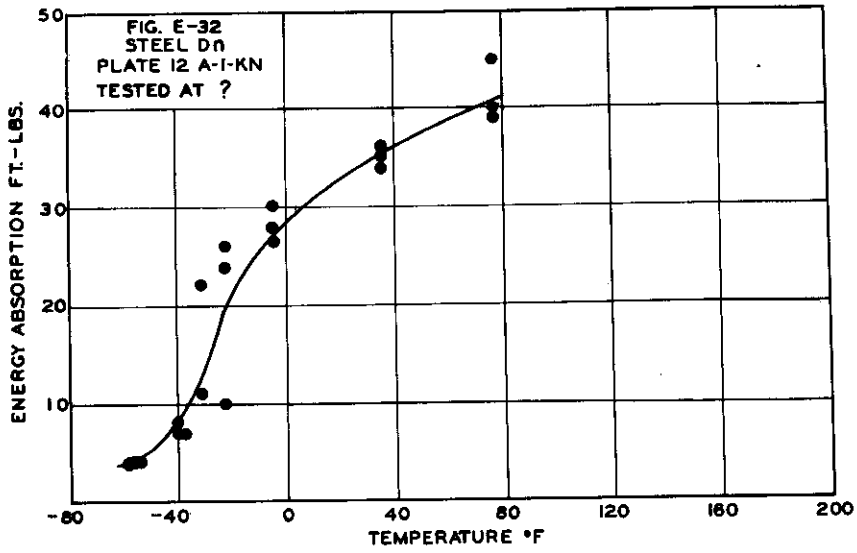


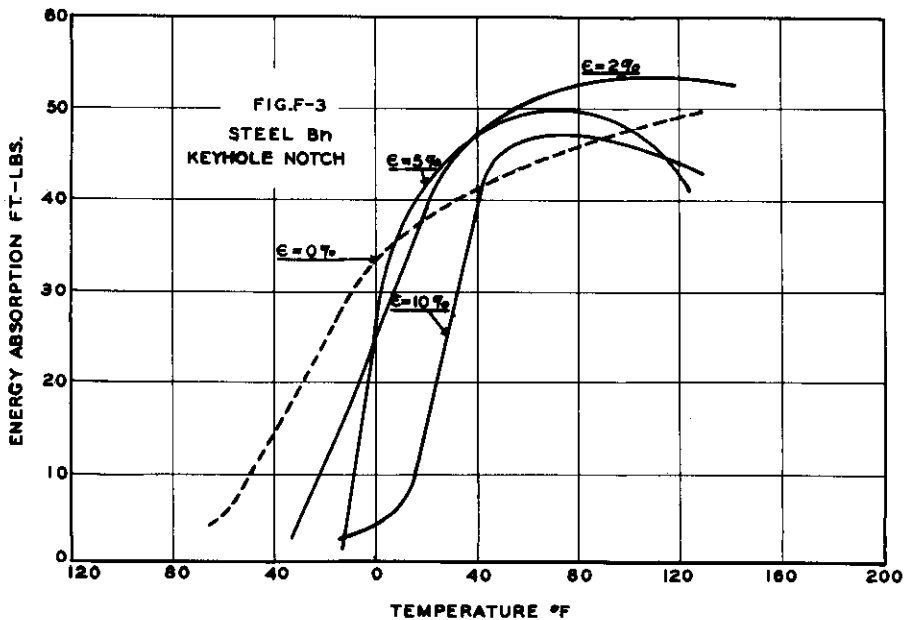
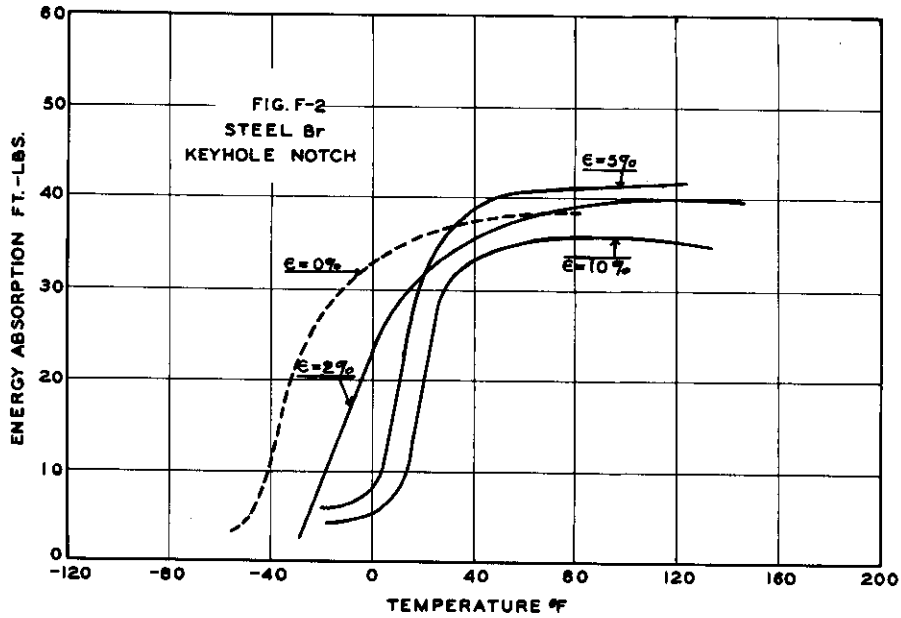
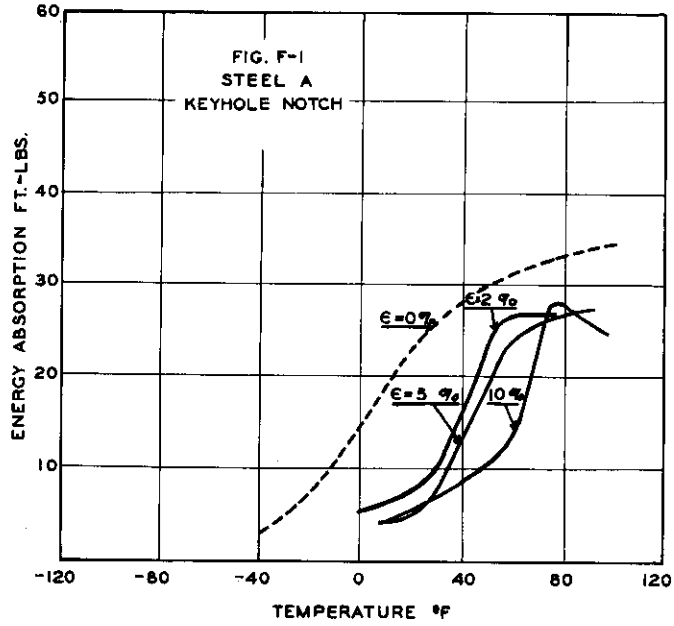


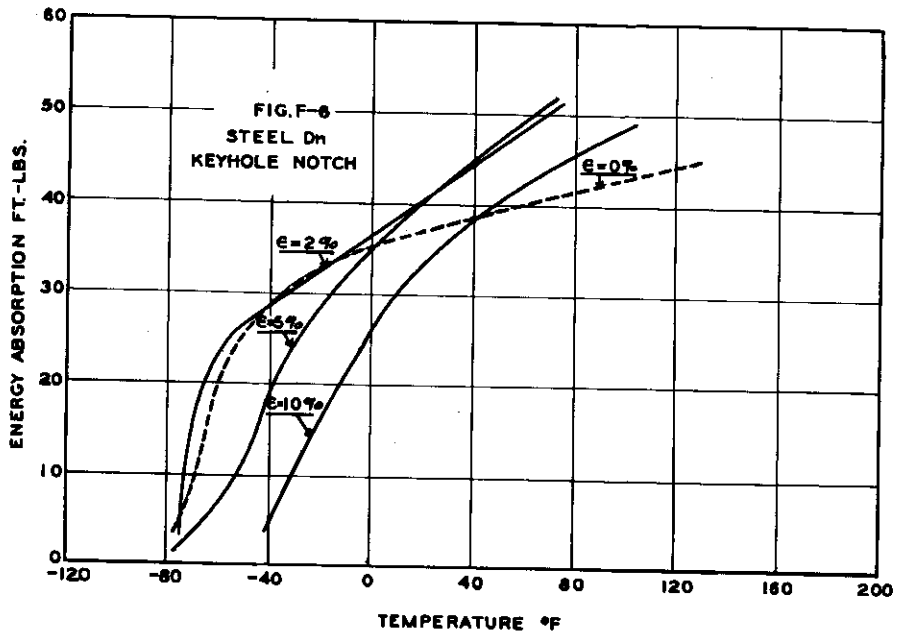
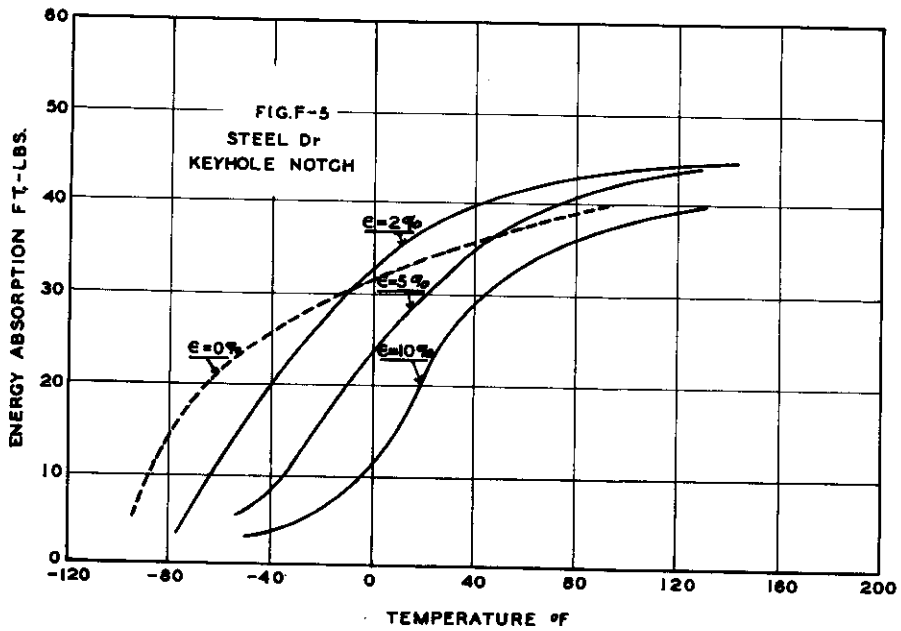
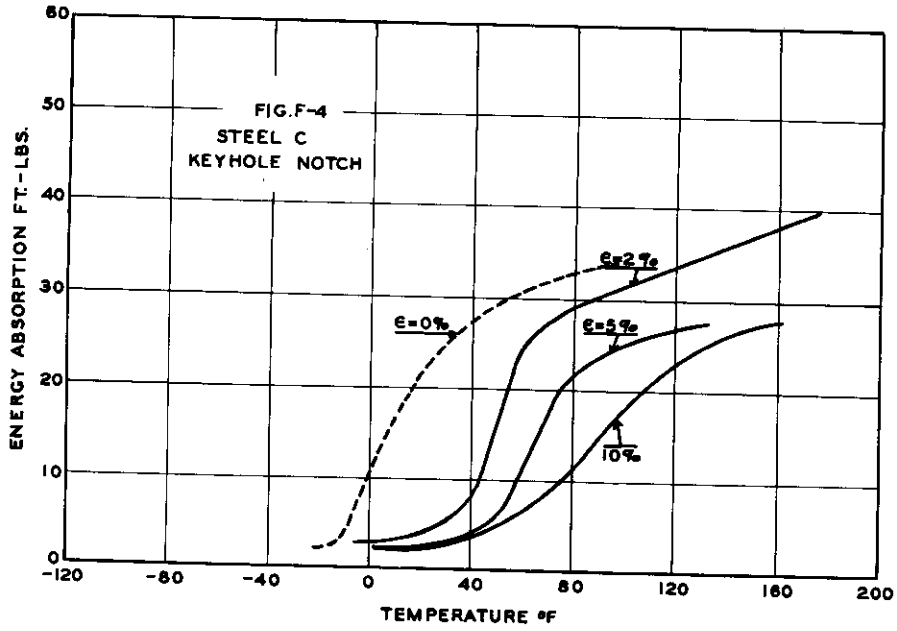


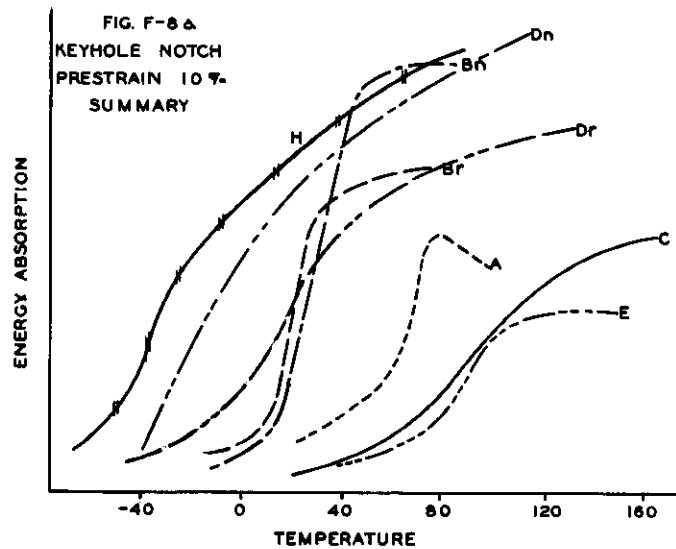
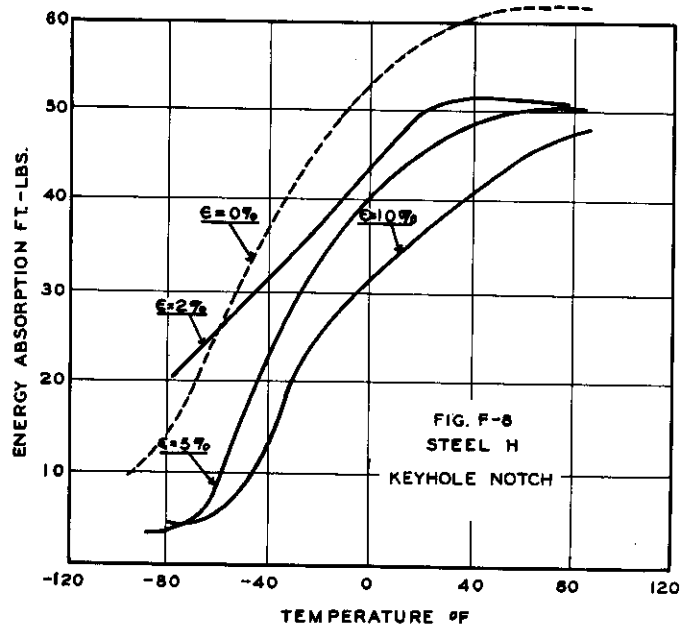
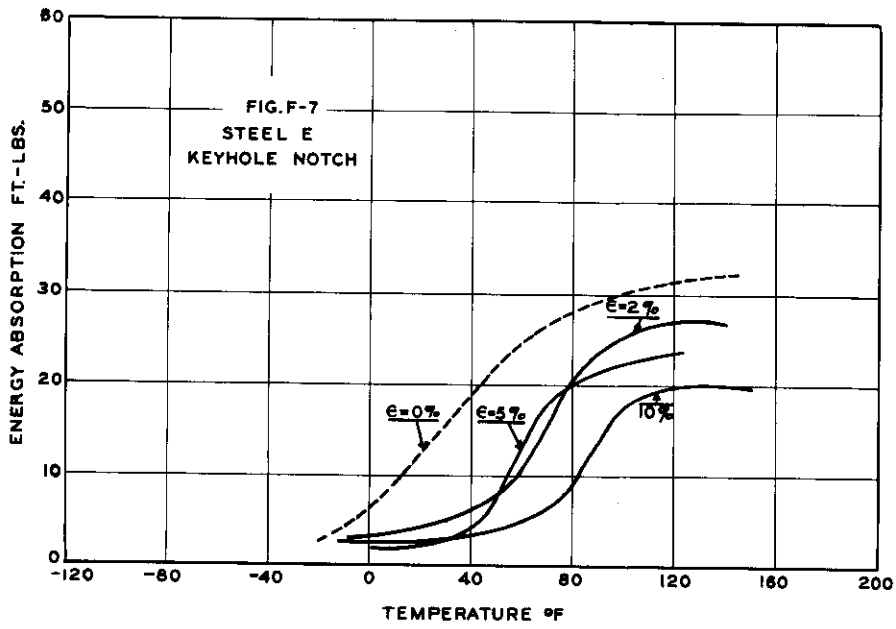


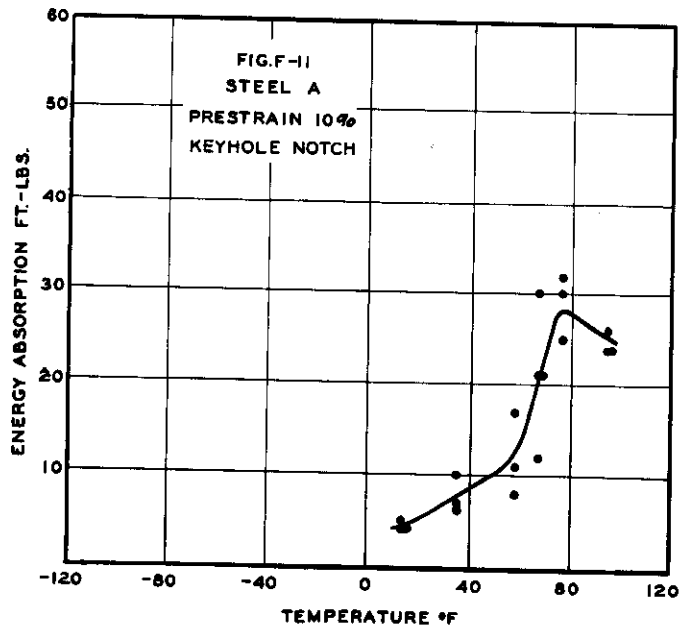
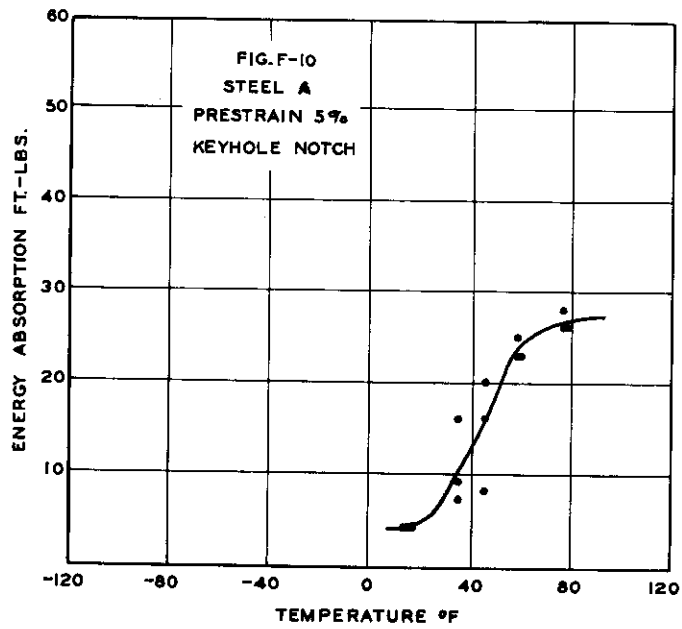
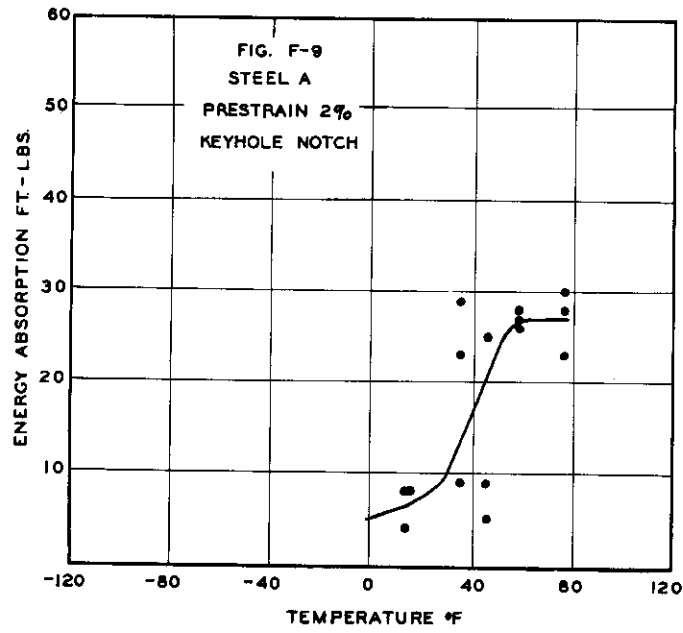


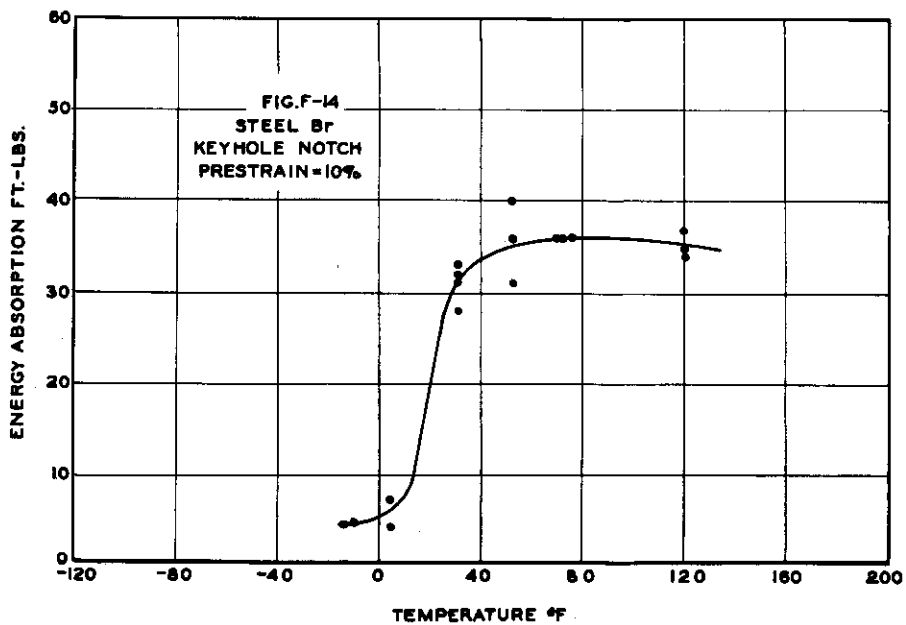
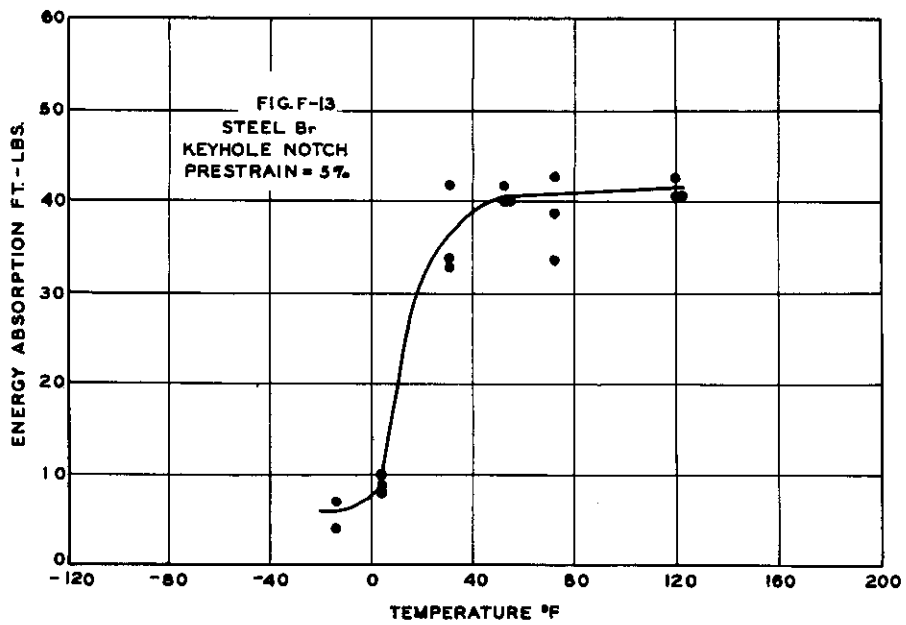
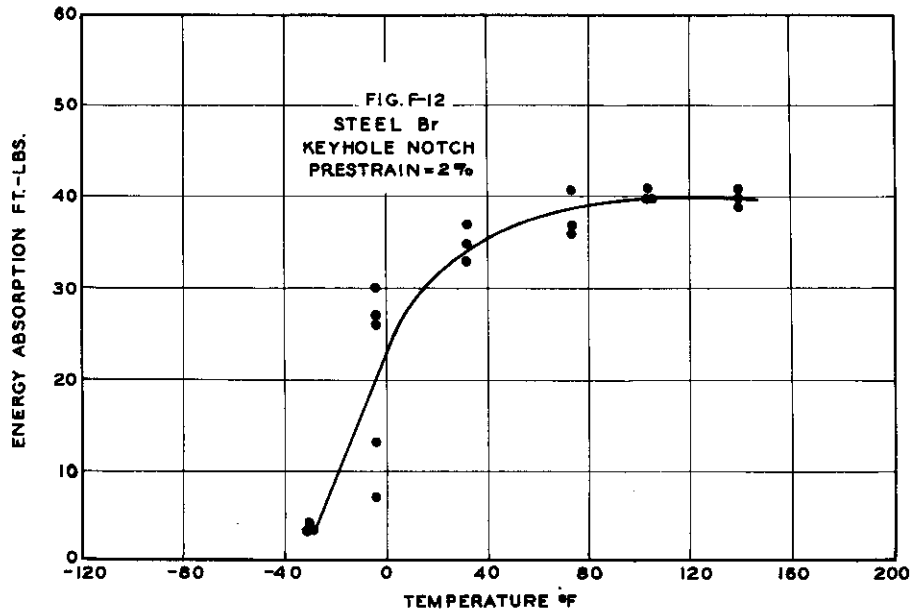


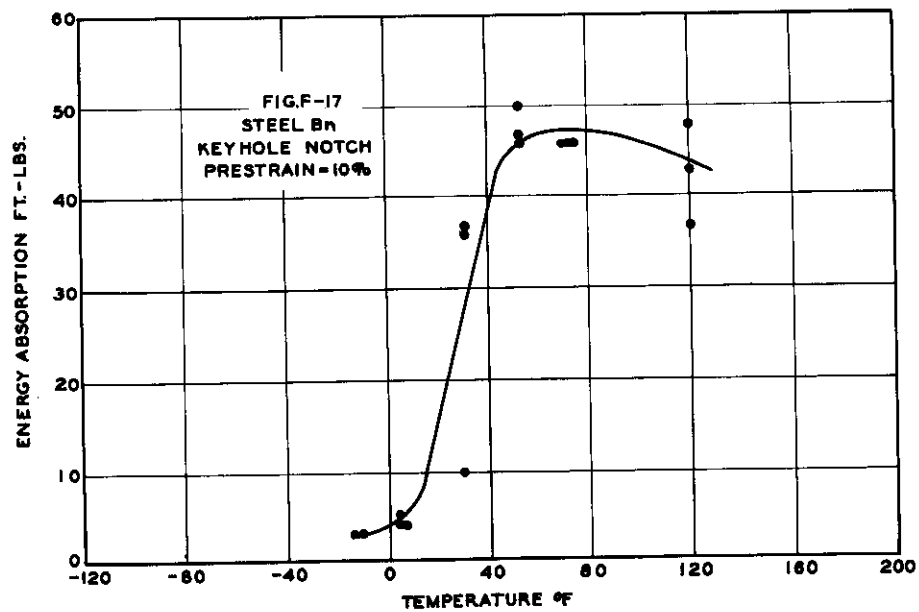
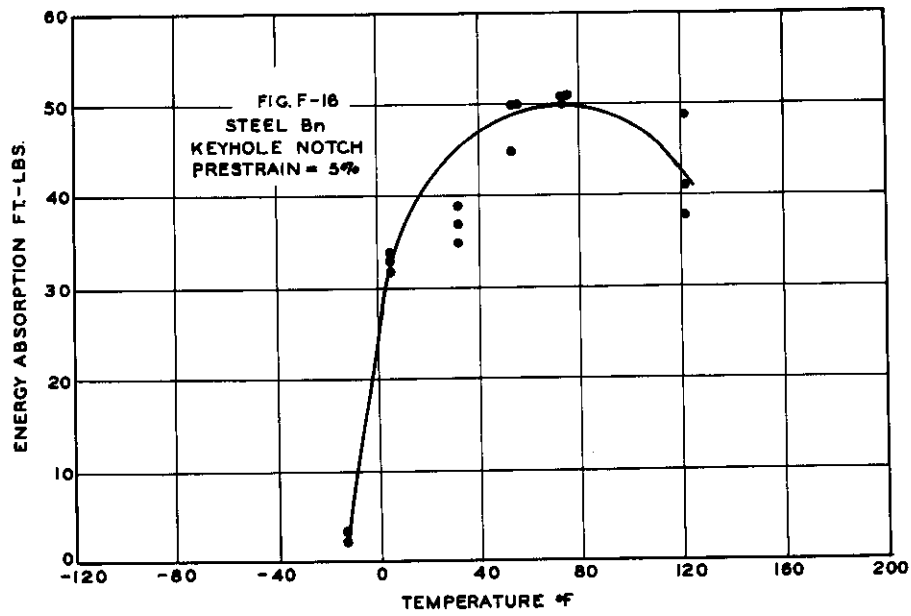
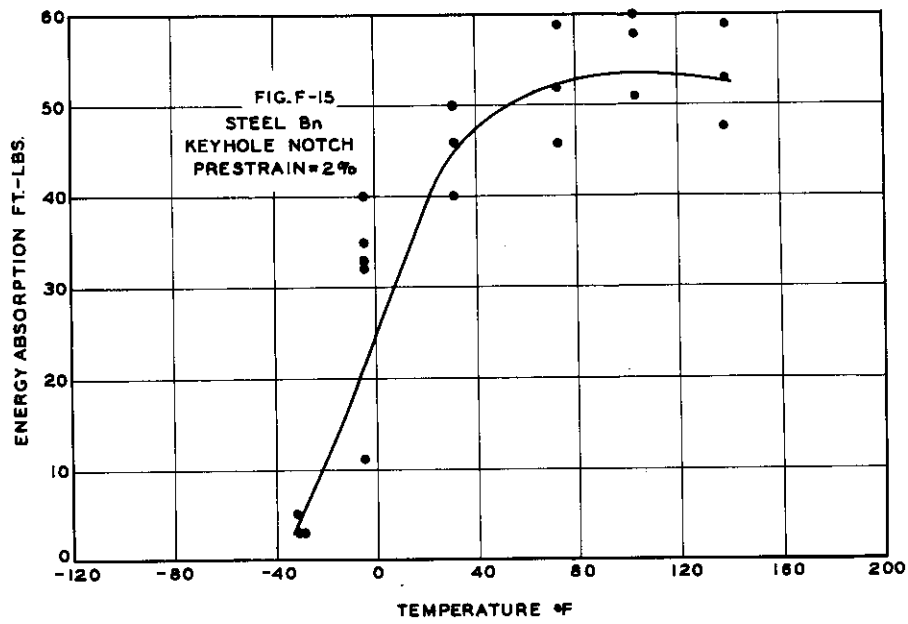


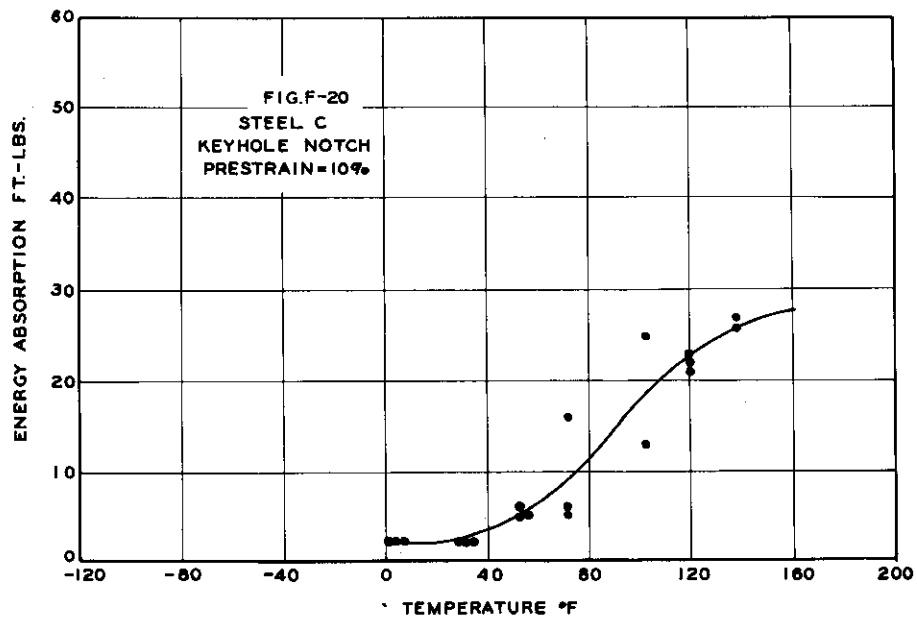
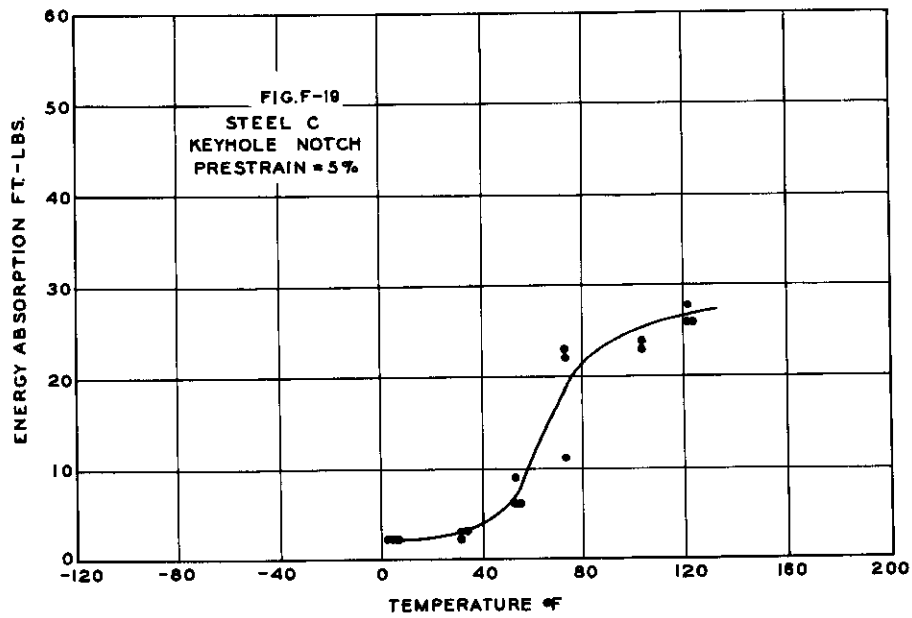
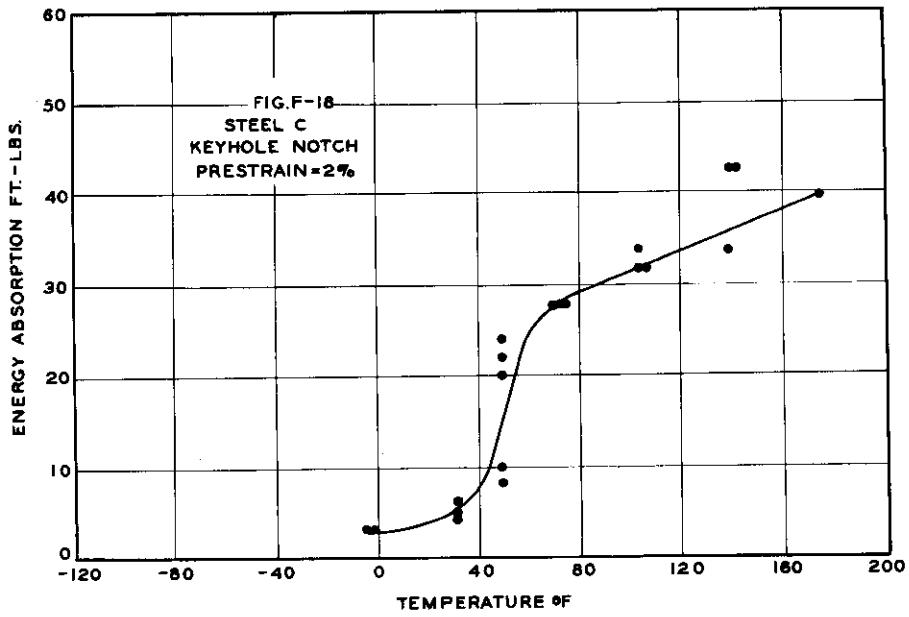


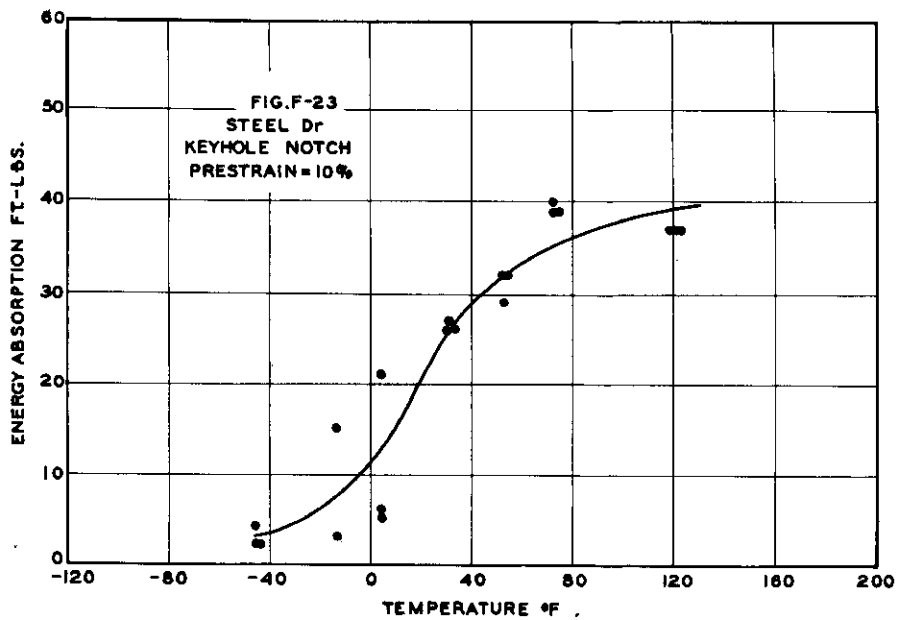
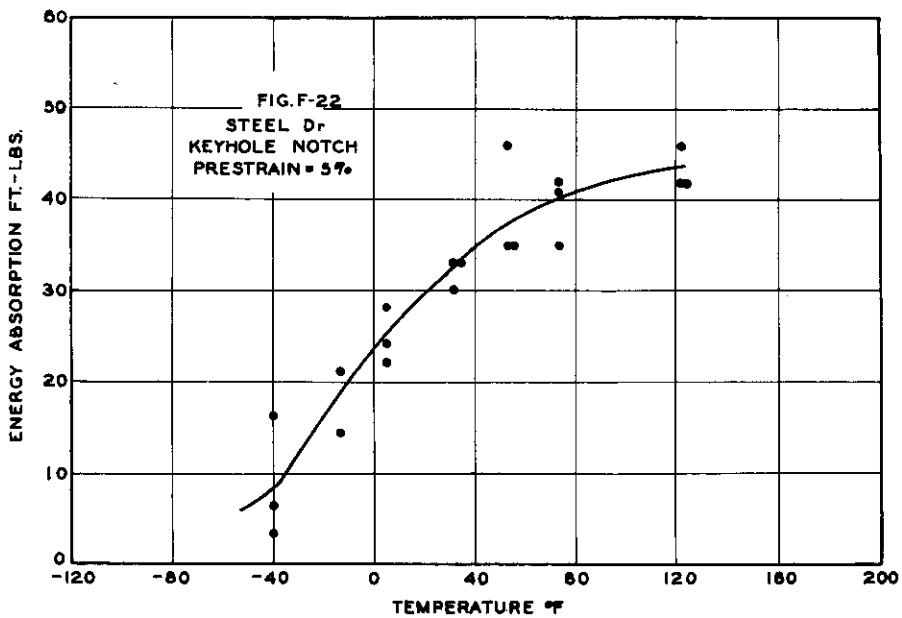
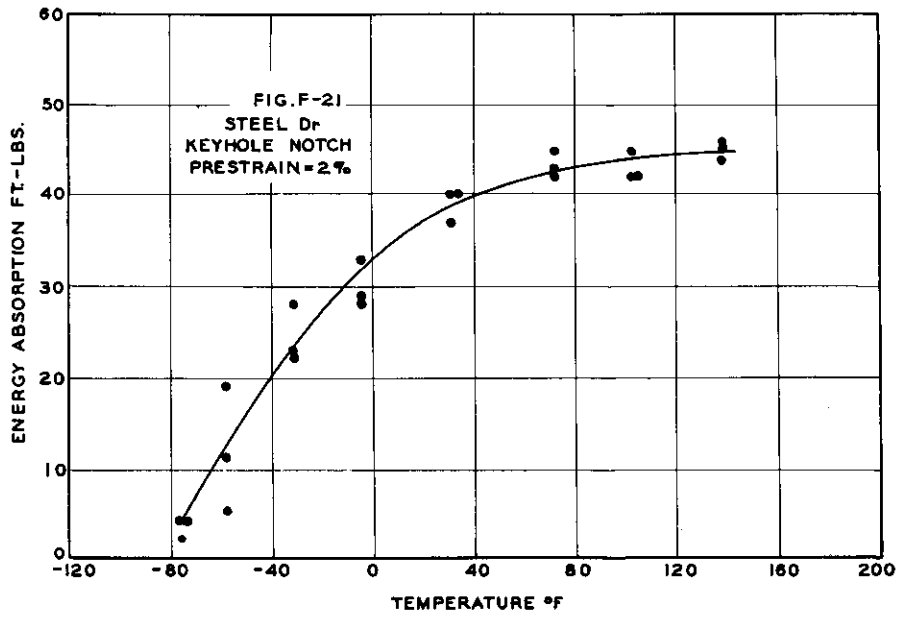


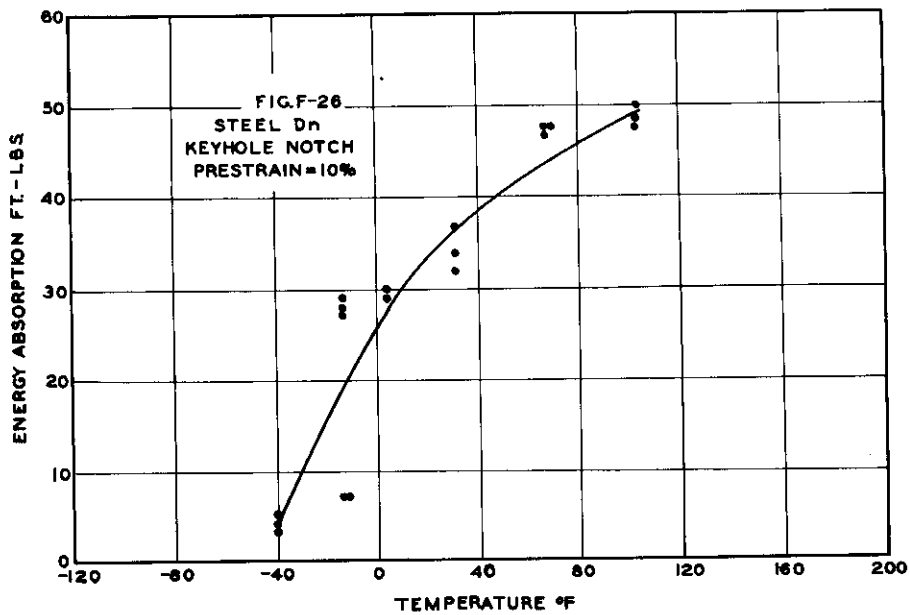
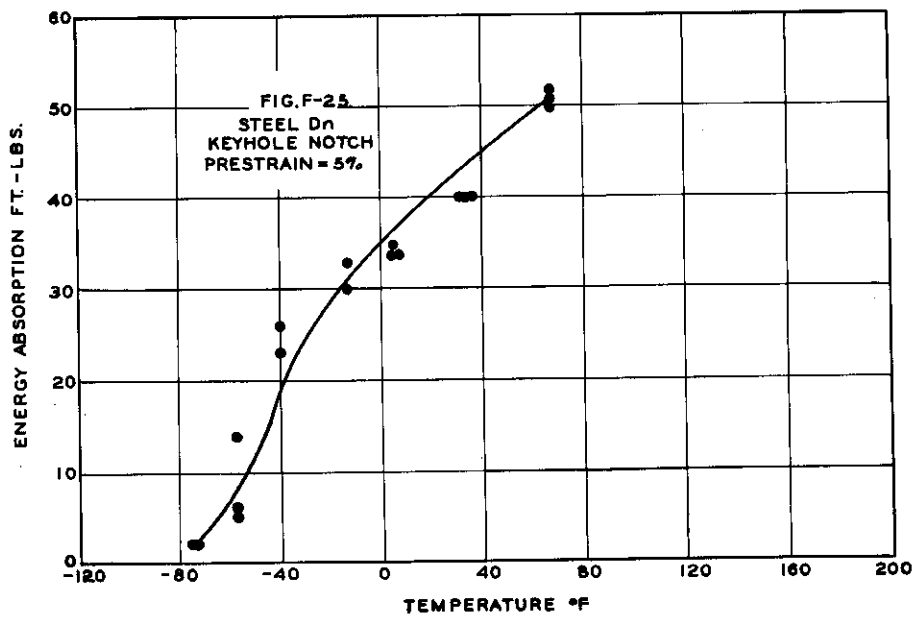
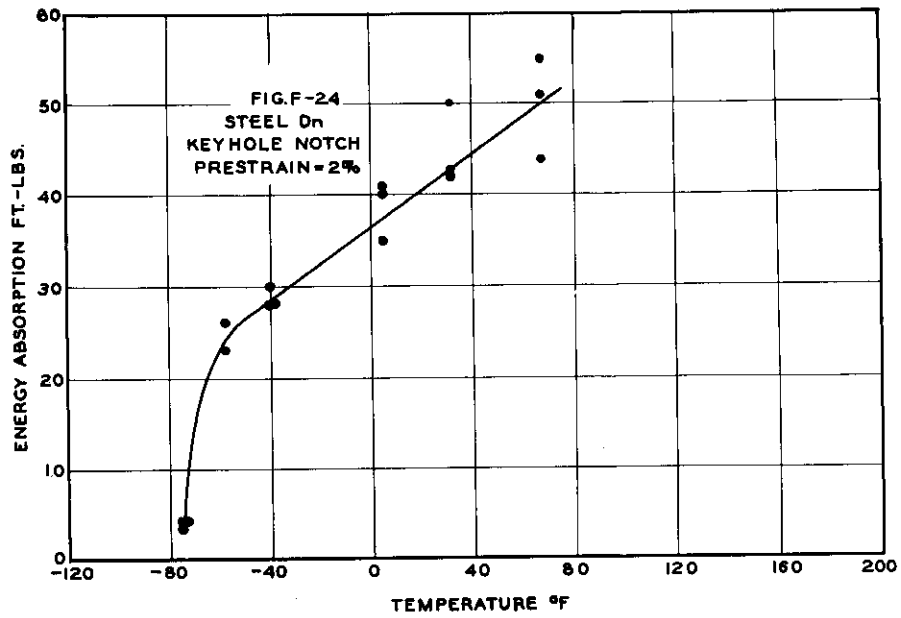


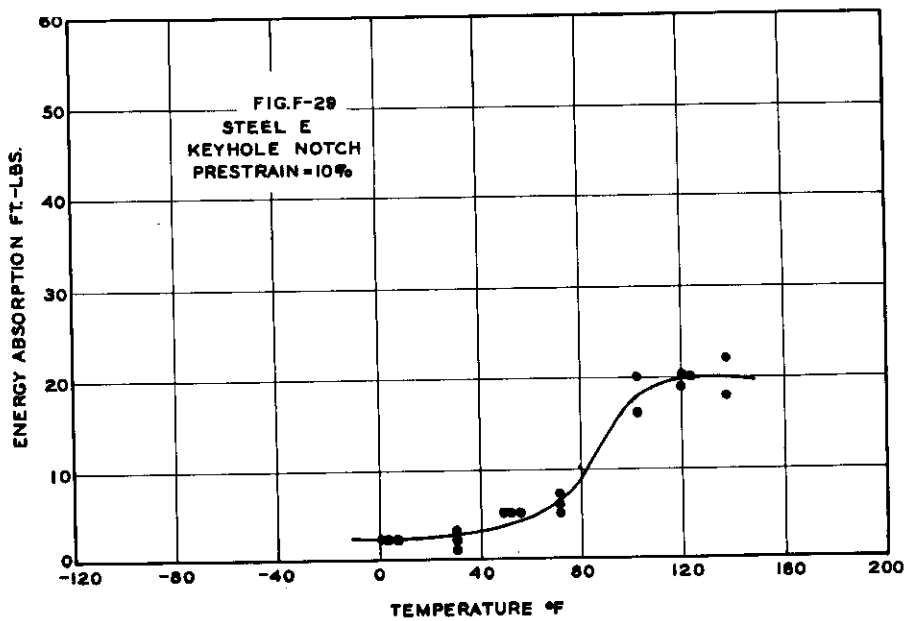
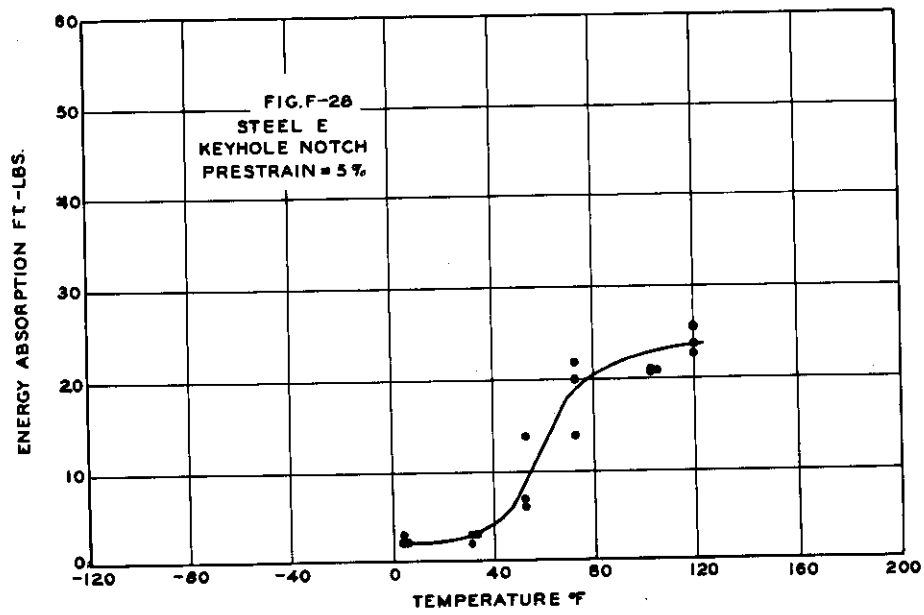
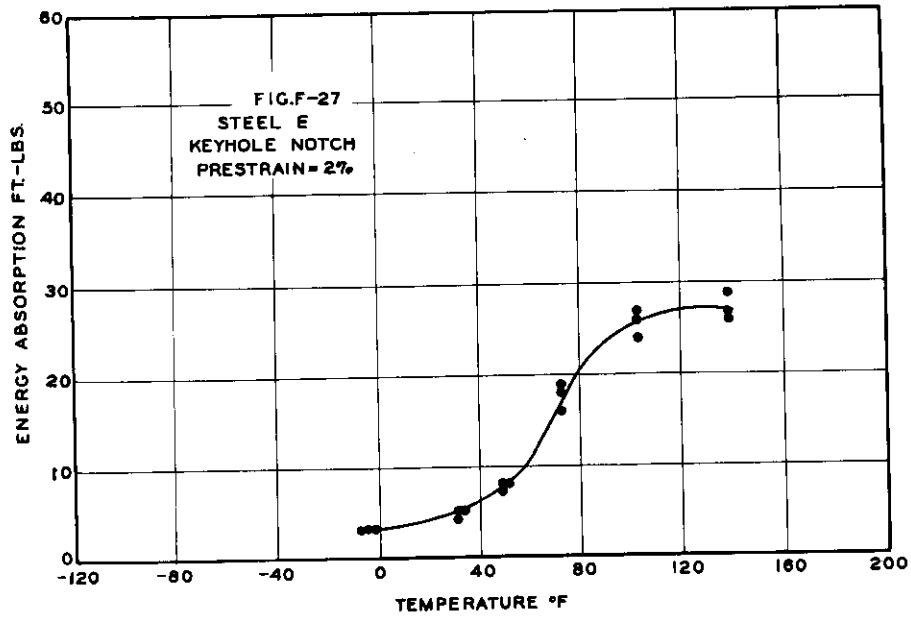


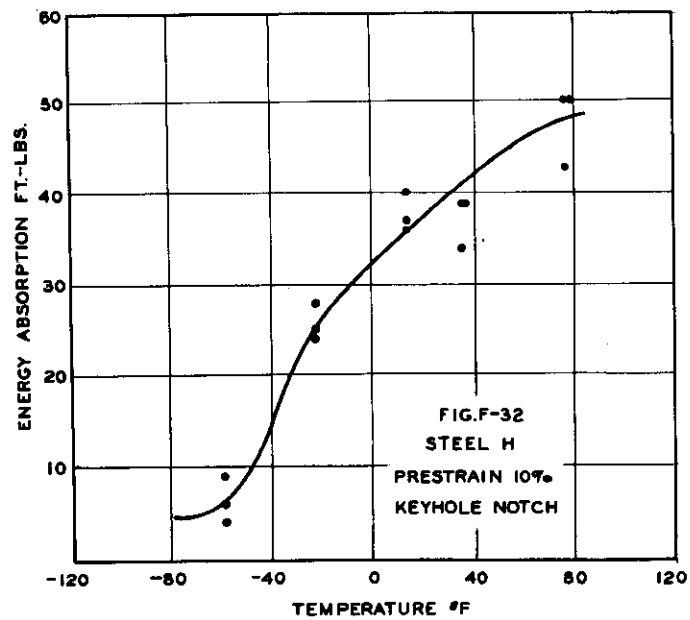
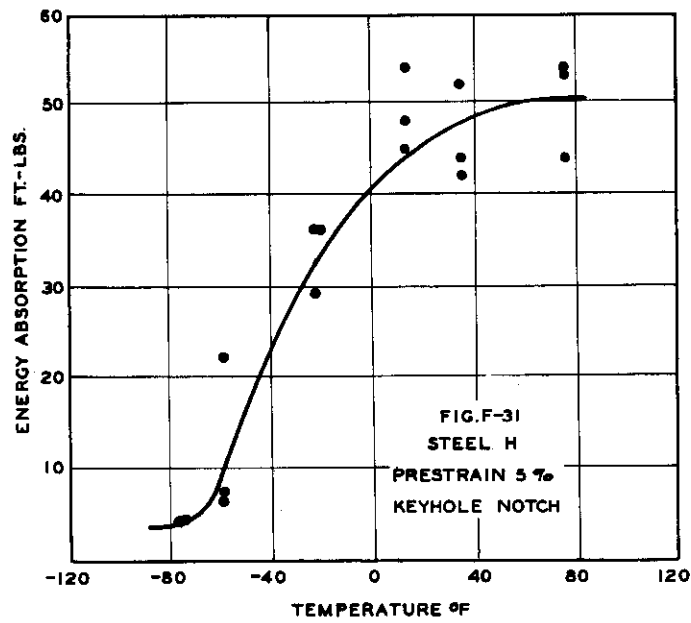
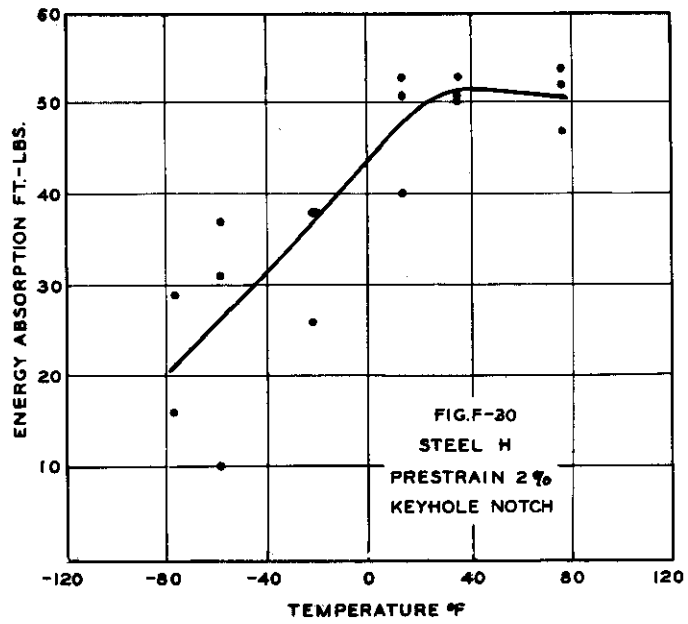


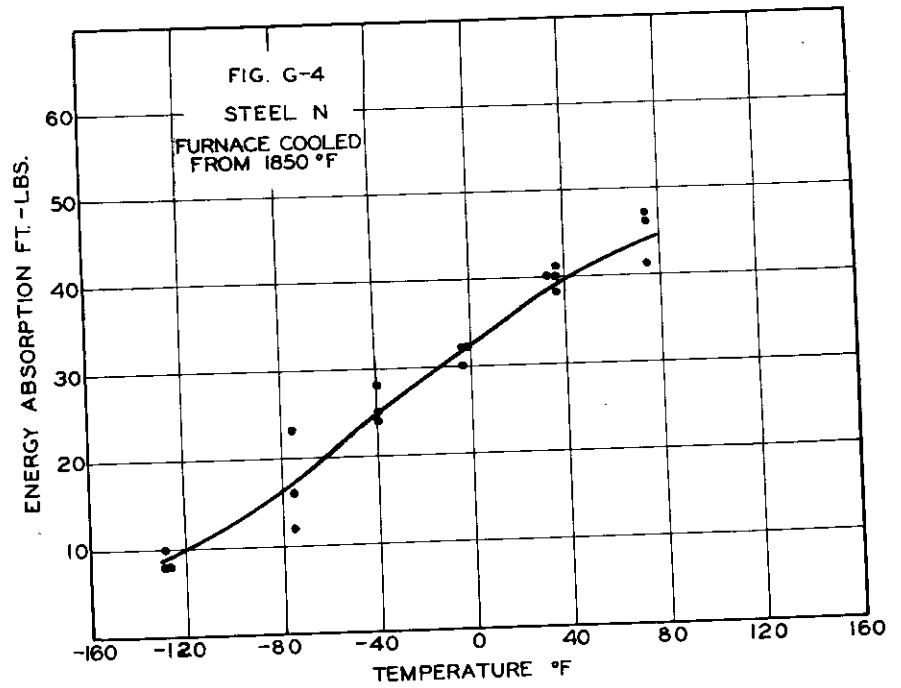
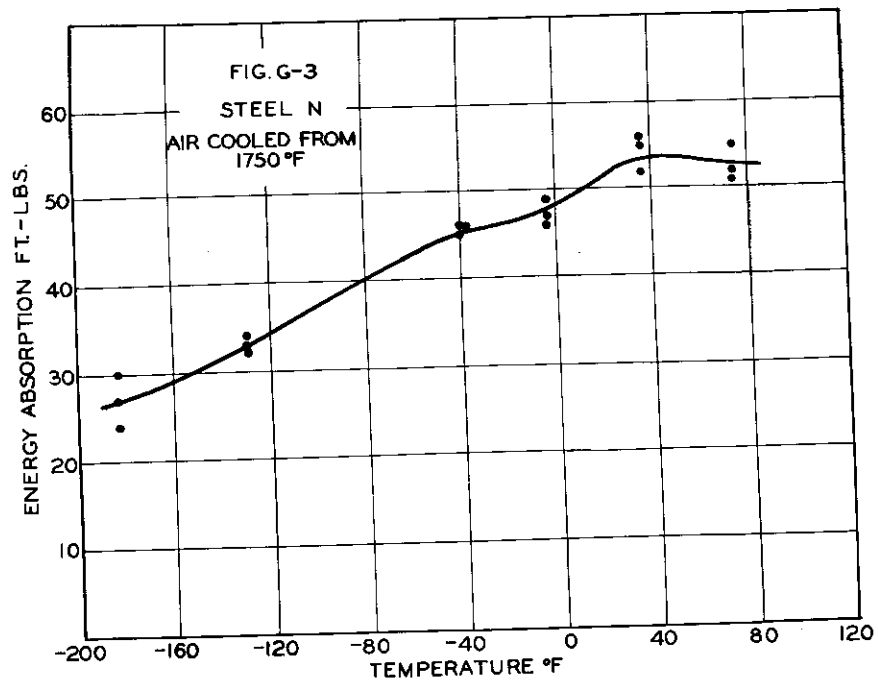
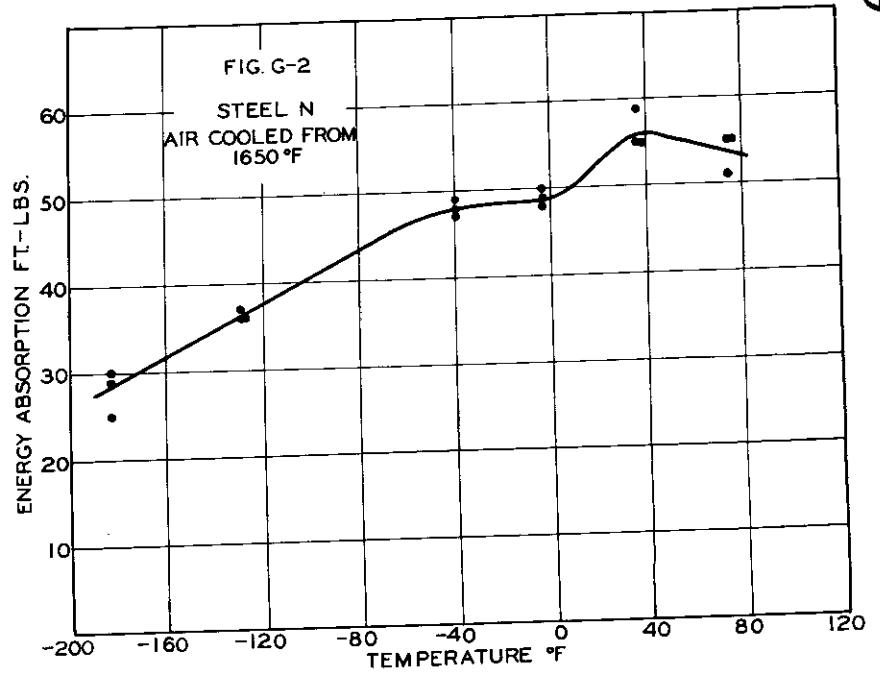
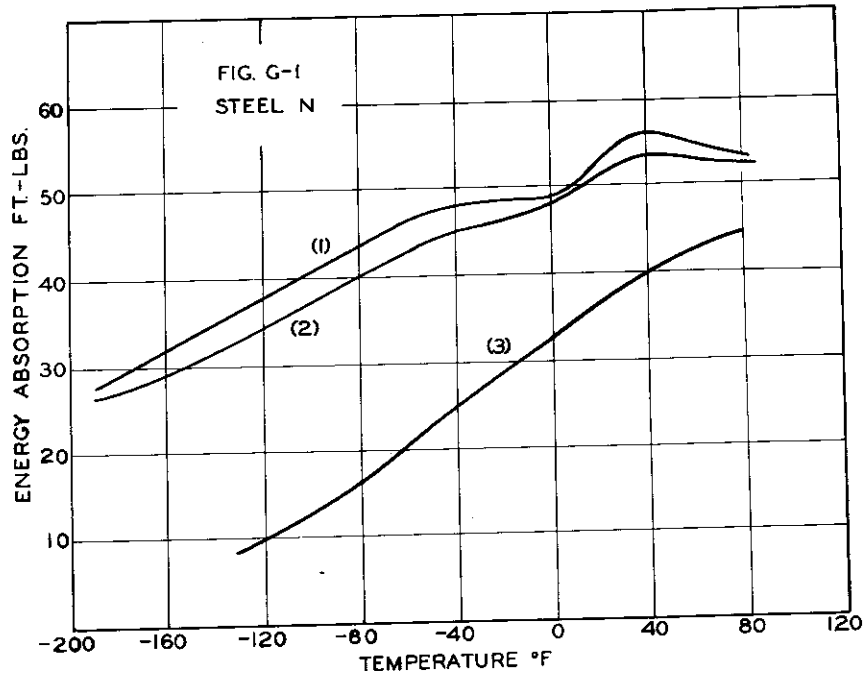






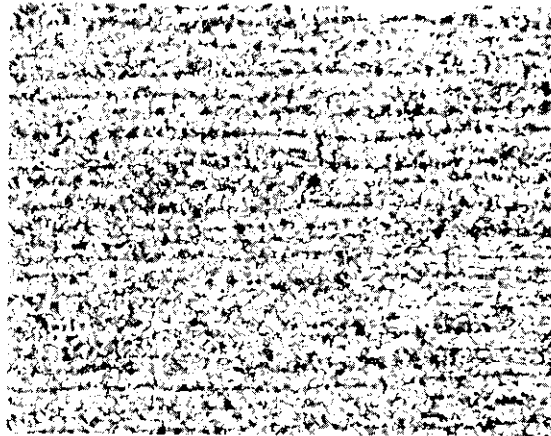




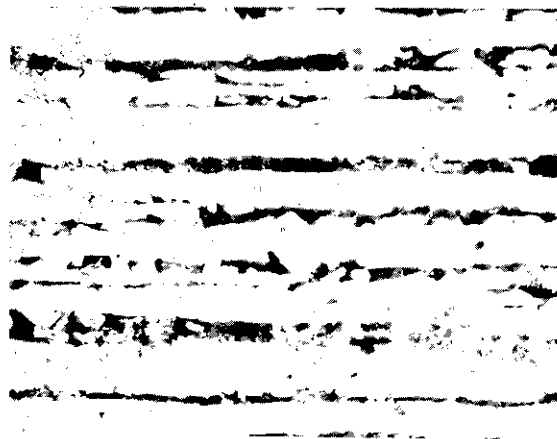




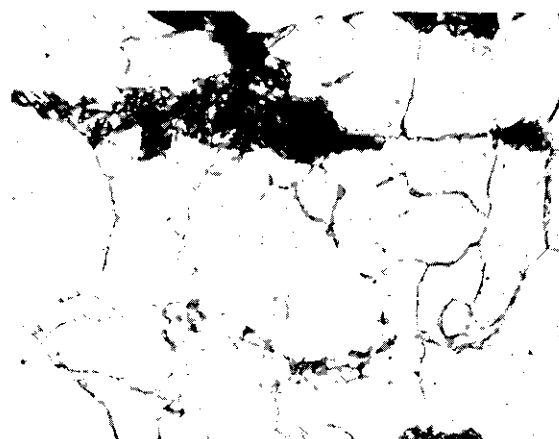
a. Air Cooled from
1650 F. X 100



b. Air Cooled from
1750 F. X 100

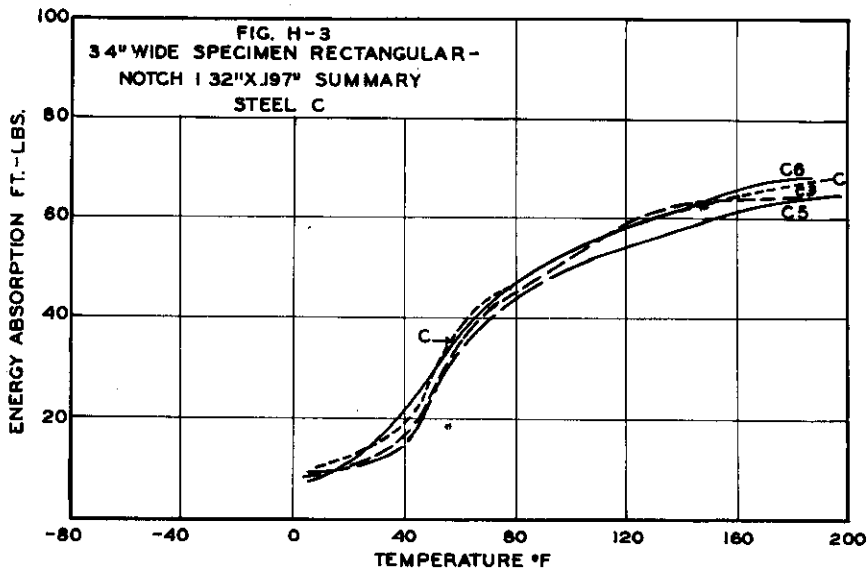
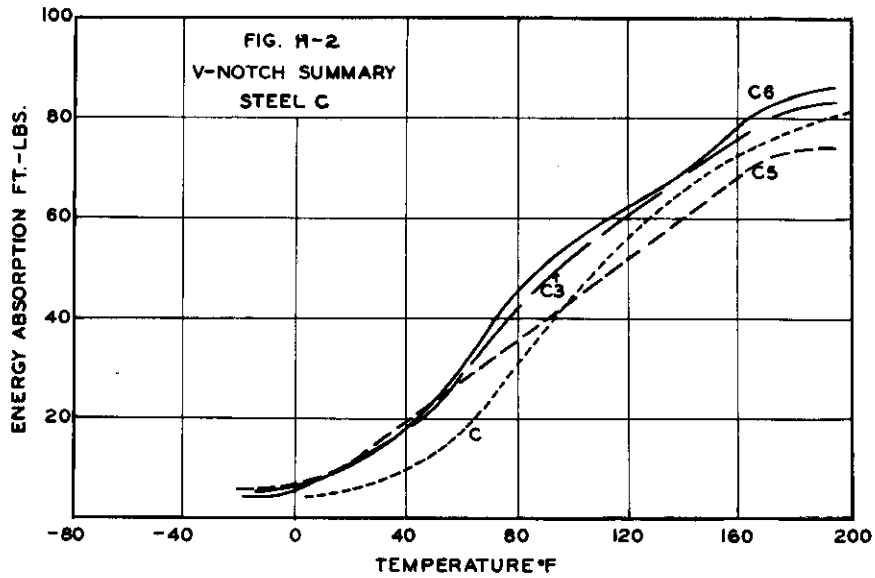
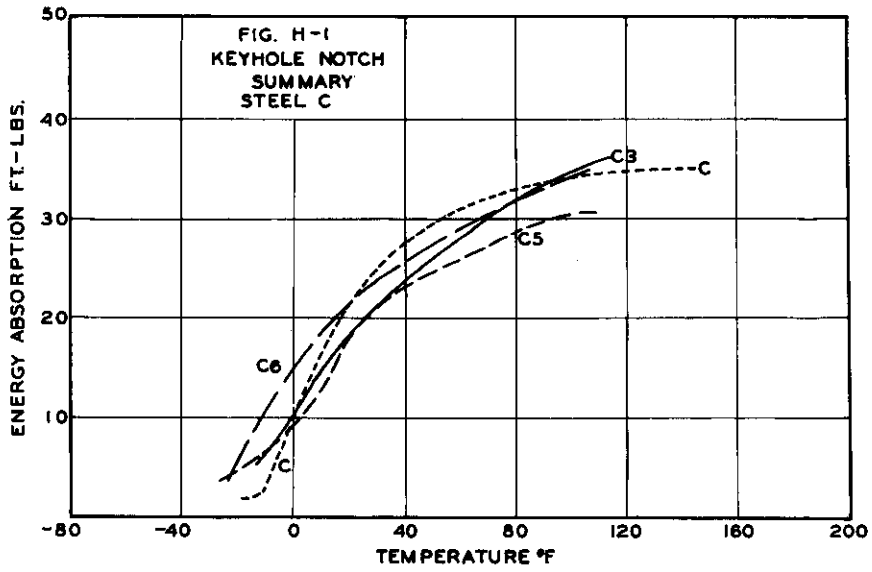


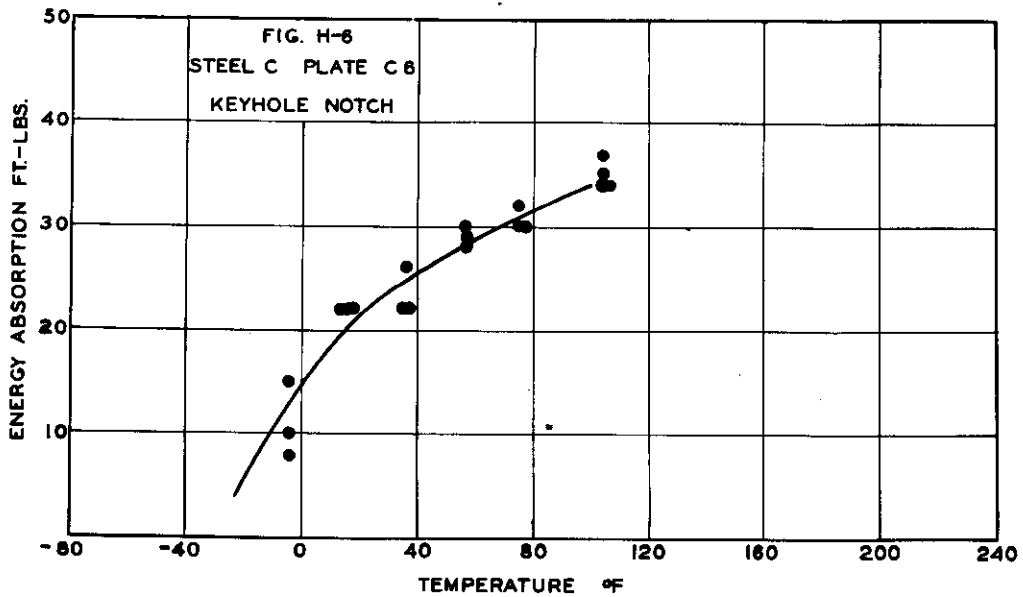
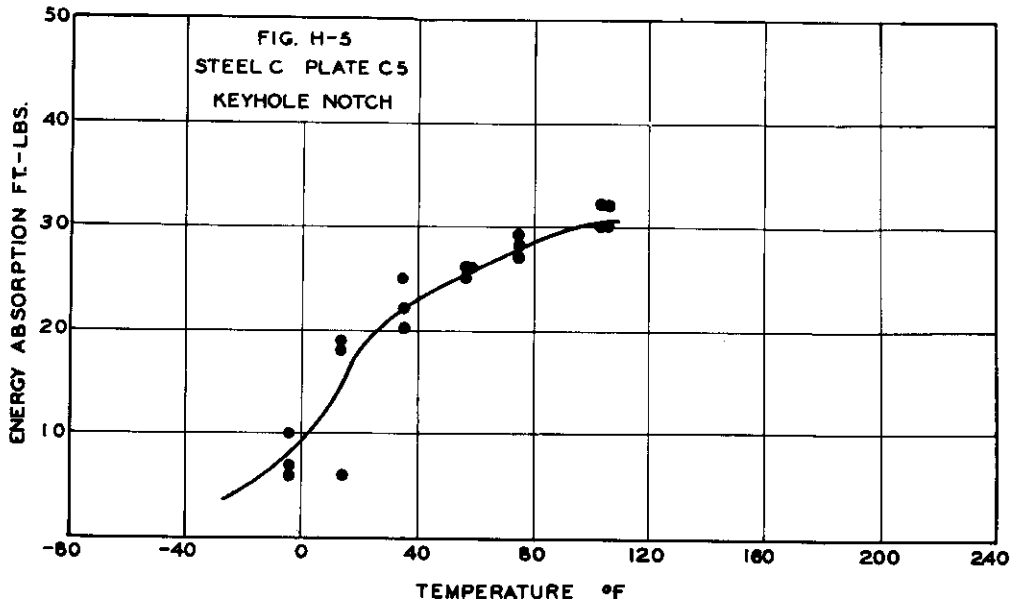
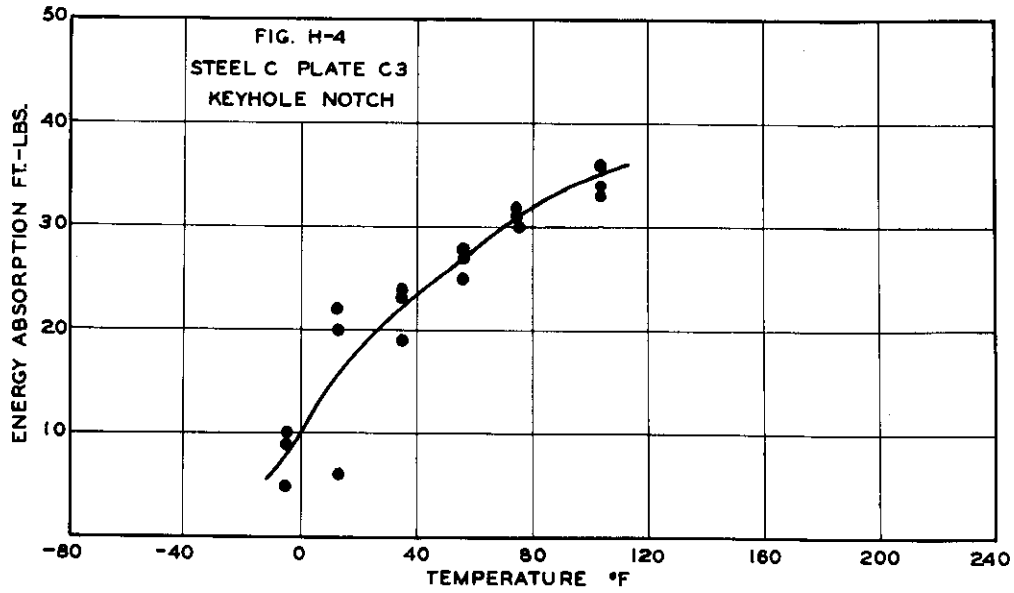
c. Furnace Cooled
from 1850 F.
X 100

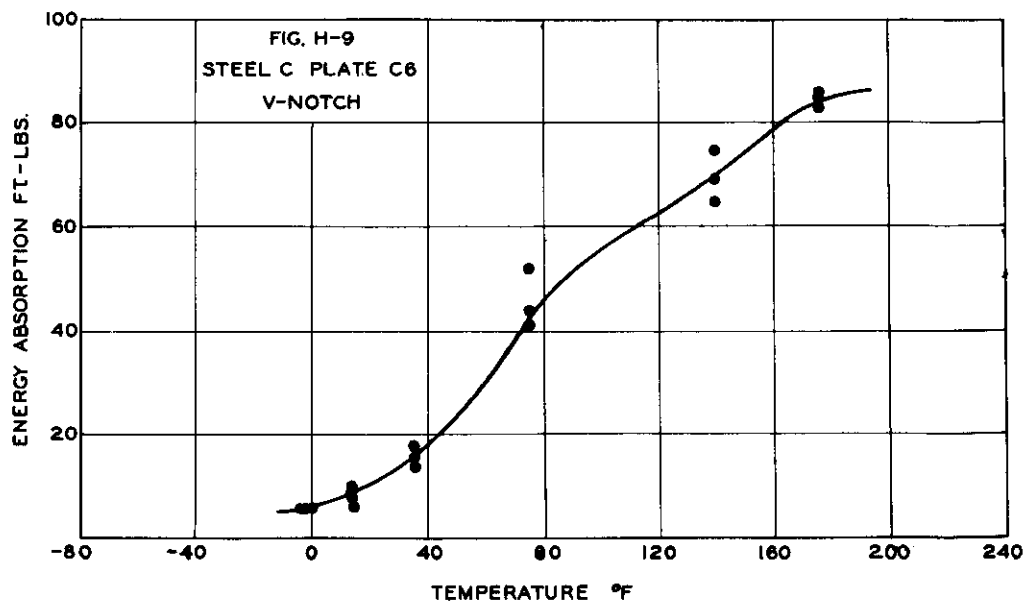
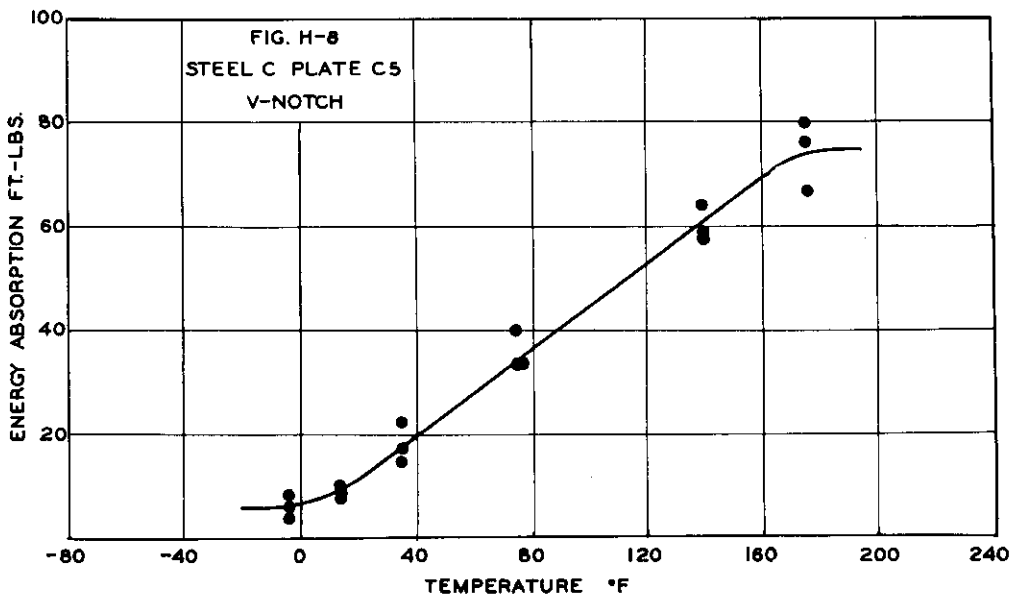
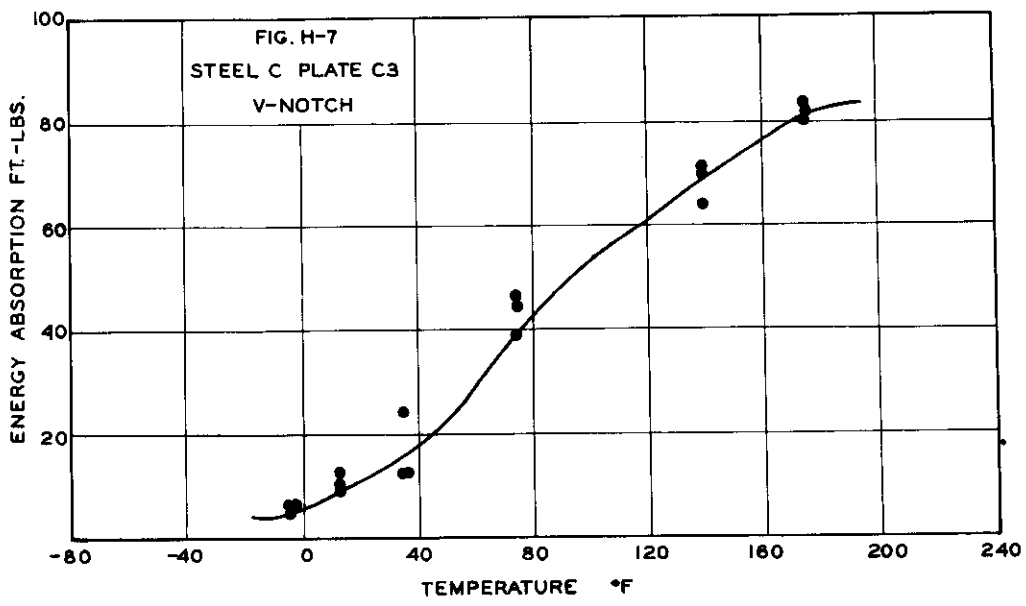


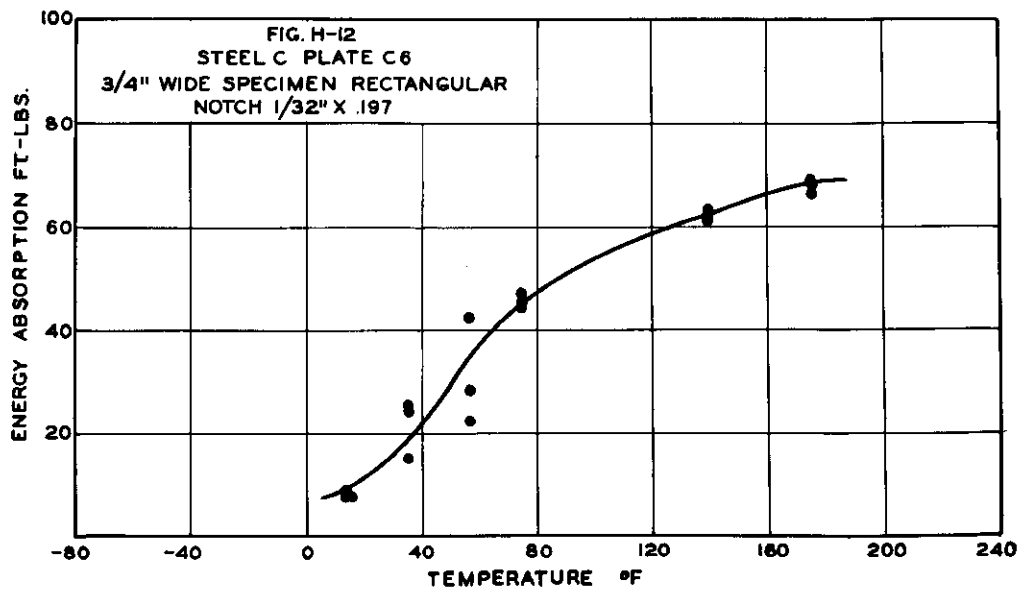
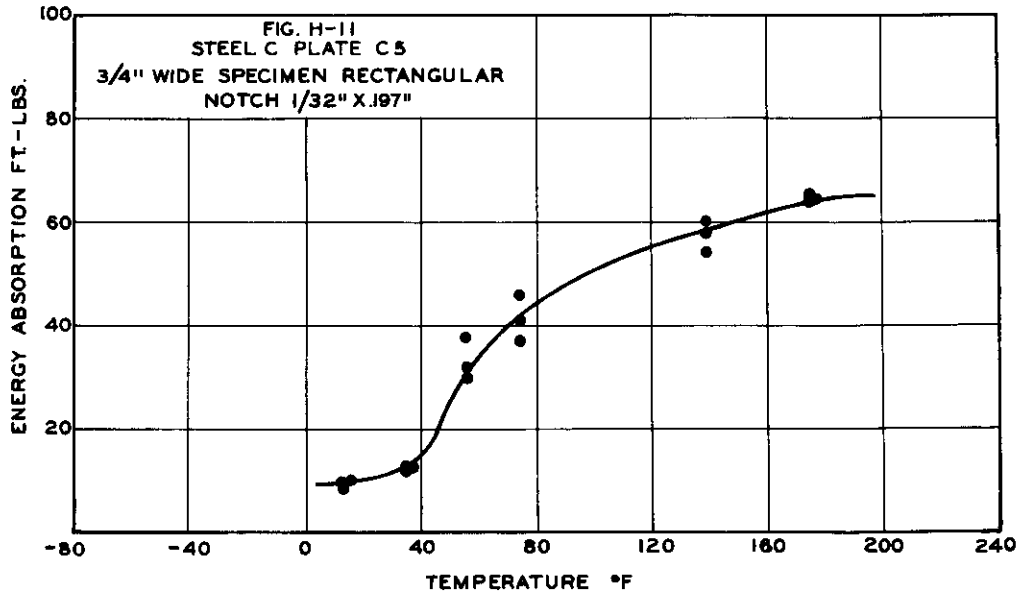
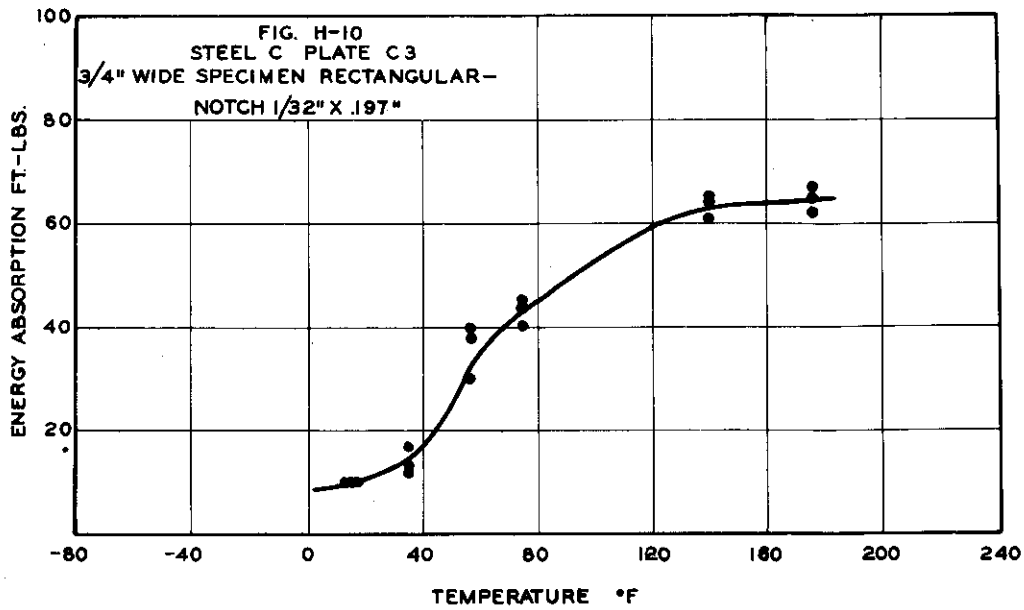
d. Furnace Cooled
from 1850 F.
X 600

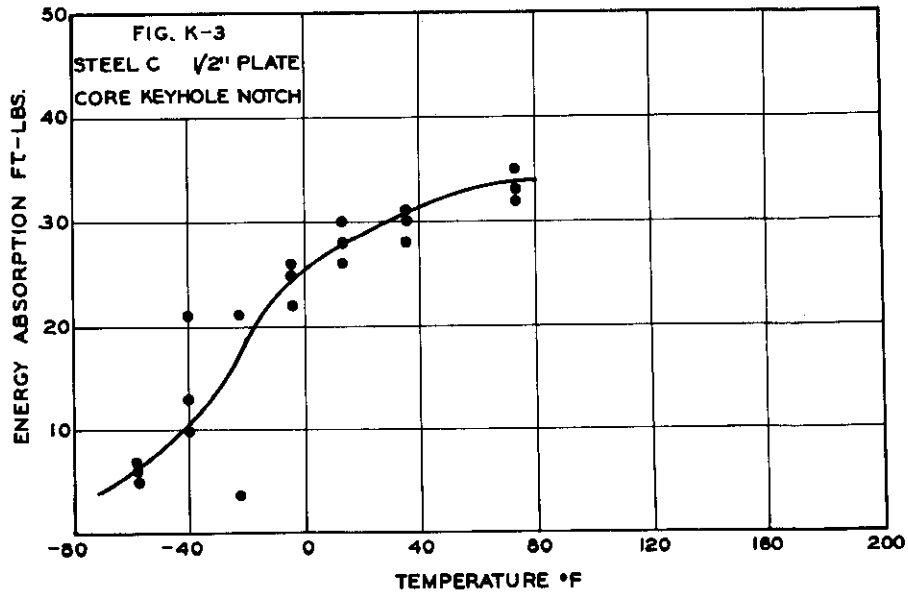
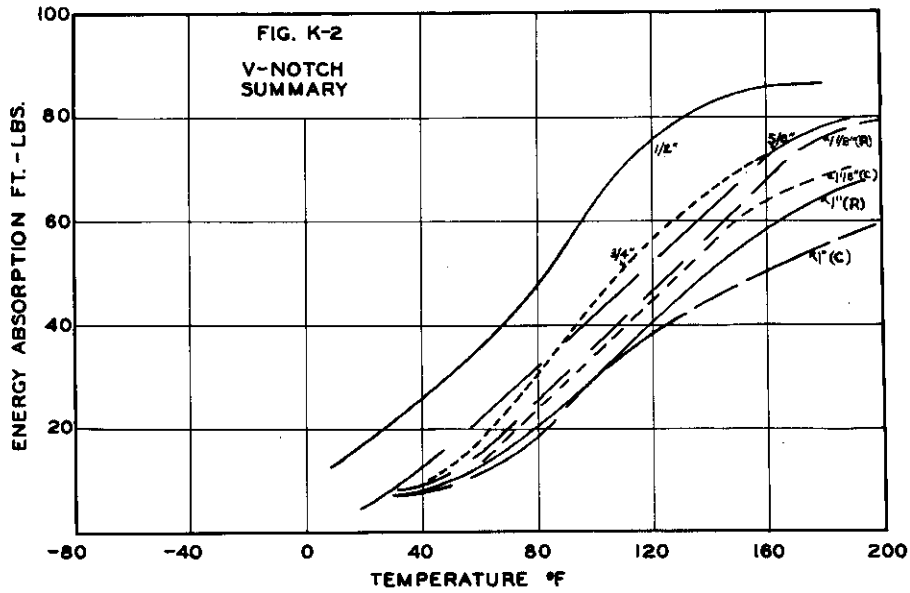
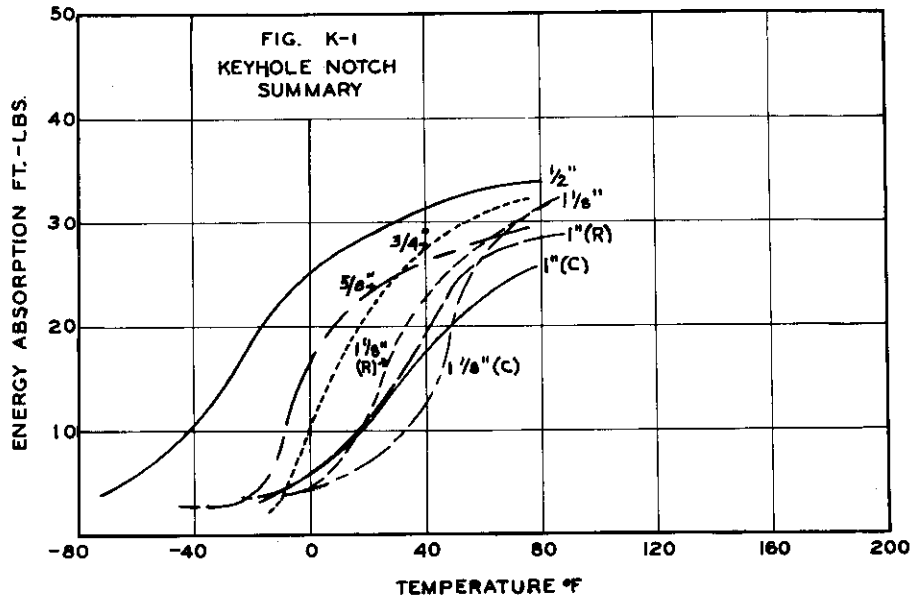
Fig. G-5 Photomicrographs of Steel N
After Different Heat Treatments

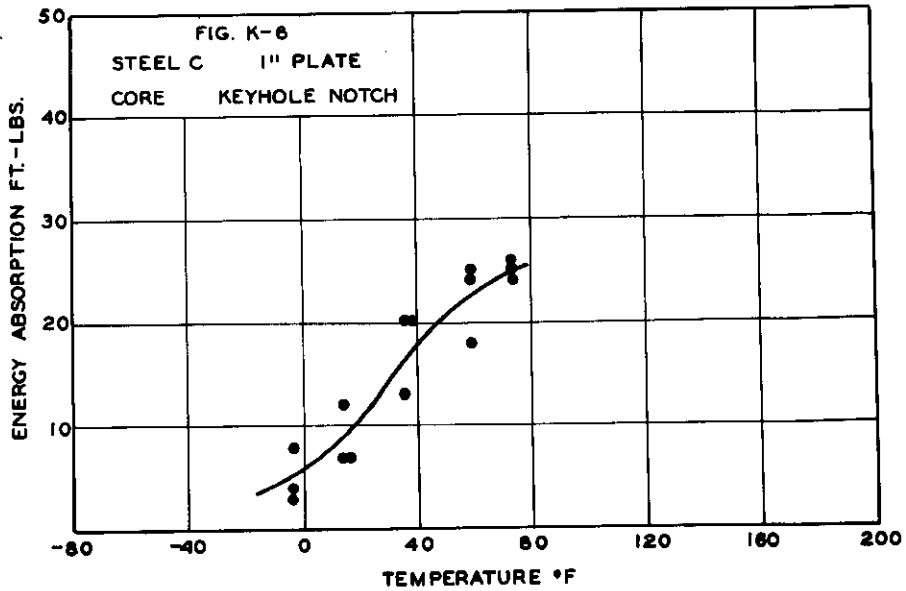
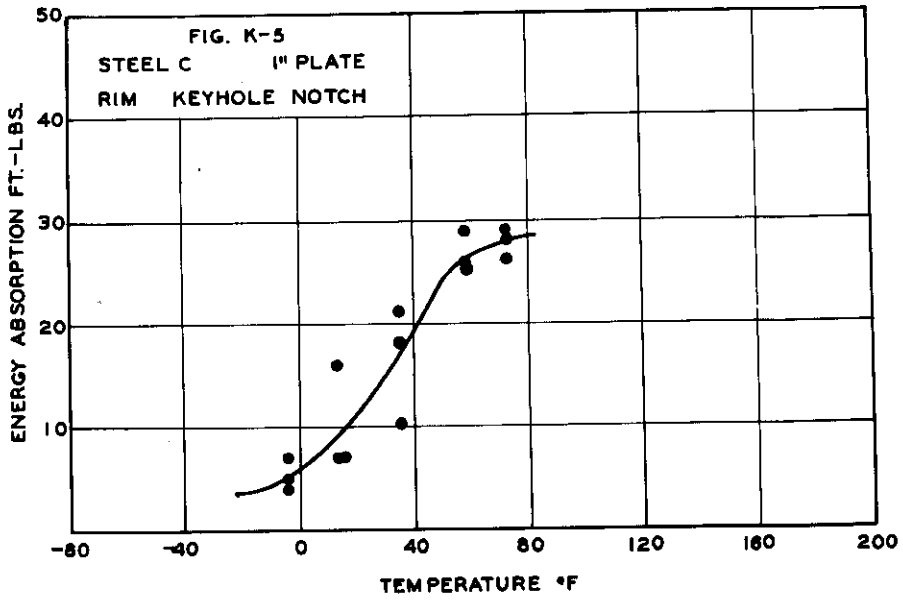
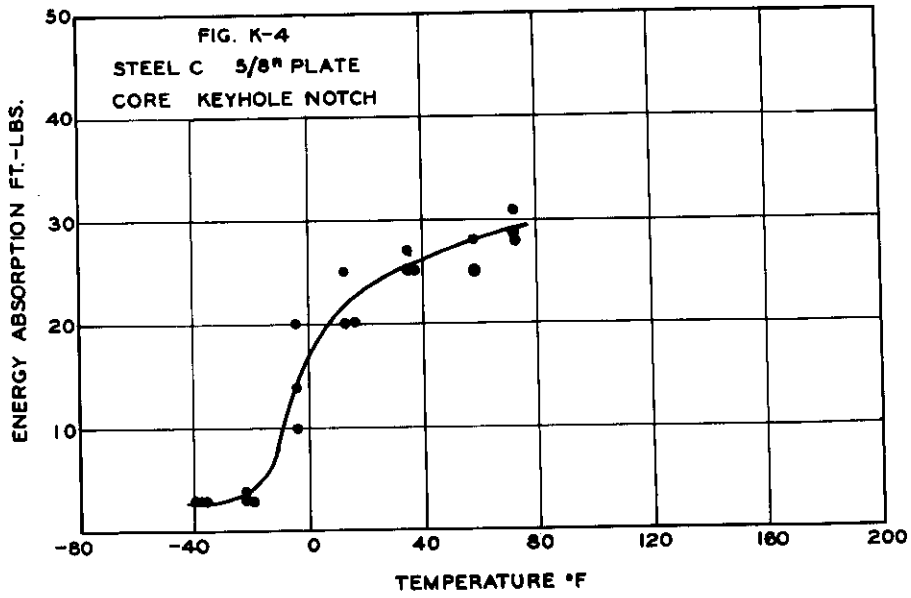


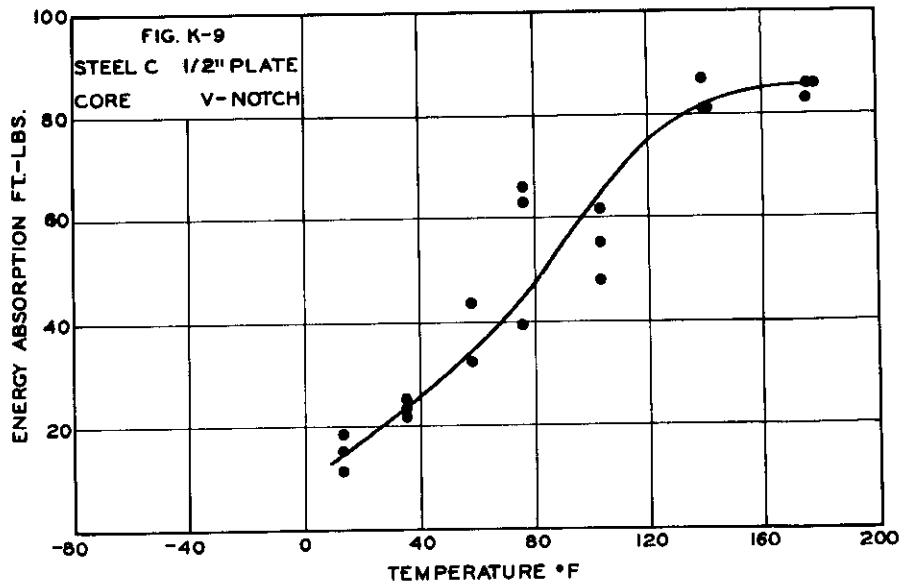
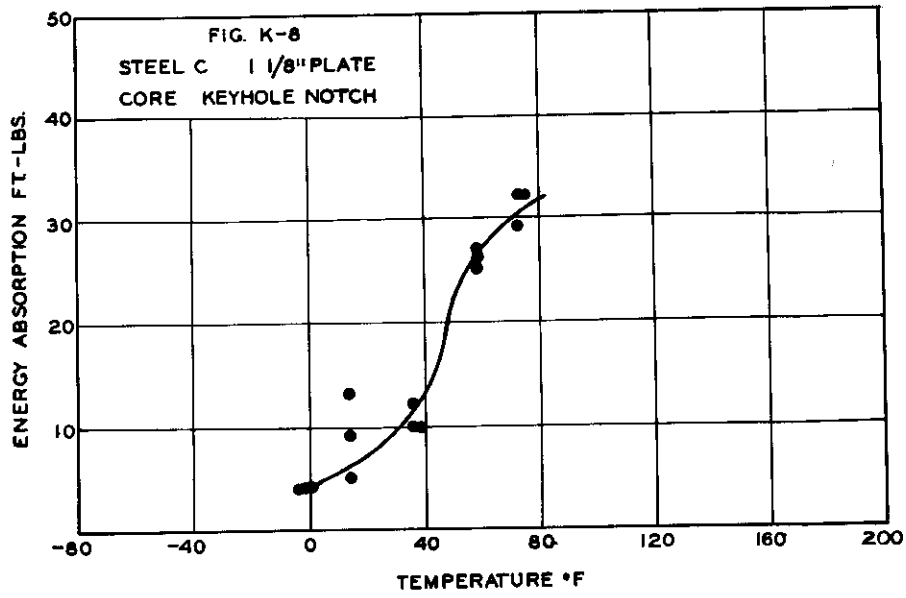
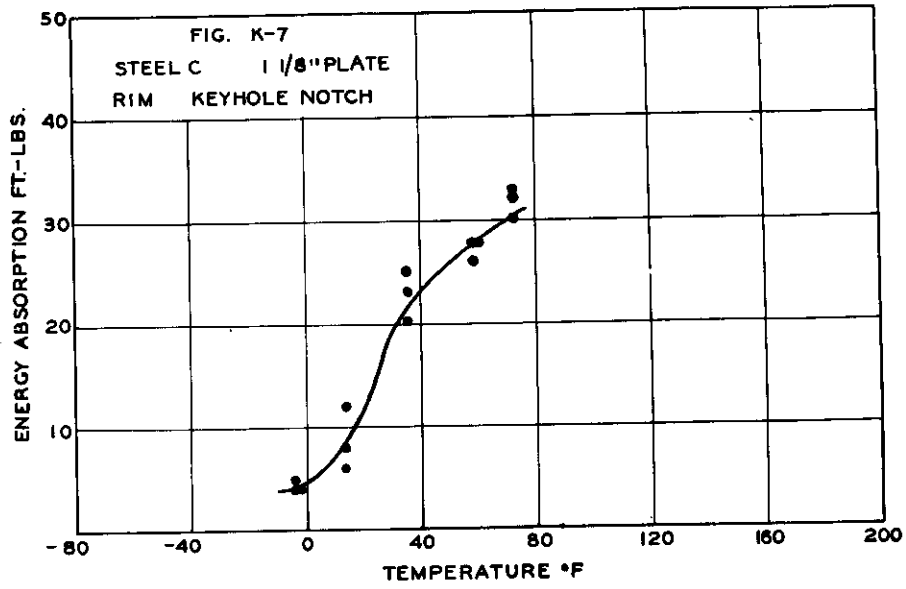


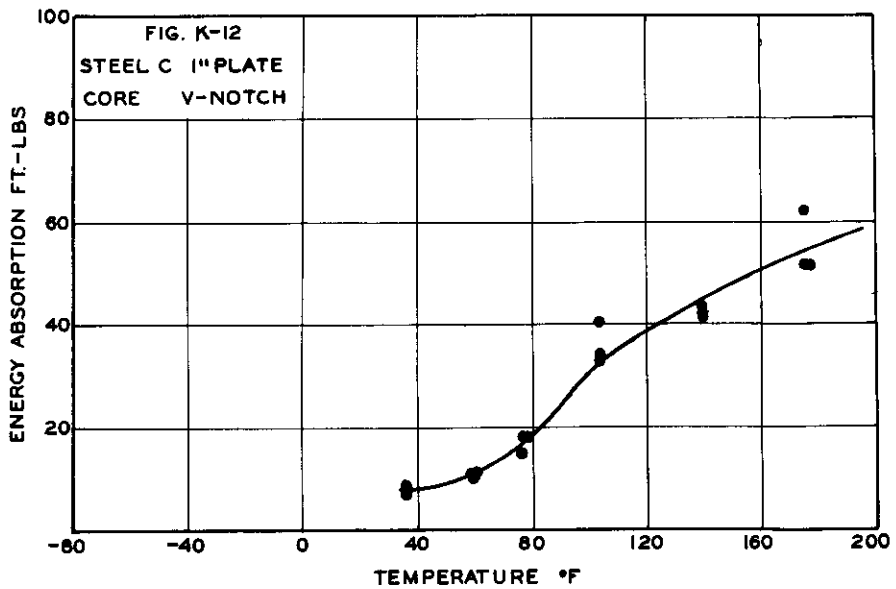
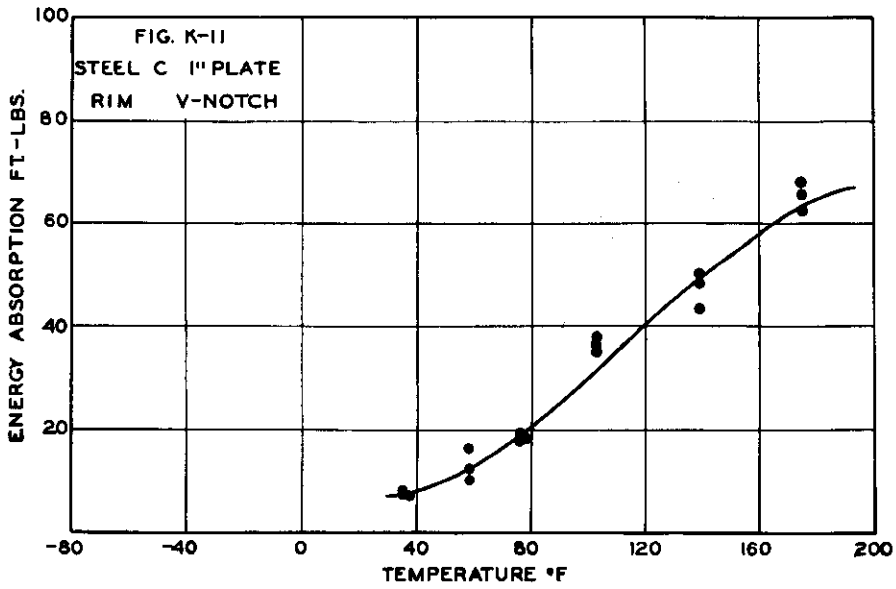
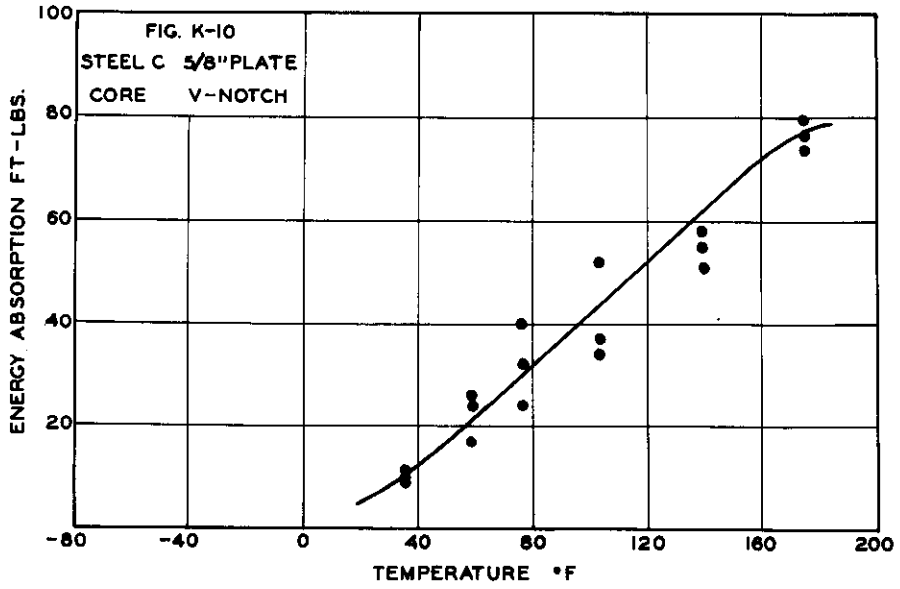


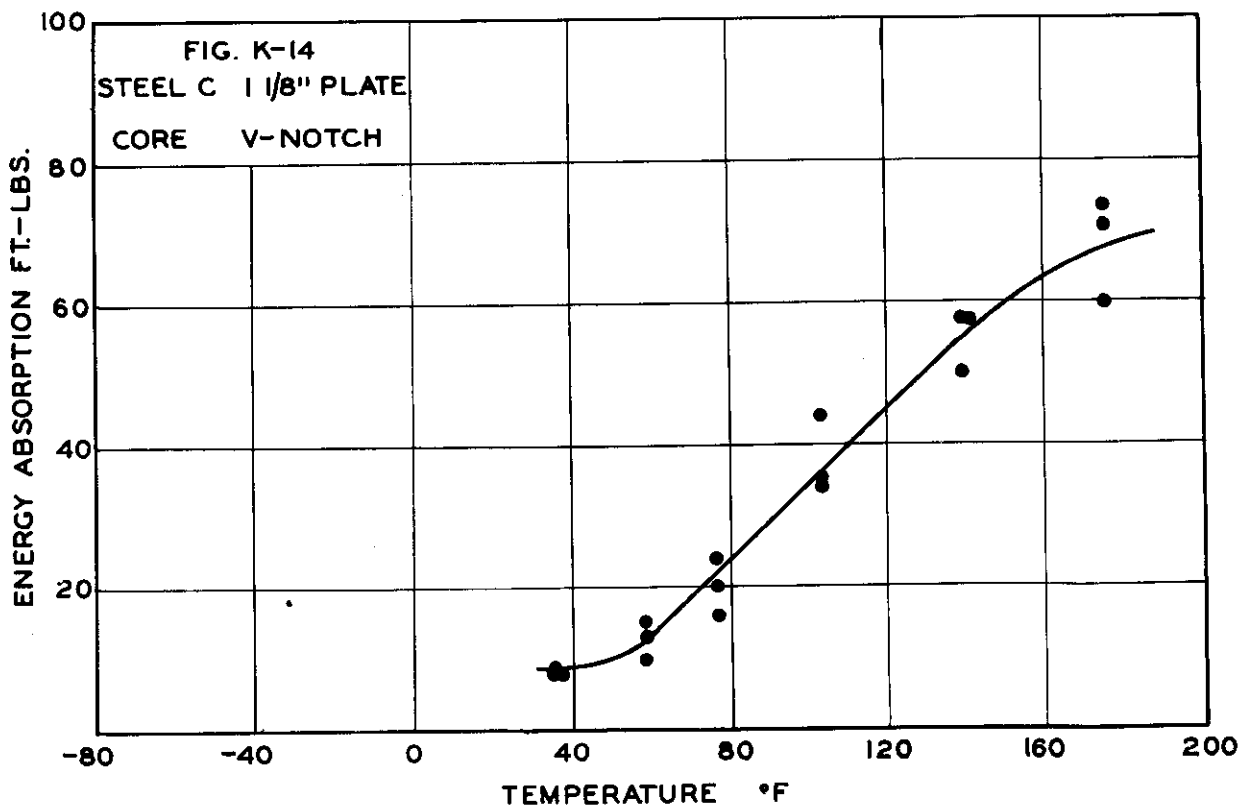
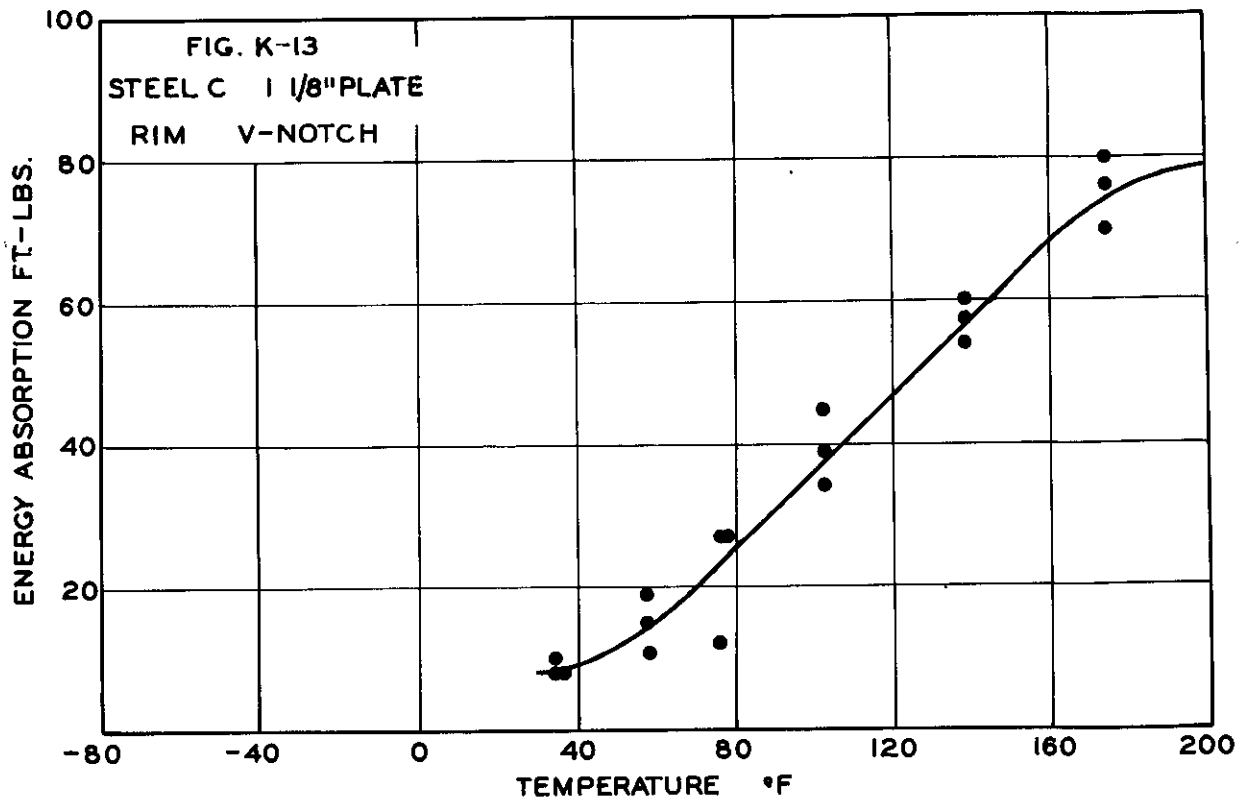




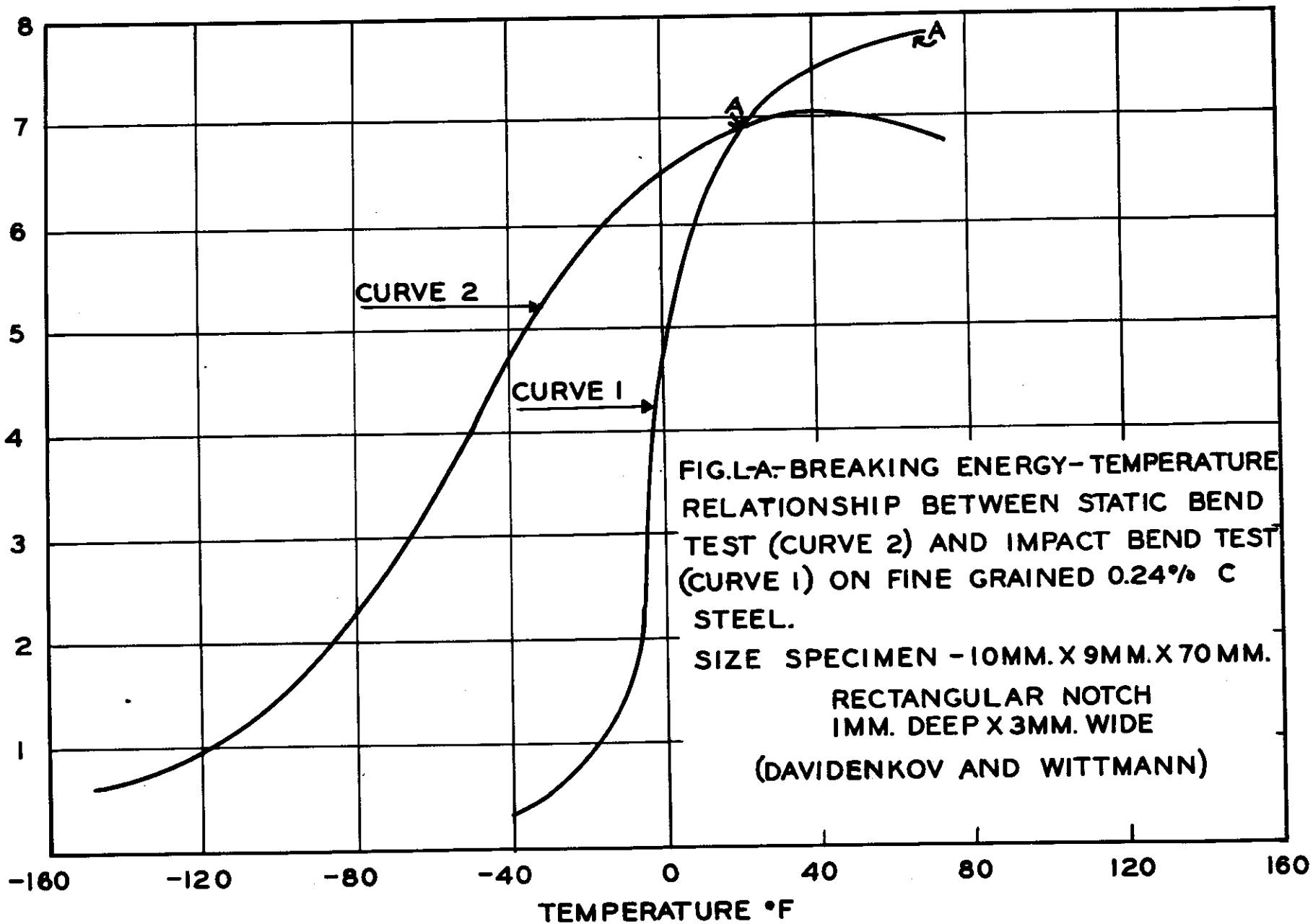








BREAKING ENERGY - METER KILOGRAMS



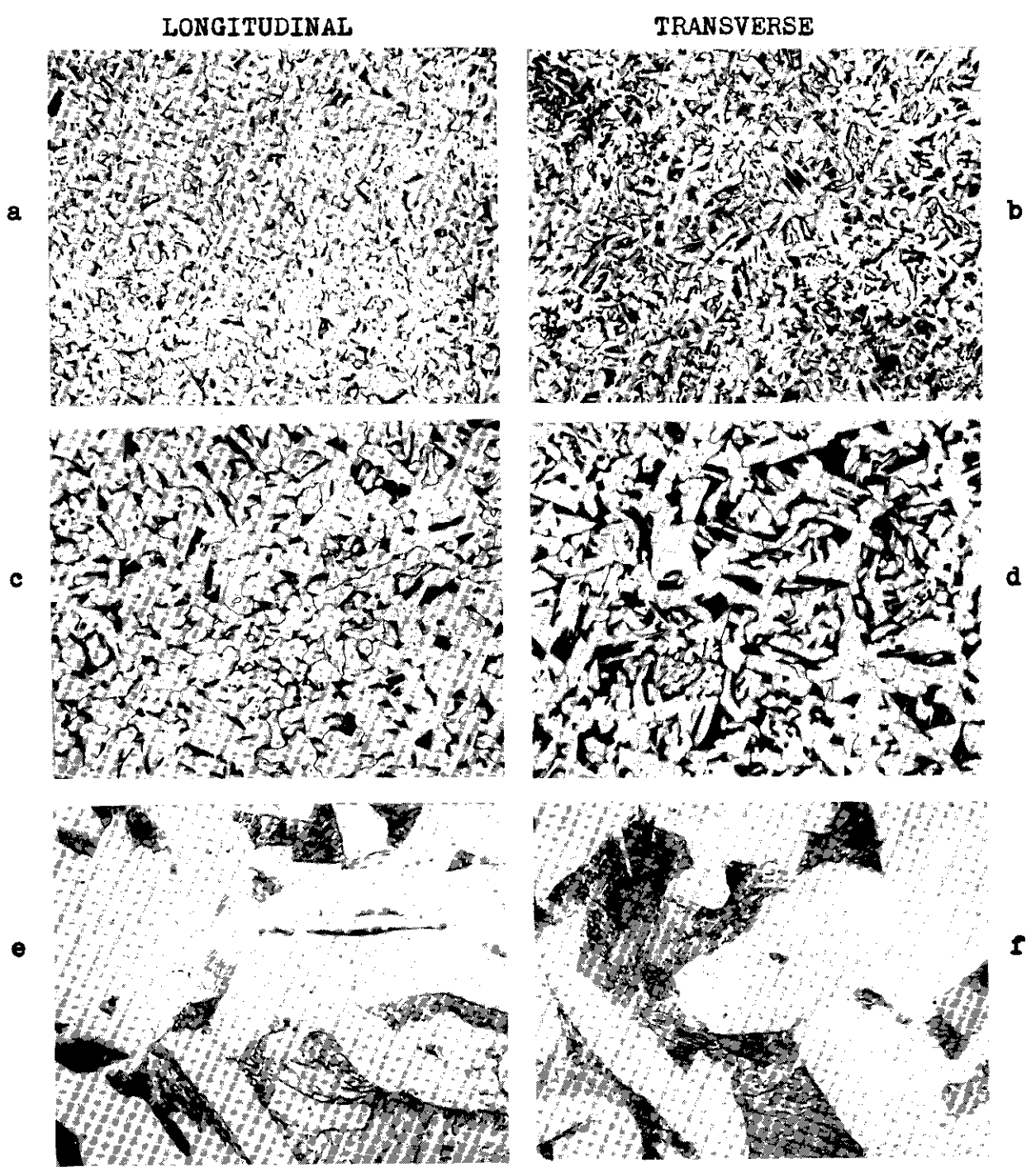


Fig. M-1 Photomicrographs, Etched Steel E. (Rim)

a,b X 50
c,d X 100
e,f X 600

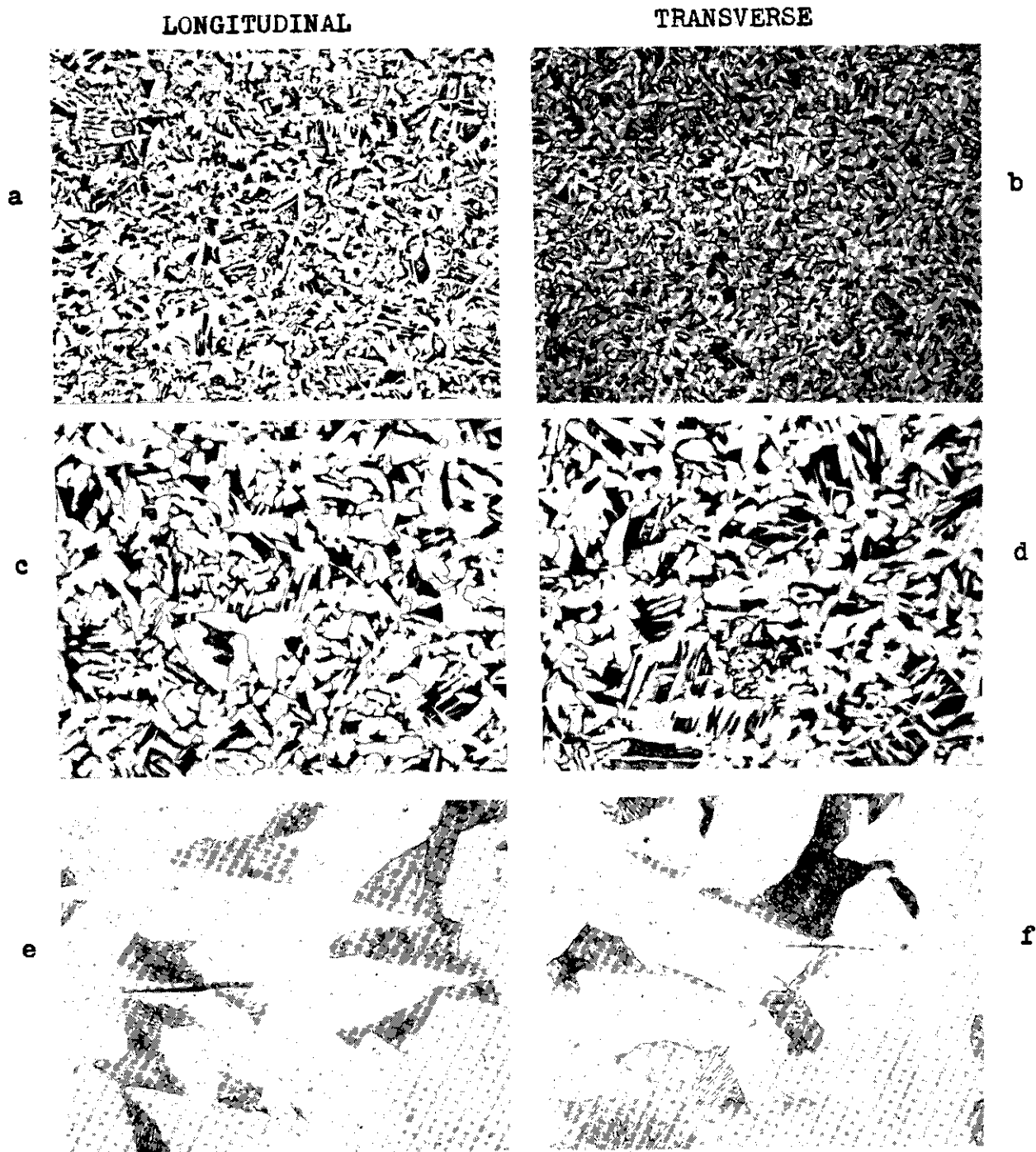


Fig. M-1a Photomicrographs, Etched Steel E. (Core)

a,b X 50
 c,d X 100
 e,f X 600



Fig. M-2 Photomicrographs, Etched Steel C.

a, b X 50
 c, d X 100
 e, f X 600

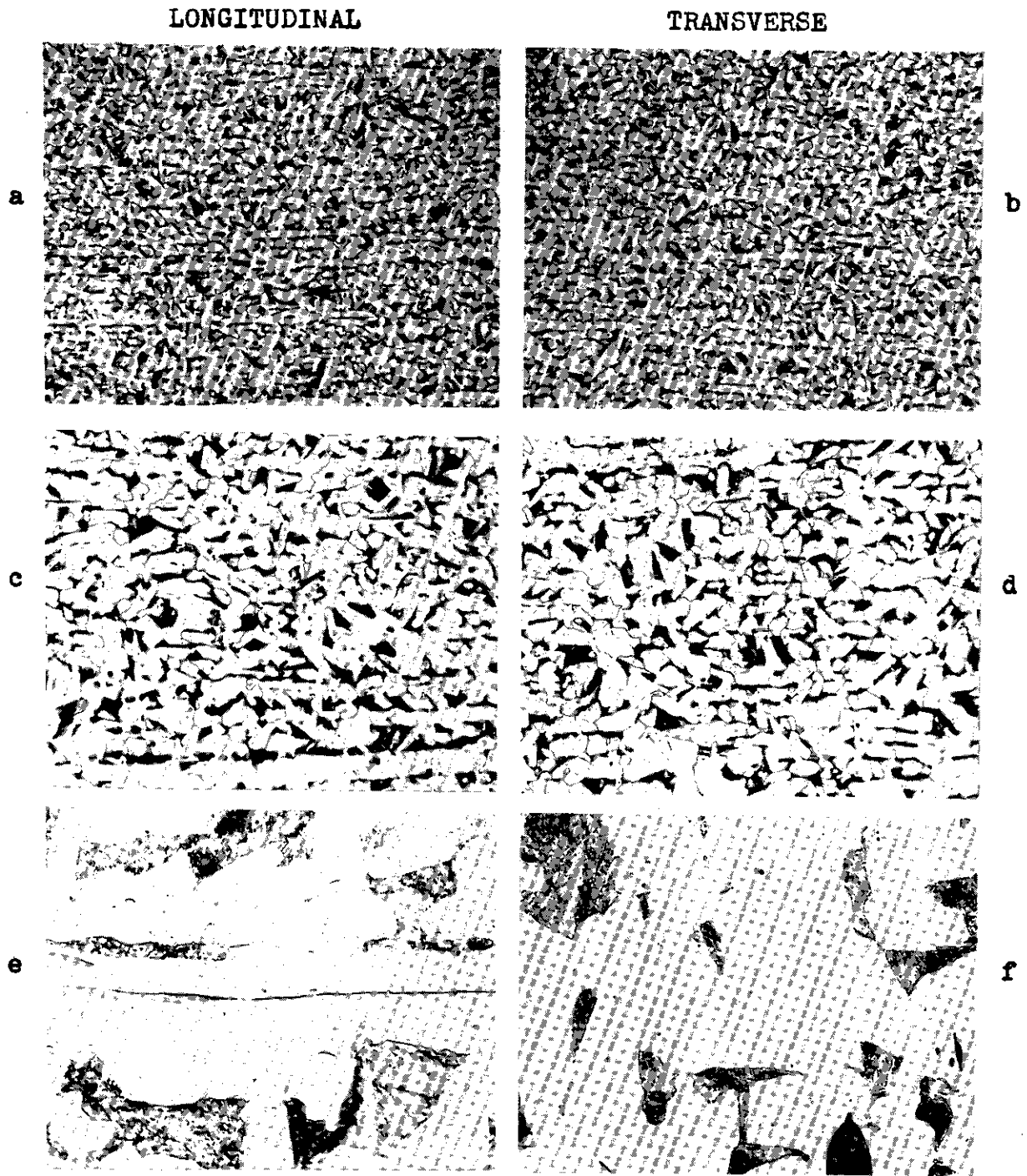


Fig. M-3 Photomicrographs, Etched Steel A.

a,b X 50
 c,d X 100
 e,f X 600

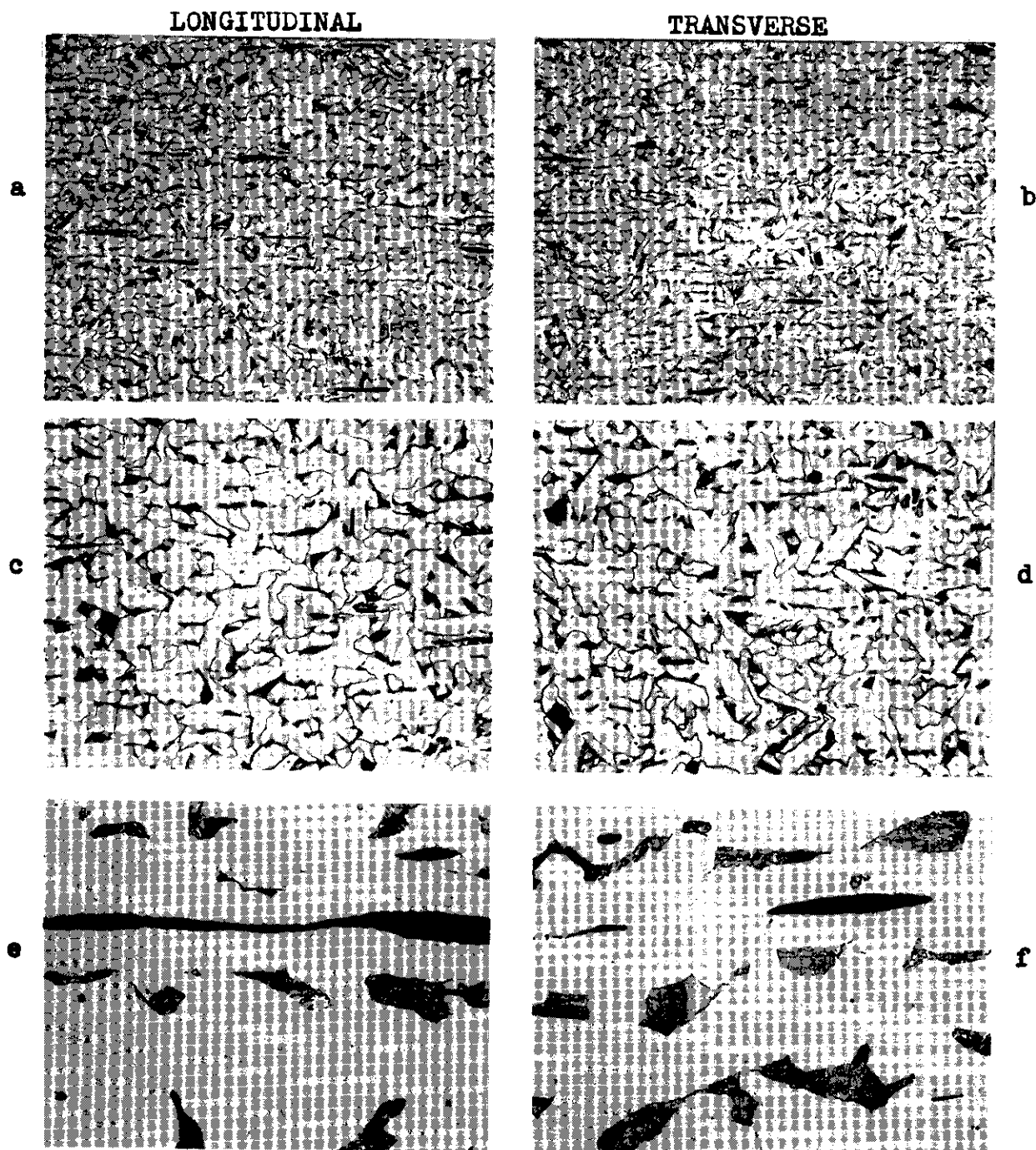


Fig. M-4 Photomicrographs, Etched Steel Br.

a,b X 50
c,d X 100
e,f X 600

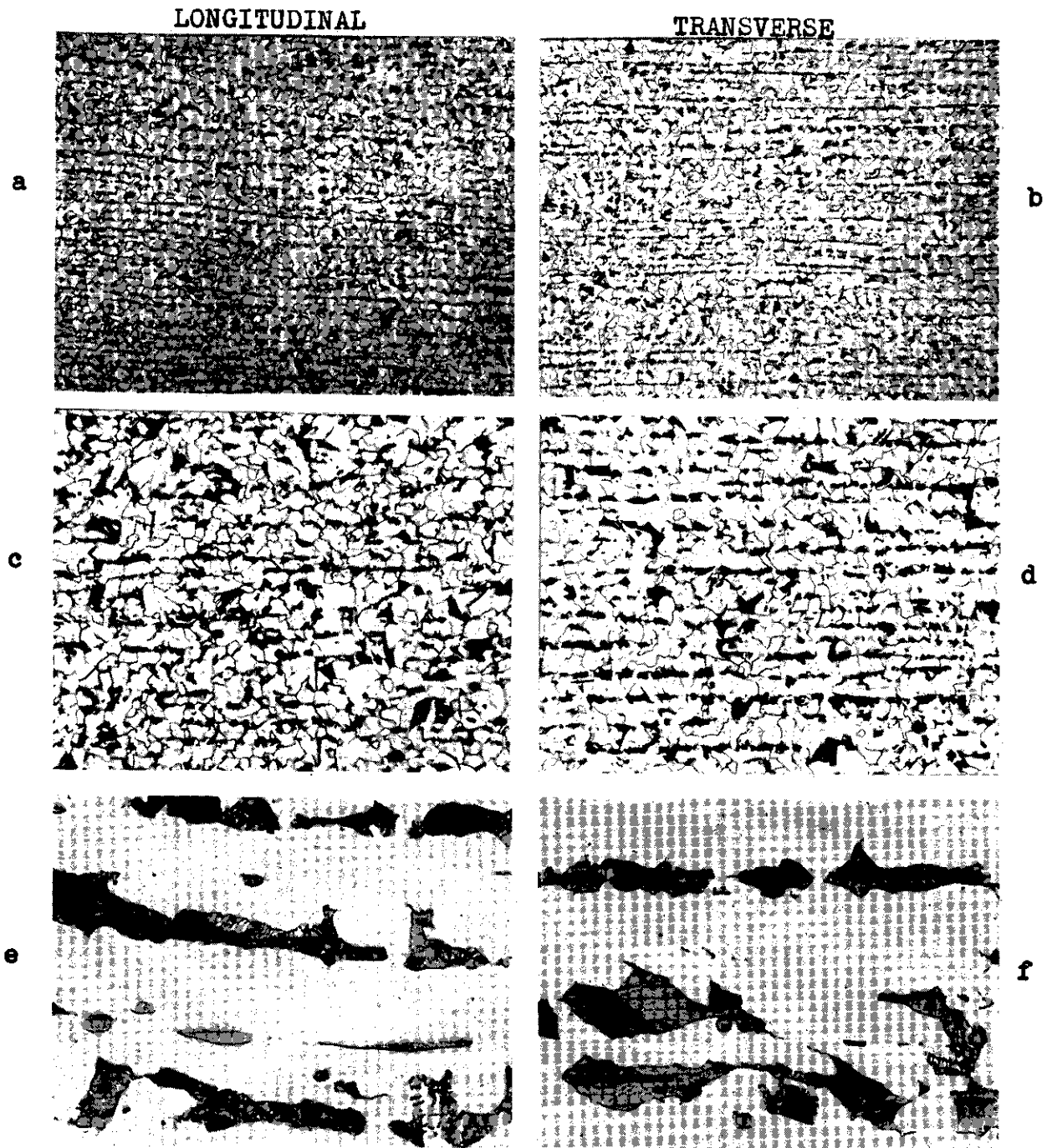


Fig. M-5 Photomicrographs, Etched Steel Bn.

a,b X 50
 c,d X 100
 e,f X 600

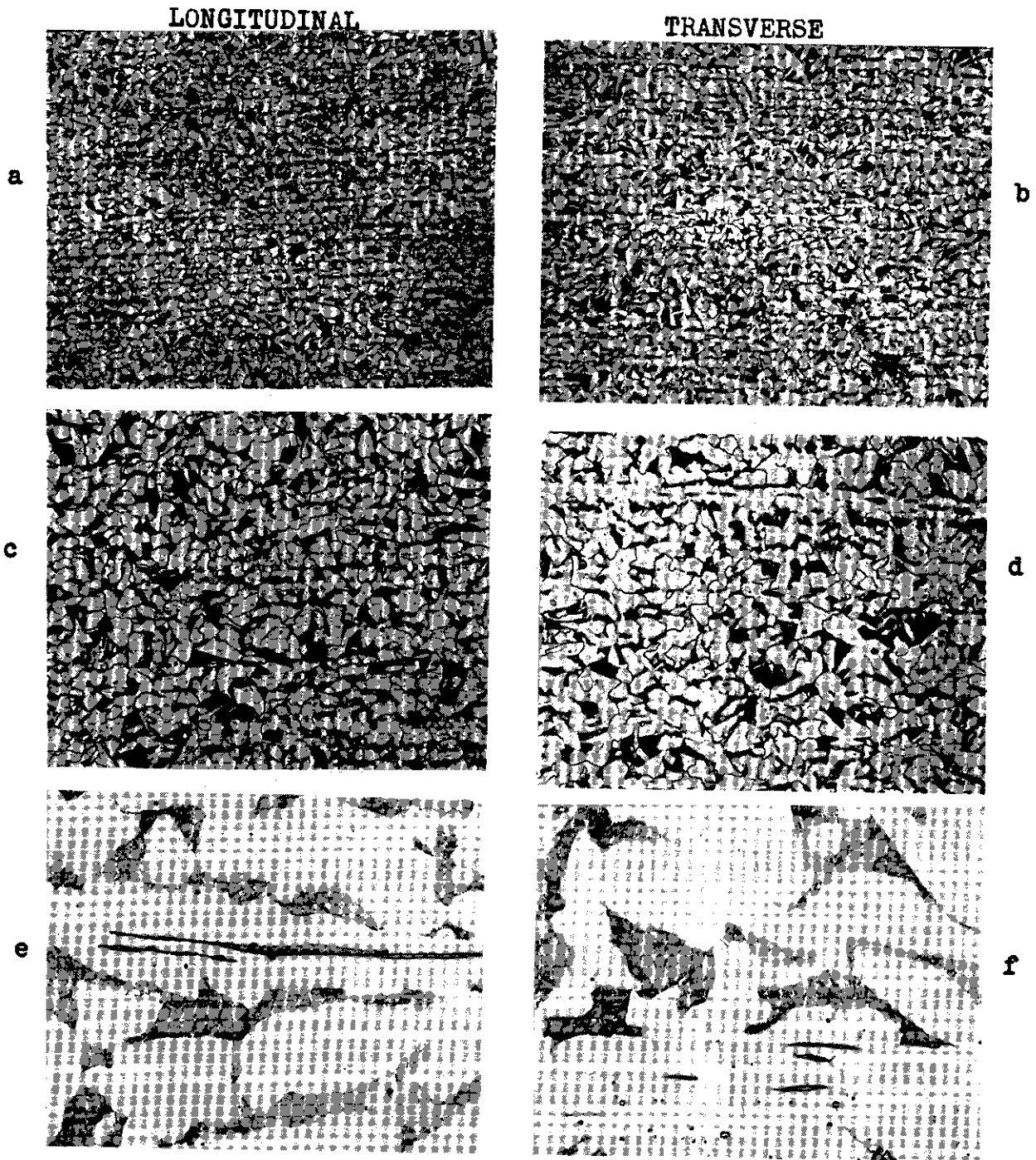


Fig. M-6 Photomicrographs, Etched Steel Dr.

a,b X 50
 c,d X 100
 e,f X 600

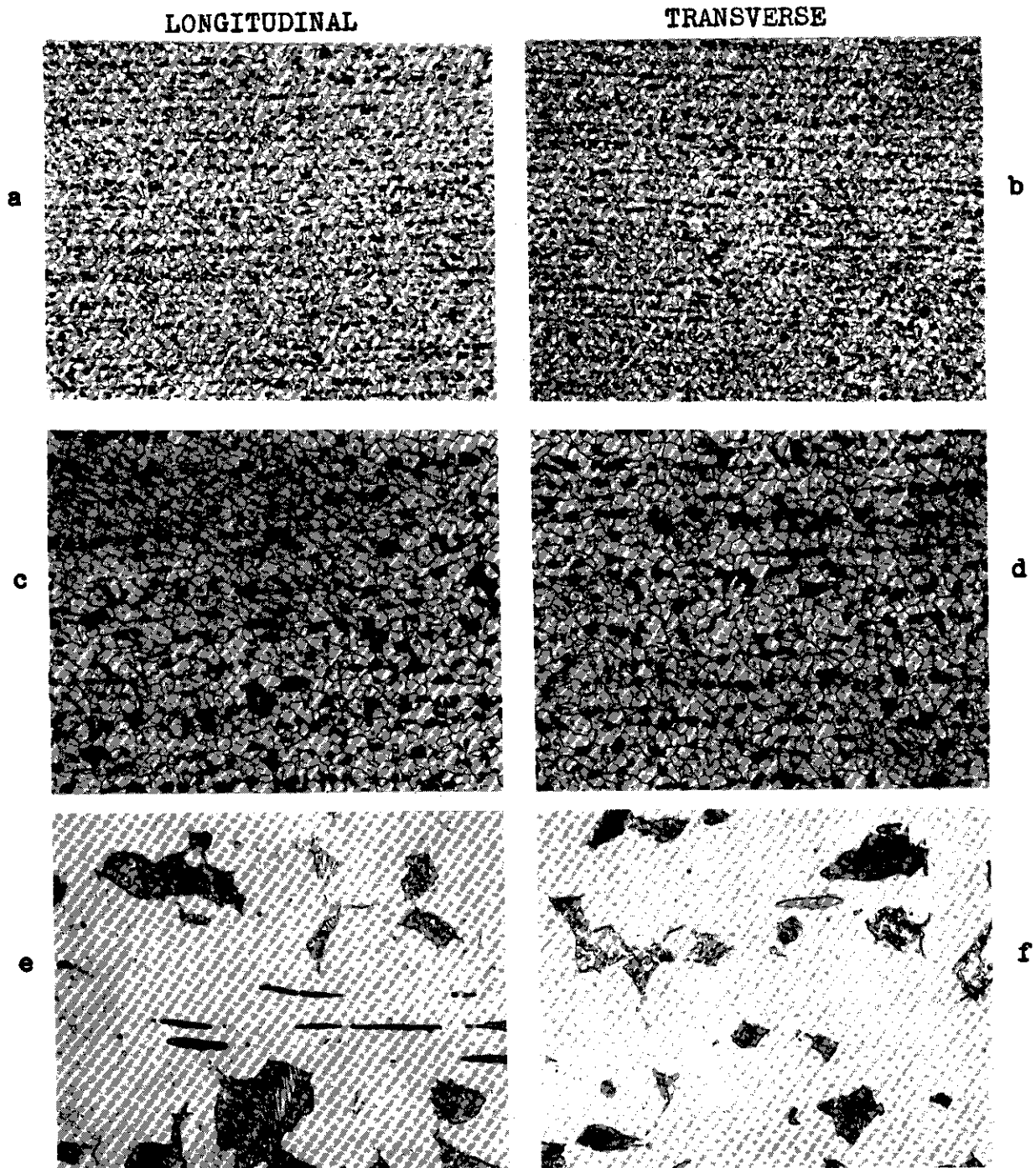


Fig. M-7 Photomicrographs, Etched Steel Dn.

a,b X 50
c,d X 100
e,f X 600

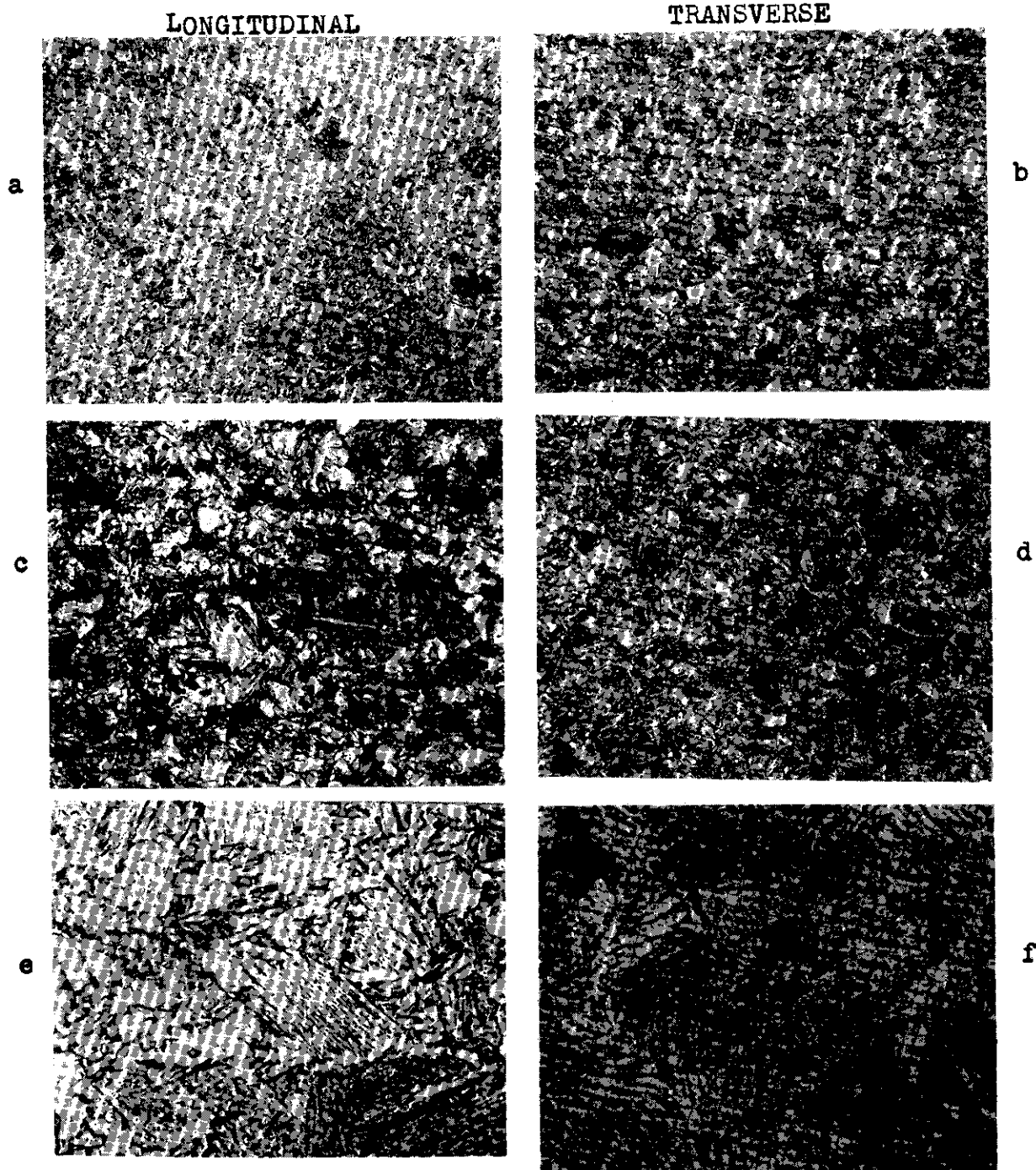
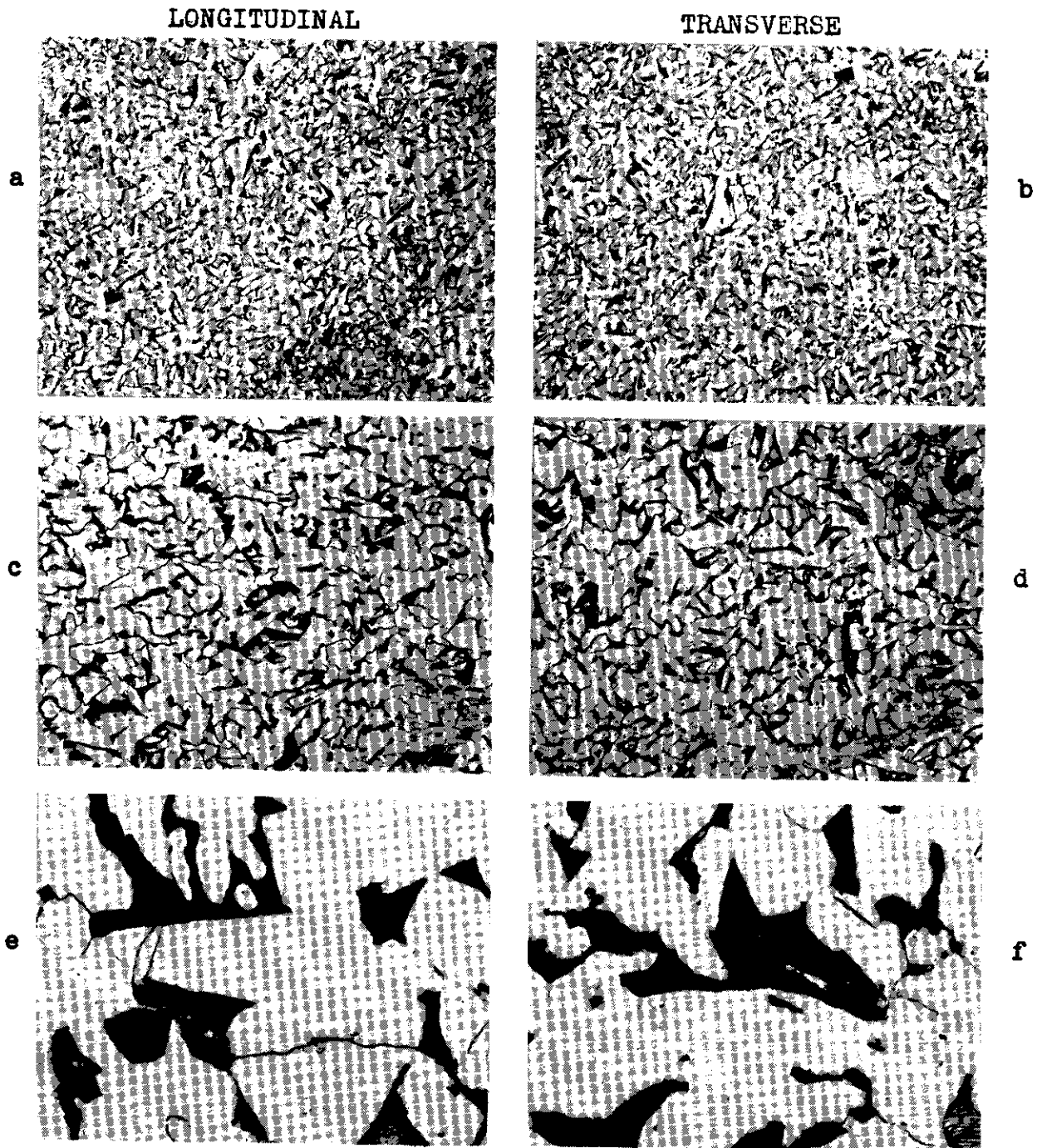


Fig. M-8 Photomicrographs, Etched Steel Q.

a, b X 50
c, d X 100
e, f X 600



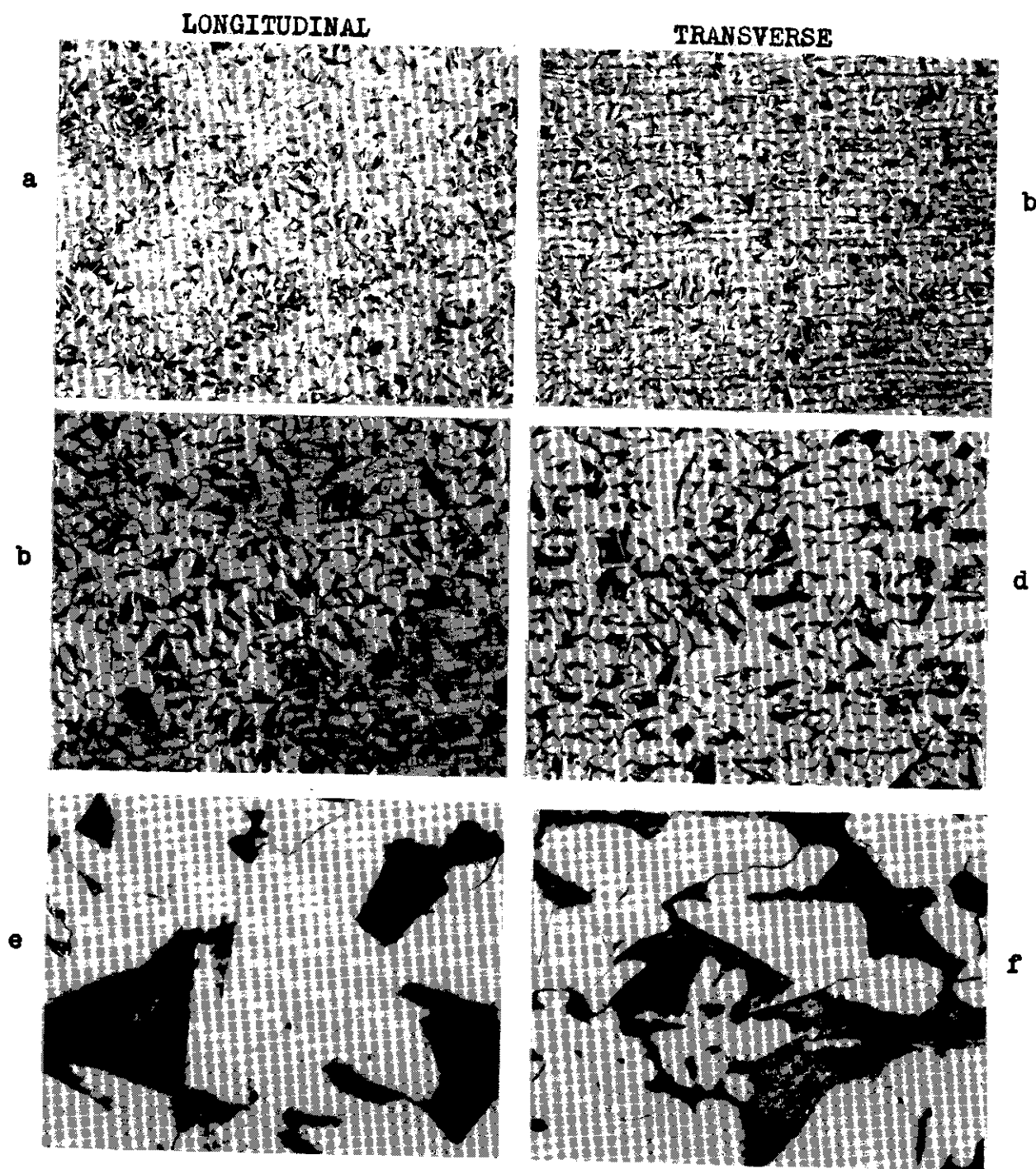


Fig. M-10 Photomicrographs, Etched Steel G.

a, b X 50
c, d X 100
e, f X 600

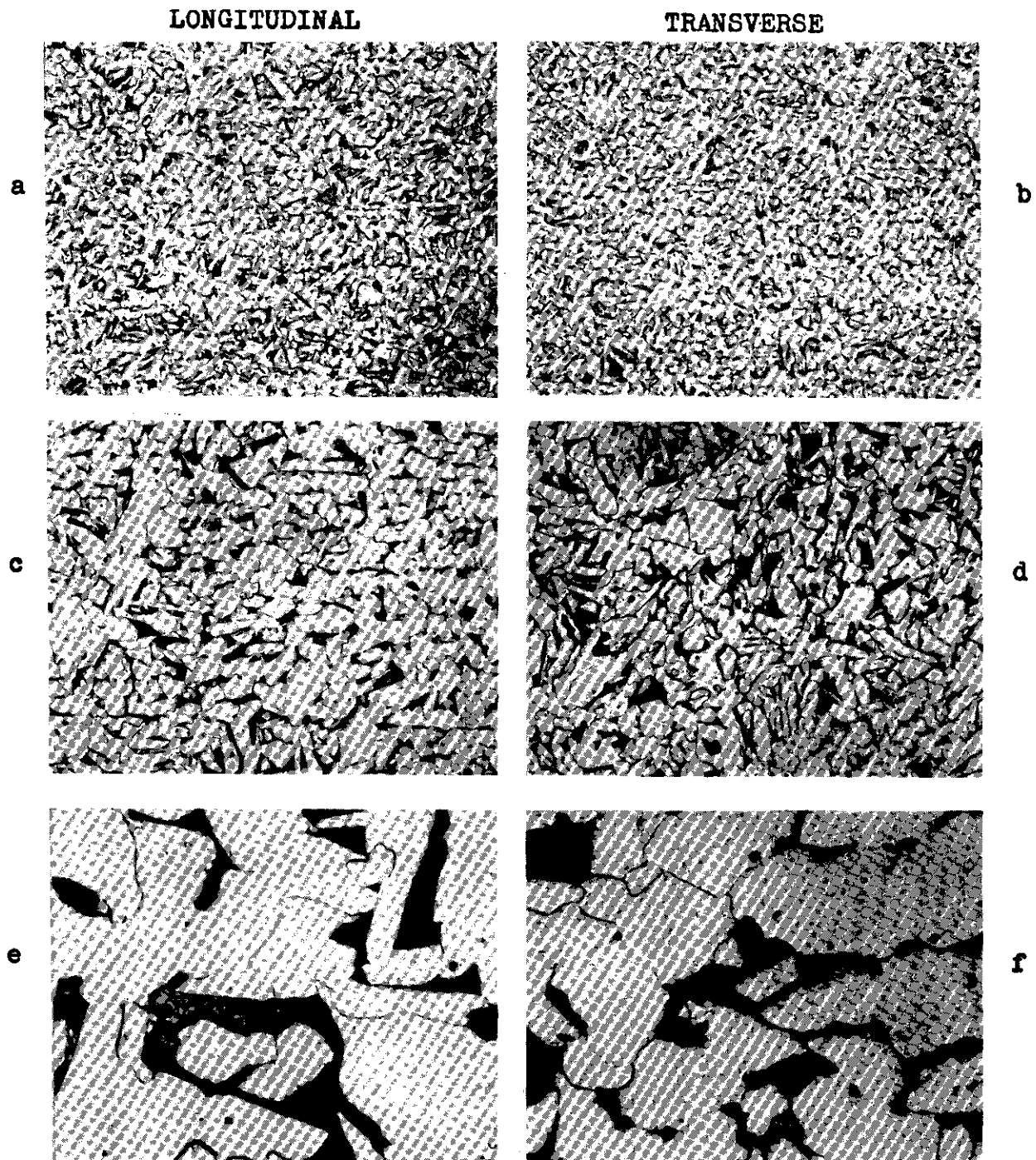


Fig. M-11 Photomicrographs, Etched Steel H.

a, b	X	50
c, d	X	100
e, f	X	600

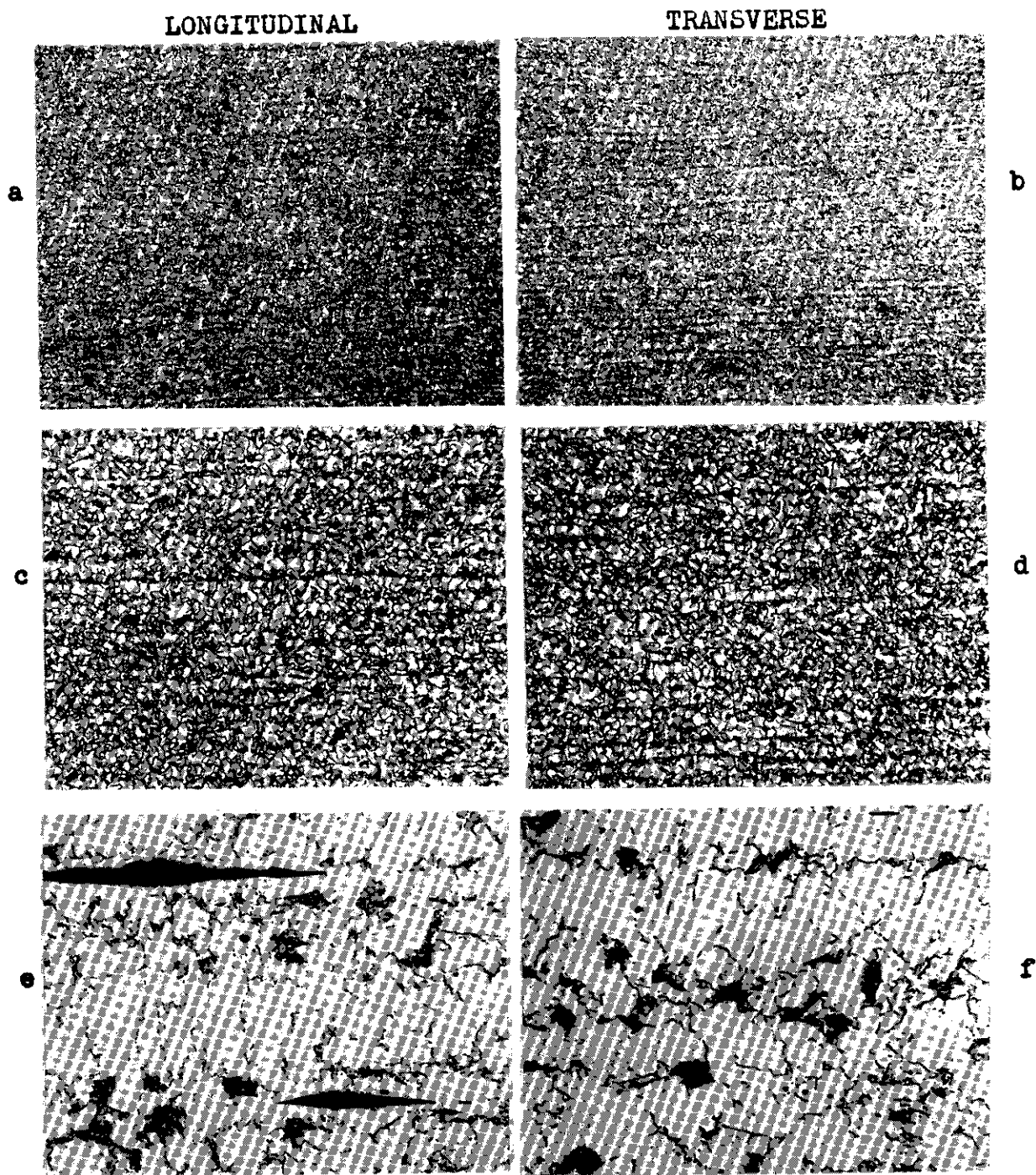


Fig. M-12 Photomicrographs, Etched Steel N.

a, b X 50
c, d X 100
e, f X 600

